POLITECNICO DI MILANO
School of Civil, Environmental and Land Management Engineering
Master of Science in Civil Engineering for Risk Mitigation

POLITECNICO
MILANO 1863

Flood hazard and damage assessment for the Namuapala village in northern Mozambique under different modeling scenarios

Supervisor: Dr. Alessio Radice
Co-supervisor: M.Sc. Ana Maria Rotaru

MSc thesis by:
Zeynep Ergün - 965544

Academic Year 2022/2023

Acknowledgments

Firstly, I would like to express my deep gratitude to my thesis advisor, Dr. Alessio Radice of the Department of Civil and Environmental Engineering at Politecnico di Milano, for his professional knowledge, meticulous guidance throughout the entire process, and, most importantly, for his understanding. I will always be grateful for the opportunity to work with him, whom I feel deeply respect.

I would like to extend my gratitude to my co-supervisor, Ana Maria Rotaru. It is an immeasurable value of Rotaru's unwavering support, patience, friendship, and sincerity, which have consistently grown from the first day to the last. I am eternally grateful to her for always helping me overcome my concerns and doubts by creating a comfort zone for me and for never leaving me alone on this journey. I would like to point out that the high quality of all her work, particularly her unwavering determination, diligence, and dedication, consistently serves as a profound wellspring of motivation for me, and I feel privileged to have worked with her.

Lastly, I express my appreciation to my dear friends Beril and İlke, my sister Zühre, and my roommate Mohadese, who have consistently provided unwavering faith and support while consistently listening and understanding all the challenges and doubts I encountered throughout this process.

Thank you.

Zeynep

November 2023

ABSTRACT (English)

Floods are one of the most devastating weather-related hazards that are affecting millions of people all over the world every year. The impacts of climate change are anticipated to increase the frequency and intensity of these events, leading to an escalation in future flood risk. This heightened risk is further compounded by expected changes in land use, as increasing urbanization places more people in flood-prone areas, intensifying the exposure of communities to these devastating events.

Developing countries are particularly vulnerable to the destructive consequences of floods due to a combination of socioeconomic and environmental factors. These nations often face challenges in infrastructure development, including inadequate flood control measures, inefficient water resource management, poorly constructed housing, and limited access to early warning systems.

One of the most significant challenges in assessing flood risk in developing countries is due to data scarcity, which raises uncertainties around assessing flood impact. Given the constraints of incomplete data, reliance on assumptions becomes essential. These assumptions, while necessary, introduce complexities and potential inaccuracies into the risk assessment process. In data-scarce regions recognizing and thoroughly scrutinizing the implications of these assumptions on damage assessment outcomes are crucial steps toward enhancing the reliability of flood risk assessments.

This study is part of a series of three theses conducted within a project led by the NGO Oikos in Mozambique. The data and the modeling align with the approaches used in previous theses, and the focus of this study is to address uncertainties arising from earlier research findings. In detail, this study presents a comparative analysis of the results obtained using different hydrologic and hydraulic modeling assumptions for the rural community of Namuapala in the province of Cabo Delgado. The modeling assumptions encompass sub-basin selection in hydrological modeling and terrain geometry utilized in hydraulic modeling. Using a comprehensive modeling chain composed by hydrological, hydraulic, and damage assessment, various model sets based on different assumptions were created considering four return period scenarios. The results obtained from the different model sets were compared to evaluate the effects of the assumptions employed on hazard and damage assessment.

This research not only contributes to improving flood risk assessments in data-scarce regions but also provides valuable insights into the complex relationship between hydro-dynamic modeling assumptions and damage assessment outcomes. By explicitly addressing uncertainties and building on previous research, this study enhances our understanding of flood risk dynamics and supports future studies in similar regions.

Keywords: flood risk; developing countries; data scarcity; uncertainties; hydro-dynamic modeling

ABSTRACT (Italiano)

Le alluvioni rappresentano uno dei pericoli naturali più devastanti che colpiscono milioni di persone in tutto il mondo ogni anno. Si prevede che gli impatti dei cambiamenti climatici aumenteranno la frequenza e l'intensità di tali eventi, accrescendo il rischio di future alluvioni. Questo aumento del rischio è ulteriormente accentuato dai cambiamenti previsti nell'uso del territorio, poiché la crescente urbanizzazione colloca un numero maggiore di persone in aree soggette al rischio alluvionale, aumentando l'esposizione delle comunità a tali eventi catastrofici.

I paesi in via di sviluppo sono particolarmente vulnerabili alle conseguenze distruttive delle alluvioni a causa di una combinazione di fattori socioeconomici e ambientali. Queste nazioni spesso presentano limiti nello sviluppo delle infrastrutture, tra cui misure insufficienti di controllo delle alluvioni, gestione inefficiente delle risorse idriche, edifici mal costruiti e limitato accesso ai sistemi di allarme rapido.

Una delle sfide più significative nella valutazione del rischio di alluvioni nei paesi in via di sviluppo è rappresentata dalla scarsità di dati, che aumenta le incertezze nella valutazione dell'impatto delle alluvioni. Considerando i vincoli derivanti dai dati incompleti, diventa essenziale fare affidamento su delle ipotesi. Queste ipotesi, sebbene necessarie, introducono complessità e potenziali imprecisioni nel processo di valutazione del rischio. Nelle regioni con dati limitati, riconoscere ed esaminare attentamente le implicazioni di tali ipotesi sui risultati della valutazione dei danni rappresenta un passo cruciale per migliorare l'affidabilità delle valutazioni del rischio di alluvioni.

Questo studio fa parte di una serie di tre tesi condotte all'interno di un progetto guidato dalla ONG Oikos in Mozambico. I dati e la modellizzazione si allineano con gli approcci utilizzati nelle tesi precedenti e l'obiettivo di questo studio è affrontare le incertezze derivanti dai risultati della ricerca precedente. In particolare, lo studio presenta un'analisi comparativa dei risultati ottenuti da diverse ipotesi di modellazione per la comunità rurale di Namuapala nella provincia di Cabo Delgado. Le ipotesi di modellazione includono la selezione dei sottobacini nella modellazione idrologica e la geometria del terreno utilizzata nella modellazione idraulica. Utilizzando una catena completa di modellazione, composta da valutazione idrologica, idraulica e dei danni, sono stati creati diversi set di modelli basati su diverse ipotesi, considerando quattro scenari di tempi di ritorno. I risultati ottenuti dai diversi set di modelli sono stati confrontati per valutare gli effetti delle ipotesi impiegate sulla valutazione dei pericoli e dei danni.

Questa ricerca non solo contribuisce a migliorare le valutazioni del rischio di alluvioni nelle regioni con dati limitati, ma fornisce anche preziose informazioni sulla complessa relazione tra le ipotesi di modellazione idrodinamica e i risultati della valutazione del pericolo e dei danni. Affrontando esplicitamente le incertezze e basandosi su ricerche precedenti, questo studio migliora la nostra comprensione delle dinamiche del rischio alluvionale e supporta studi futuri in regioni simili.

Keywords: rischio alluvionale; paesi in via di sviluppo; scarsità di dati; incertezze; modellazione idrodinamica

ABSTRACT (Turkish)

Seller sıklıkla, dünya genelinde her yıl milyonlarca insanı etkileyen en yıkıcı doğal afetlerden biridir. İklim değişikliğinin etkilerinin, bu doğal afetlerin sıklığını ve şiddetini artırarak gelecekti sel riskinin artmasına neden olması beklenmektedir. Bu riskin artışı, beklenen arazi kullanımındaki değişiklikler tarafından daha da vurgulanmaktadır, çünkü artan kentselleşme, insanları sel riskine maruz kalan alanlara daha fazla yerleştirmekle birlikte toplulamları bu felaket olaylarına daha fazla açık hale getirmektedir.

Gelişmekte olan ülkeler, selin yıkıcı sonuçlarına karşı özellikle sosyoekonomik ve çevresel faktörlerin kombinasyonuyla da birleşince oldukça savunmasız duruma düşmektedirler. Bu ülkeler genellikle altyapı geliştirmede zorluklarla karşılaştıkları gibi bunlar arasında yetersiz sel kontrol önlemleri, verimsiz su kaynakları yönetimi, kötü inşa edilmiş konutlar ve erken uyarı sistemlerine de sınırlı erişim sağlamaktadırlar.

Gelişmekte olan ülkelerde sel riskinin değerlendirilmesindeki en önemli zorluklardan biri, veri eksikliğinden kaynaklanmaktadır; bu da sel etkilerinin değerlendirmesinde belirsizlikleri artırır. Veri eksikliği nedeniyle, varsayımlara güvenmek esastır. Bu varsayımlar, gerekli olsa da risk değerlendirme sürecine karmaşıklık ve potansiyel belirsizlikler ekler. Sınırlı verilere sahip bölgelerde, bu varsayımların değerlendirme sonuçları üzerindeki etkilerini tanımak ve dikkatlice incelemek, sel risk değerlendirmelerinin güvenilirliğini artırmak için kritik bir adımdır.

Burada sunulan çalışma, Mozambik'te Oikos adlı İtalyan bir sivil toplum kuruluşu tarafından yönetilen bir projenin parçası olarak gerçekleştirilen üç yüksek lisans tezinin bir parçasıdır. Veriler ve modellemeler önceki tezlerde kullanılan yaklaşımlarla uyumlu olmakta birlikte bu çalışmanın ana odak noktası, önceki araştırma bulgularından kaynaklanan belirsizliklere çözüm bulmaktır. Bu çalışma, Mozambik ülkesinde bulunan Cabo Delgado ilinin Namuapala köyü için farklı hidrolojik ve hidrolik modelleme varsayımlarının karşılaştırılmalı bir analizini sunmaktadır. Modelleme varsayımları, hidrolojik modellemede alt havza seçimi ve hidrolik modellemede kullanılan arazi geometrisini içermektedir. Hidrolojik, hidrolik ve hasar değerlendirmesinden oluşan kapsamlı bir modelleme zinciri kullanılarak, farklı varsayımlara dayanan çeşitli model setleri, dört farklı geri dönüş süresi senaryosunu içerecek şekilde oluşturulmuştur. Farklı model setlerinden elde edilen sonuçlar, varsayımların tehlike ve hasar değerlendirmesi üzerindeki etkilerini değerlendirmek için karşılaştırılmıştır.

Burada sunulan araştırma, veri yetersizliği bulunan bölgelerdeki sel riski değerlendirmelerini geliştirmenin yanı sıra hidro-dinamik modelleme varsayımları ile hasar değerlendirme sonuçları arasındaki kompleks ilişki hakkında değerli analizler sunmaktadır. Belirsizliklere açık ve anlaşılır bir yaklaşımla önceki yapılan araştırmalara dayanarak bu çalışma, sel riski değerlendirmesindeki dinamiklerini anlamlandırmaya katkı sağlarken benzer bölgelerdeki gelecekte yürütülecek çalışmalara destek olmaktadır.

Anahtar kelimeler: sel riski; hidrodinamik modelleme, veri kısıtlılığı; belirsizlikler, gelişmekte olan ülkeler

List of Contents

List of Figures

List of Tables

List of Graphs

List of Charts

Chapter 1: Introduction

1.1 Context

Mozambique is a Sub-Saharan African country bordered by Tanzania, Malawi, Zambia, Zimbabwe, South Africa, and Eswatini. It is one of the least developed countries in the world and has the rank of 185 out of 191 countries according to the 2022 Human Development Index. (UNHCRR, 2023) The country faces numerous obstacles commonly seen in less developed countries, encompassing elevated levels of poverty, restricted availability of healthcare and education, and an over-reliance on a small number of economic sectors like agriculture and natural resources. Development initiatives are additionally impeded by corruption and political instability. Although Mozambique has a high poverty rate, it is also situated in a region at higher risk due to its extensive 2,470 km coastline, which makes it highly susceptible to tropical depressions and typhoons. (Mondlhane, 2004) Given these socio-economic factors, it is inevitable that the country will face challenges in coping with and recovering from natural disasters.

Figure 1-1: Mozambique. Source: (Encyclopedia Britannica. https://www.britannica.com/place/Mozambique)

The country suffers most from cyclones, droughts, and floods as climate-related hazards. On an annual basis, approximately 2 million individuals in the coastal regions of Mozambique are impacted by cyclones, making them the most notable and frequent hazard. Additionally, flooding poses a risk to lowland areas, highland areas, and urban regions, with around 200,000 people being affected each year on average. (World Bank, 2019) The main factors affecting floods in Mozambique are local heavy rains, cyclonic winds, flooding of national basins, as well as management problems in river basins of neighboring countries. Considering the presence of multiple rivers flowing from the central African highland plateau into the Indian Ocean, as well as several minor river basins in the northeastern region, it is inevitable that a considerable risk of flood hazard exists in this country. The relatively flat topography of the country, combined with the scarcity of vegetation, further increases its exposure and vulnerability to floods. (Cea et al., 2022)

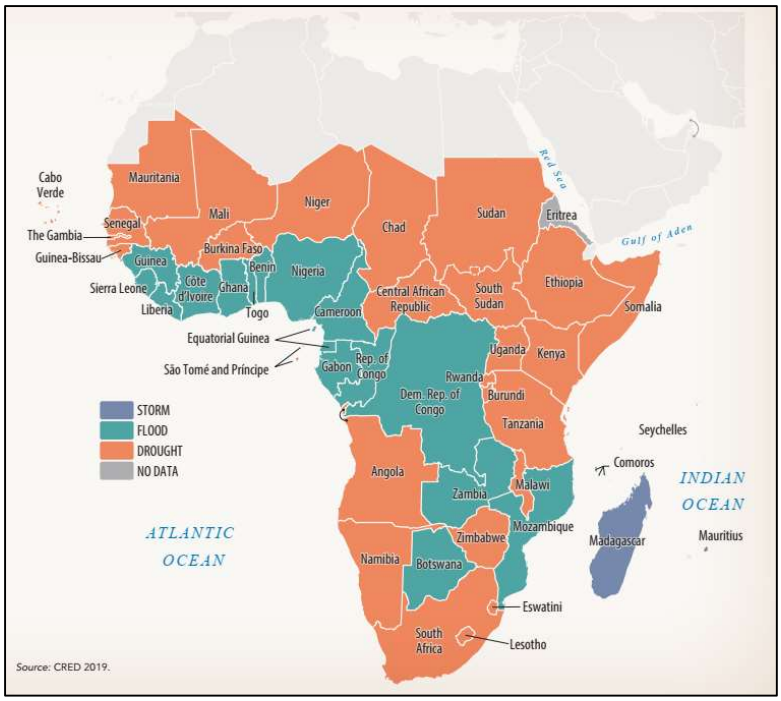

Figure 1-2 : Natural Hazards Affecting the Most People across Sub-Saharan African Countries, 2000–19. Source: (World Bank, 2019)

In recent years, Mozambique has been hit by several devastating tropical cyclones, such as Tropical Cyclones Idai and Kenneth. On the night of 14 March 2019, Tropical Cyclone Idai made landfall in central Mozambique. The rivers overflowed, resulting in floodwater reaching depths of over 10 meters. It is estimated that more than 600 people lost their lives, and it affected more than 1.5 million in the four provinces of Sofala, Manica, Zambezia, and Tete. It is estimated that Cyclone Idai caused around 1.4 billion US dollars in total damage and 1.39 billion US dollars in loss (PDNA of Cyclone Idai, 2019). Unluckily, six weeks after this event, another tropical cyclone, Kenneth, struck northern Mozambique on April 25, 2019. It was recorded as the most powerful hurricane to strike the African continent. The storm-induced flooding resulted in the displacement of 95,388 individuals and caused extensive damage to approximately 715,000 hectares of agricultural land. One of the strongest tropical cyclones of recent times was Gombe. It made landfall on March 11, 2022, and its consequences were devastating for the country, causing the displacement of 740,000 people in Nampula and Zambezia provinces. (WFP, 2022) Severe Tropical Cyclone Gombe caused the death of 61 people, while the total number of affected people recorded reached 488,5702, and a total of 46,265 houses have been destroyed. (IFRC, 2022) Nevertheless, the surge in these tropical events can be attributed to the rising ocean temperatures resulting from the effects of climate change in recent years. (Cea et al., 2022)

Among the general population, the intersection of extreme poverty and susceptibility to floods is most pronounced in sub-Saharan Africa. Therefore, there is an urgent imperative to enhance disaster prevention and recovery capabilities in regions where these factors overlap most significantly (Rentschler et al., 2022). However, factors such as high summer precipitation in the region, lack of reliable data, sensitivity to climate change, and dependence on the agricultural sector contribute to the complexity of flood risk assessment in the region and create difficulties in effectively understanding and managing flood risks.

1.1.2 The effect of climate change on natural disasters

Climate change is significantly impacting Sub-Saharan Africa, particularly regarding natural disasters. According to the 2021 Global Climate Risk Index, Mozambique is at the top of the list of countries most likely to be affected by climate change (Eckstein et al., 2021). These disasters, including cyclones, droughts, and floods, are becoming more frequent and intense due to climate change. Countries hit by hurricanes are often more vulnerable to other hazards and the effects of climate change due to their lack of recovery capacity. According to The Centre for Research on the Epidemiology of Disasters, the frequency of floods between 1970 and 1979 increased more than ten times compared to that between 2010 and 2019. The number of people impacted by floods has also witnessed a significant rise over the years. From 1970-1979, approximately 3.5 million people were affected by floods, whereas between 2010-2019, this number escalated to around 28.1 million people affected. The increasing occurrence of natural disasters and changes in temperature and precipitation patterns can threaten agricultural production, leading to food insecurity and economic losses. Aggregate production shortfalls from drought or flood cause food scarcity and increase acute food insecurity (Hendrix et al., 2013). As a result of these combined factors, it is projected that 22 African countries may experience a scarcity of water or stress on water resources by the year 2025 (Coulibaly et al., 2020; Cooper et al., 2008). The main source of livelihood and income for the Mozambican people is still agriculture. Mozambique's agricultural sector accounts for 30% of GDP and 77% of overall employment. (World Bank, 2019) Agriculture is practiced on less than 10% of arable land and largely in flood- and drought-prone areas, and challenges such as low productivity, low value-added and poor market access, and the dominance of rain-fed agriculture make the sector vulnerable to shocks, hindering higher earnings (Sida, 2019). Given the heavy dependence on the agricultural sector, this issue becomes even more critical and exacerbates the vulnerability compared to other developed countries. It is causing a perpetual cycle of poverty and instability that affects millions of people.

1.1.3 The Risk Mitigation in Mozambique

The National Institute of Disaster Management (INGD) has coordinated disaster risk management activities in Mozambique since 1999. Under the Ministry of State Administration, INGD is responsible for emergency coordination, promoting disaster prevention through mobilization of the population and government, safeguarding human lives, ensuring coordinated efforts in disaster emergencies across various sectors, coordinating early warning systems, raising public awareness about disasters, and utilizing arid and semi-arid areas.

The structure of INGD has evolved since 2007 with the National Emergency Operations Centre (CENOE), which is responsible for multi-sectoral coordination structure for emergency response at regional, provincial, and district levels, and the National Civil Protection Unit (UNAPROC), which is responsible for the search and rescue of disaster victims. Additionally, INGD has integrated the Post-Disaster Reconstruction Support Office (GACOR). At the local level, the Local Disaster Risk Management Committee (CLGRC), comprised of dedicated volunteers, plays a crucial role as the initial responders during disaster events and works to empower community members (World Bank, 2019).

In a possible emergency, weather bulletins and warnings are transmitted to INGD by the National Institute of Meteorology (INAM). In case of danger, INGD notifies the Regional Planning and Infrastructure Service (SDPI) and then passes the weather bulletin to a community leader. The Early Warning System is completed when the leader communicates with the Local Disaster Risk Management Committee (CLGRC). CLGRC also must sensitize the community to the risks by keeping in touch with INGD before the rainy season (Paz Idarraga & Rotaru, 2023). Hydraulic resource

management occurs at a regional level and is carried out by public organizations known as ARAs, an acronym for Regional Water Administration. Administração Regional de Aguas do Norte (ARA-Norte) is the administration in charge of the basins in Cabo Delgado Province. The responsibilities of ARA-Norte are such as management of hydrographic basins focusing on the land use planning and water domain protection zones, collection, processing, analysis, and storage of hydro-climatological data, implementation of structural measures aimed at defending against floods and mitigating droughts and so on. Unfortunately, ARA-Norte does not yet have the capacity and resources to fulfill these responsibilities. The main reasons for this are a lack of knowledge of water resources, an appropriate monitoring network, and awareness among stakeholders (Ferrer, 2014).

1.1.4 The Study Area

Acknowledging the challenges in assessing flood risk in Mozambique attributed to limited data availability and the consequential uncertainties associated with flood impact assessments, this research focuses on assessing the flood hazard and damage assessment for Namuapala village, situated in the Metuge District in Cabo Delgado province in northern Mozambique. The Rio Muaguide River basin, which is located in Cabo Delgado province with an area of 1740 km^2 and a river length of 132 km, was selected to perform the hydrological and hydraulic analyses (Figure 1-3). The river flows through the districts of Ancuabe and Metuge into the Indian Ocean and it is characterized by a well-defined path of 130 km that braids into multiple sub-reaches in the last 15 km. The climate in Cabo Delgado is categorized as sub-humid, featuring an extended dry season from May to November and a rainy season from December to April. Despite this, the temperatures in the northern region remain relatively stable throughout the year, experiencing a slight decrease from May to August, particularly in inland areas influenced by cool air from the south. The province receives an annual rainfall ranging from 800 to 1000 mm, with occasional intense rainfall leading to significant flooding across the region (Corti & Rotaru, 2019).

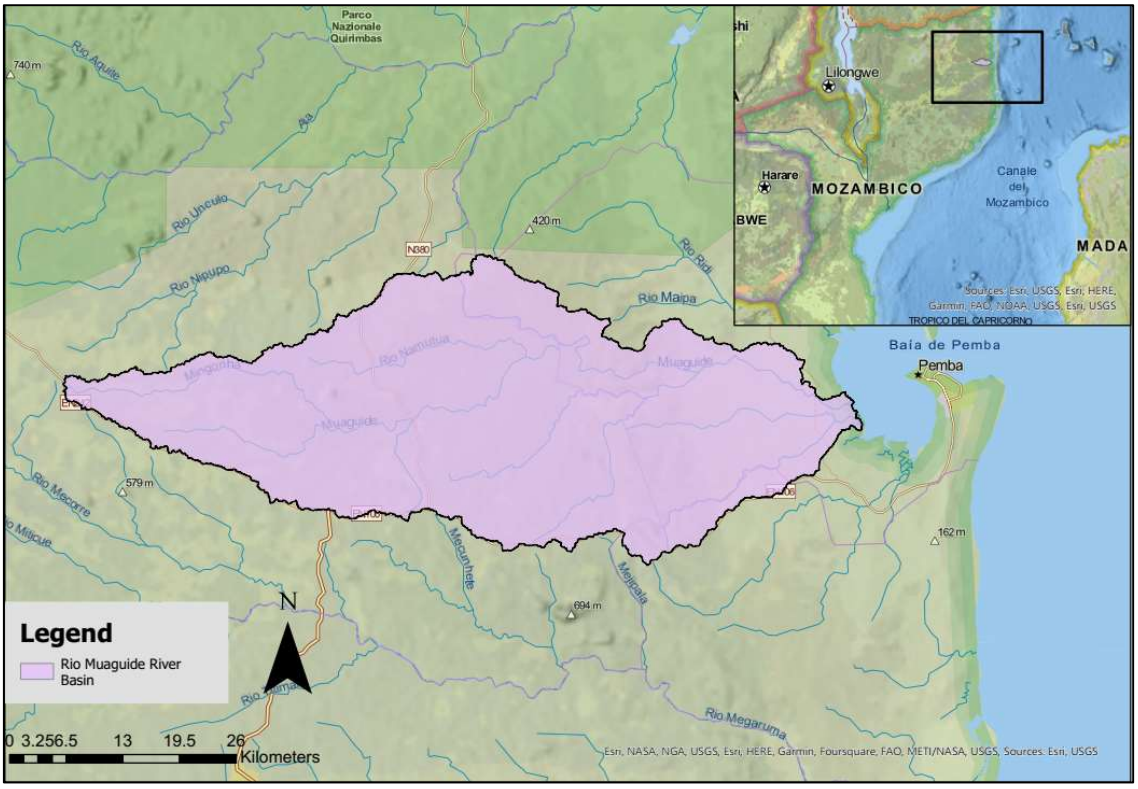

Figure 1-3: Study Area

The research documented here follows the prior two theses (Corti & Rrokaj, 2019) and (Paz Idarraga & Rotaru, 2023), also conducted as a part of the PRONTIDÃO project led by Oikos, which is a non-governmental organization (NGO). This organization aims to produce tangible solutions to climate change in Mozambique by supporting local people in preparing for and mitigating impacts. The data and modeling used in this study are compatible with the approaches used in previous theses and are based on previous research findings. According to the recent research of Paz Idarraga & Rotaru (2023), the village of Namuapala, located in the low region of the river basin, is most likely to be affected by the impact of floods among the other villages considered. For this reason, this study focuses on the Namuapala village (Figure 1-4) regarding flood hazard and damage assessment.

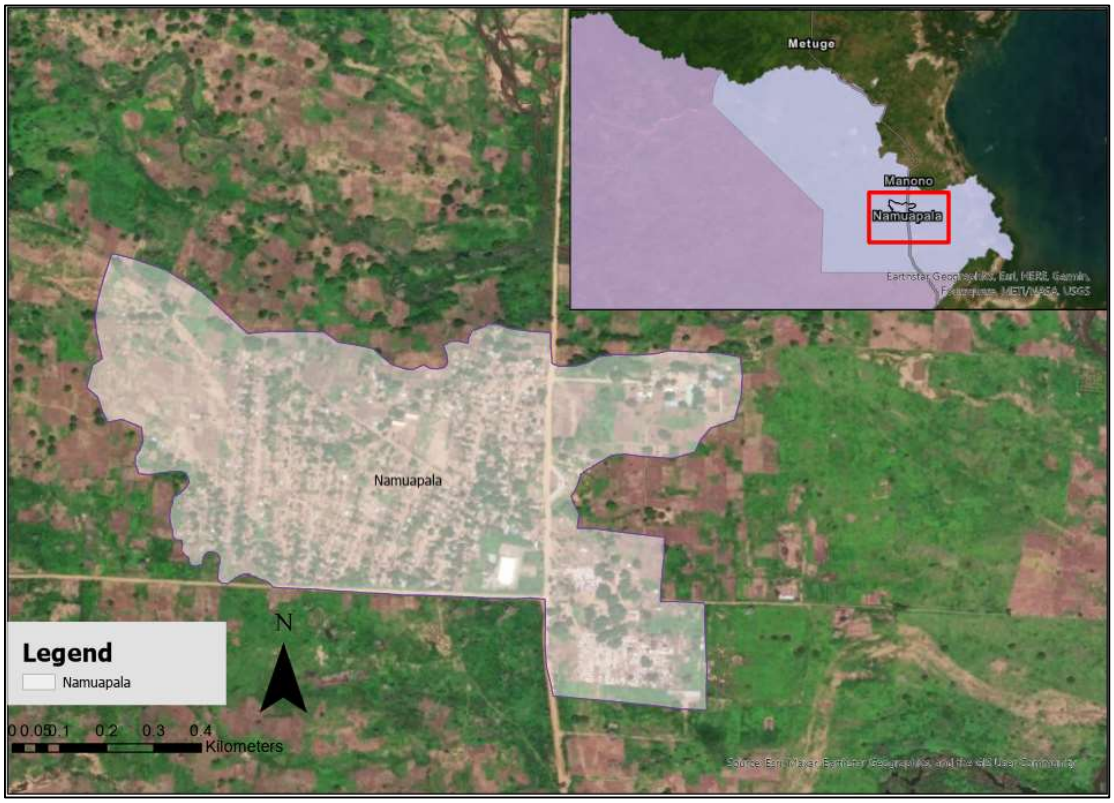

Figure 1-4: Focus village.

1.1.5 The conducted prior studies in the Cabo Delgado province for flood risk assessment and mitigation

1) The SIXHIARA Project, Phase IV (iCarto & ARA-NORTE, 2017)

The SIXHARA Project is a collaborative effort between the Water and Environmental Engineering Group at the University of Coruna, Icarto company, and ARA-Norte. The project aims to enhance water resource management in Cabo Delgado province, Mozambique, by improving the quality and accessibility of water supply and sanitation services for the local population. Specifically, it focuses on identifying flood zones in the lower reaches of the Muaguide River basin and Messalo River basin within Cabo Delgado province in Northern Mozambique.

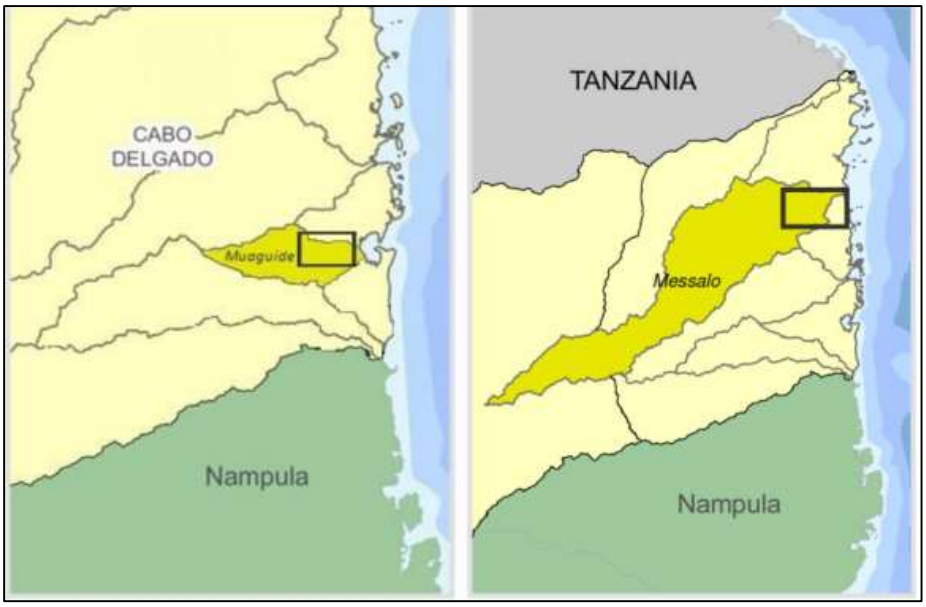

Figure 1-5: The study area of the SIXHIARA Project, Phase IV. Source :(iCarto & ARA-NORTE, 2017)

The study includes flood risk assessment and management planning by focusing on the implementation and collected recommendations to ARA-Norte authorities on the short-term flood risk assessment and management plan initial/mid-term of the relevant flood risk plans. A preliminary assessment of the flood risk was carried out and those areas with a significant potential risk of flooding were determined. Based on the assessment, an estimated area of 64 km^2 in the lower stretch of Muaguide River is prone to flooding during regional flood peaks. Within this zone, eight population centers, including Bandar, Tratara, Nangua, Nacuta, 25 de Junho, Namuapala, Pulo, and Nanjua, are at risk of flooding. The methodology employed in this study involved a three-step process, including hydrological analysis, hydraulic analysis, and geographic information systems, to obtain flood hazard and risk maps.

The initial section of the research concentrated on conducting a hydrological analysis to determine peak flows for various return periods such as 10,50,100, and 500 years. This information was essential for performing the subsequent hydraulic analysis. The calculations were carried out using the Flood Index Method, with parameters estimated regionally using the L-moments method and enveloping curves developed by Francou and Rodier to estimate the maximum regional flood peak flow value.

In the second phase of analysis, hazard risk maps were prepared. The hydraulic simulation is employed in a two-dimensional model called Iber. To carry out the hydraulic analysis for the lower stretch of Muaguide River, TanDEM-X commercial DEM was used as cartographic input data, which has a spatial resolution of 12 meters and a vertical accuracy of less than 2 meters. To perform the simulations, the maximum flows are determined from a hydrological analysis used as the upstream boundary condition. For the outflow boundary condition, a subcritical flow condition was applied downstream, while an initial condition of dry terrain was considered. To determine the roughness coefficient, Manning's roughness coefficients were employed with the subsequent values assigned: 0.04 s/$\sqrt[3]{}$m for all main bed areas, 0.05 s/$\sqrt[3]{}$m for cropland and vegetation, 0.07 s/$\sqrt[3]{}$m for wooded regions, and 0.025 s/$\sqrt[3]{}$m for areas containing bodies of water. The third block included the visualization of the results obtained from hydraulic analyses for the preparation and creation of hazard and risk maps. This operation was performed using GIS to convert these results into digital layers in raster format along with information on the relevant hazard maps. In addition to this study, a module has been developed in the Web viewer of the ARA-Norte Water Information System. This tool

aims to help calculate and analyze damage and disturbances to buildings, infrastructures, and villages through the intersection of OpenStreetMap's cadastral cartography and flood areas obtained in hydraulic modeling. As a result, ARA-Norte technicians were provided with a tool to manage and plan for floods.

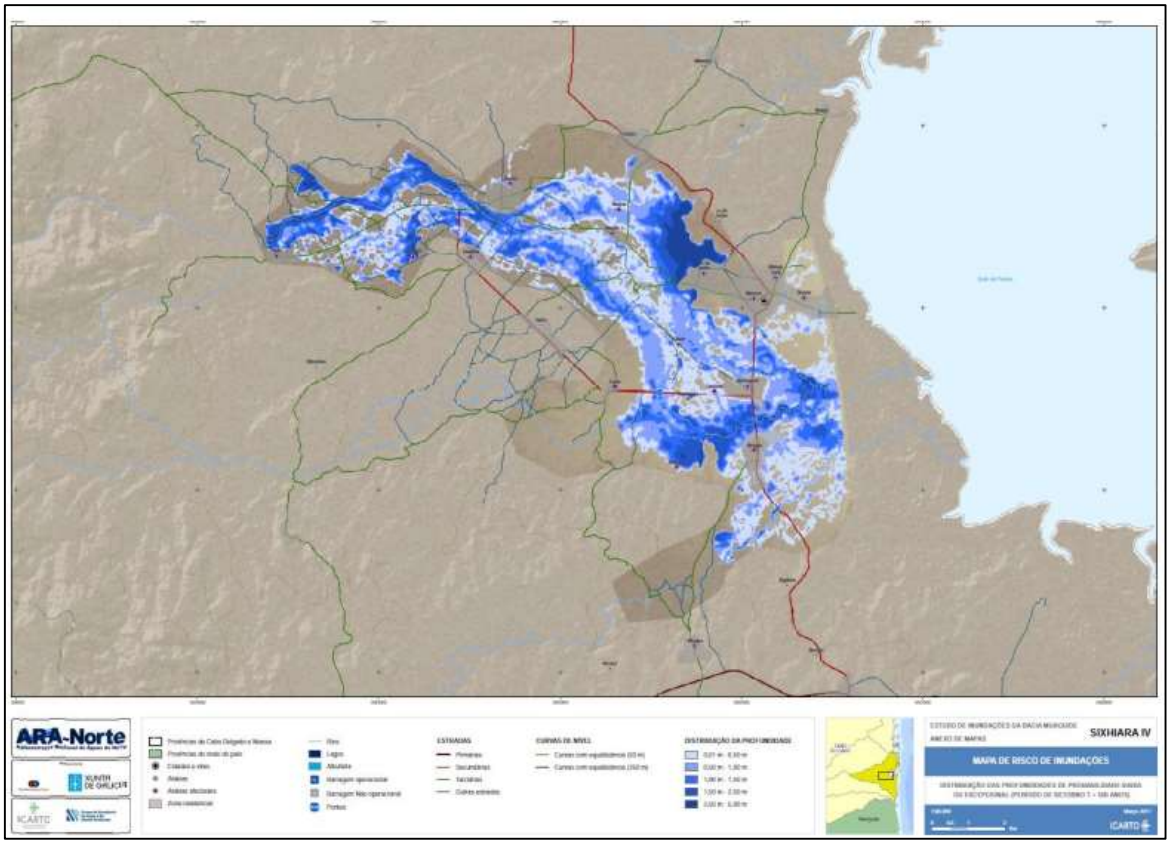

Figure 1-6: Hazard Map of 500-year return period for the lower stretches of Muaguide River. Source :(iCarto & ARA-NORTE, 2017)

2) Flood Risk Assessment and Mitigation for Rio Muaguide in Cabo Delgado, Mozambique (Corti &Rrokaj, 2019)

This study, an influential master's thesis in the field of Flood hazard in Northern Mozambique, is part of the ADAPT Project coordinated by the OIKOS Institute. This study has an important role in improving our knowledge of the flood hazard in Cabo Delgado province by emphasizing collaboration between institutions and researchers and becoming a leading source for further academic studies for the same region.

The objective of this study was to perform a flood hazard assessment for the Rio Muaguide River in the province of Cabo Delgado in Northern Mozambique and propose appropriate interventions to mitigate the flood risk. In the study, hydrologic and hydraulic numerical modeling approaches were used to achieve their objectives. The authors conducted a field trip to the area of Rio Muaguide in Cabo Delgado, Mozambique, to collect observations and data. The purpose of the mission was to collect available data regarding past events, their intensity, and GPS localization to geolocate the crucial spots and to interview local people of the villages neighboring the river to incorporate local knowledge and community participation in their research. They also collected large photographic documentation to validate the model of the flooded area and the water depth elevation extrapolated from it by comparing them with the traces left by past events and with the memory of the

inhabitants. The collected data is related to the morphology of the site, and this data is used to build numerical models with acceptable reliability. In addition, the collection and comparison of Digital Elevation Models with different resolutions, rainfall, and soil coverage data to create the models was also carried out.

The collected data was used to perform hydrological modeling to compute a synthetic hydrograph using the HEC-HMS software. The result obtained from hydrological modeling is used as input data for two-dimensional hydraulic modeling to obtain the extent of inundation areas to create hazard maps. The River2D and STORM software are used to perform hydraulic modeling. The flood modeling was performed considering a 10-year return period rainfall event and a flood hazard map corresponding to a 10-year return period produced at the end.

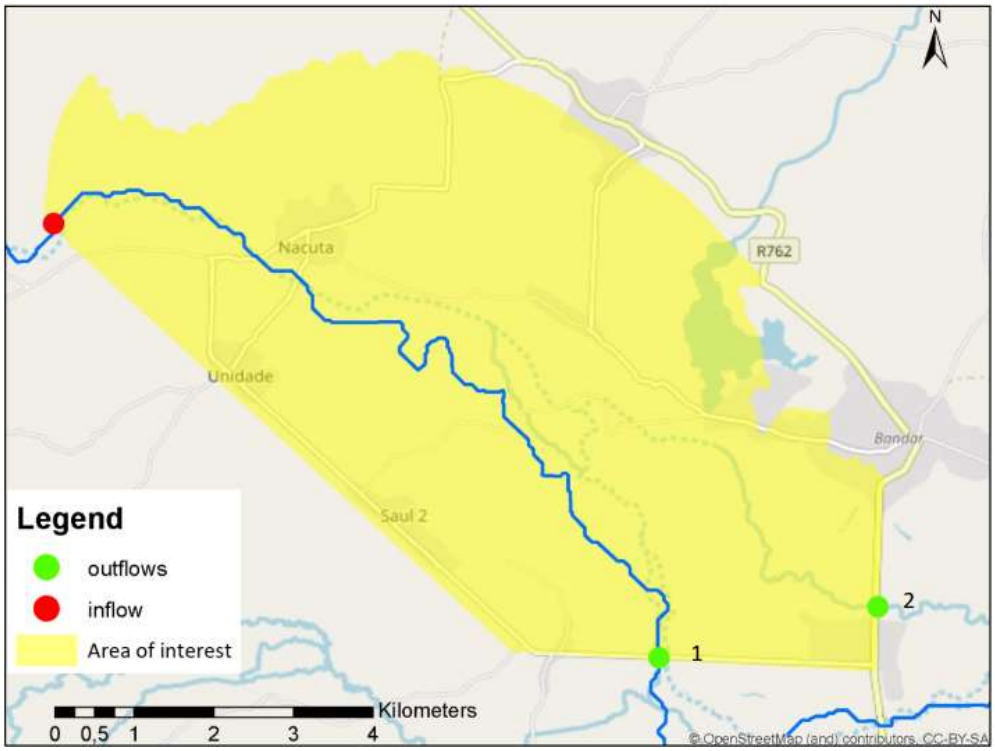

Figure 1-7: The hydraulic domain and position of the boundary conditions. Source: (Corti &Rrokaj, 2019)

The suggested mitigation measure for the region involves altering the riverbed's shape and constructing earthen levees using excavated soil. Furthermore, a water reservoir has been suggested as a solution to address water shortages during periods of low rainfall. By conducting a flood hazard study and proposing suitable mitigation measures, this study can help the community to understand the flood risk in the area better and take appropriate measures to reduce the impact of floods. The site mission is also to help future research by providing a better understanding of the local conditions and the impact of floods on the community. Additionally, the photographic documentation can be used to validate flood models and improve their accuracy. This study provides valuable insights into flood risk assessment and mitigation measures for the Rio Muaguide area in Cabo Delgado, Mozambique, which is going to be useful for future research and practical applications in the region.

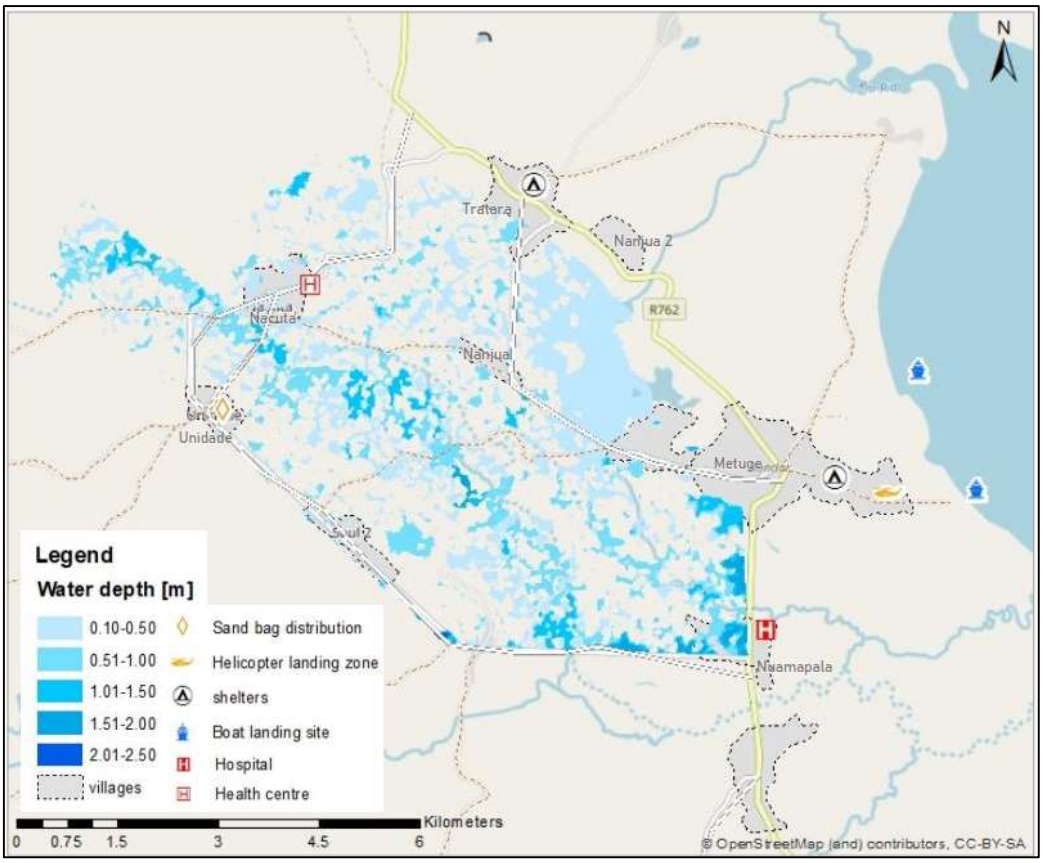

Figure 1-8: The hazard map for the 10-year return period. Source: (Corti &Rrokaj, 2019)

3) Flood Hazard and Risk Assessment in data-scarce regions: the case of the Metuge District in northern Mozambique (Paz Idarraga & Rotaru, 2023)

This study, which is another master's thesis conducted for the same region after the research of Corti & Rrokaj (2019), included a comprehensive risk assessment for the Metuge District in the Cabo Delgado province. The objective of this thesis was to develop a flood hazard and risk assessment methodology that can be easily assimilated by local technicians in data-scarce regions, specifically focusing on the Metuge district in northern Mozambique. The study aims to provide a holistic approach that includes quantitative hydrological-hydraulic modeling for the hazard component, a characterization of the population and infrastructure exposed, and the use of damage models for the physical vulnerability assessment. (Figure 1-9) In addition, the study includes a participatory approach with the CLGRC members for the validation of the results. The final objectives are to identify spatial hot spots and root causes of vulnerability, to empower the local communities, to encourage the development of effective flood risk reduction and adaptation strategies, to help the efficient allocation of resources, to raise awareness, and to strengthen the capacities of local actors.

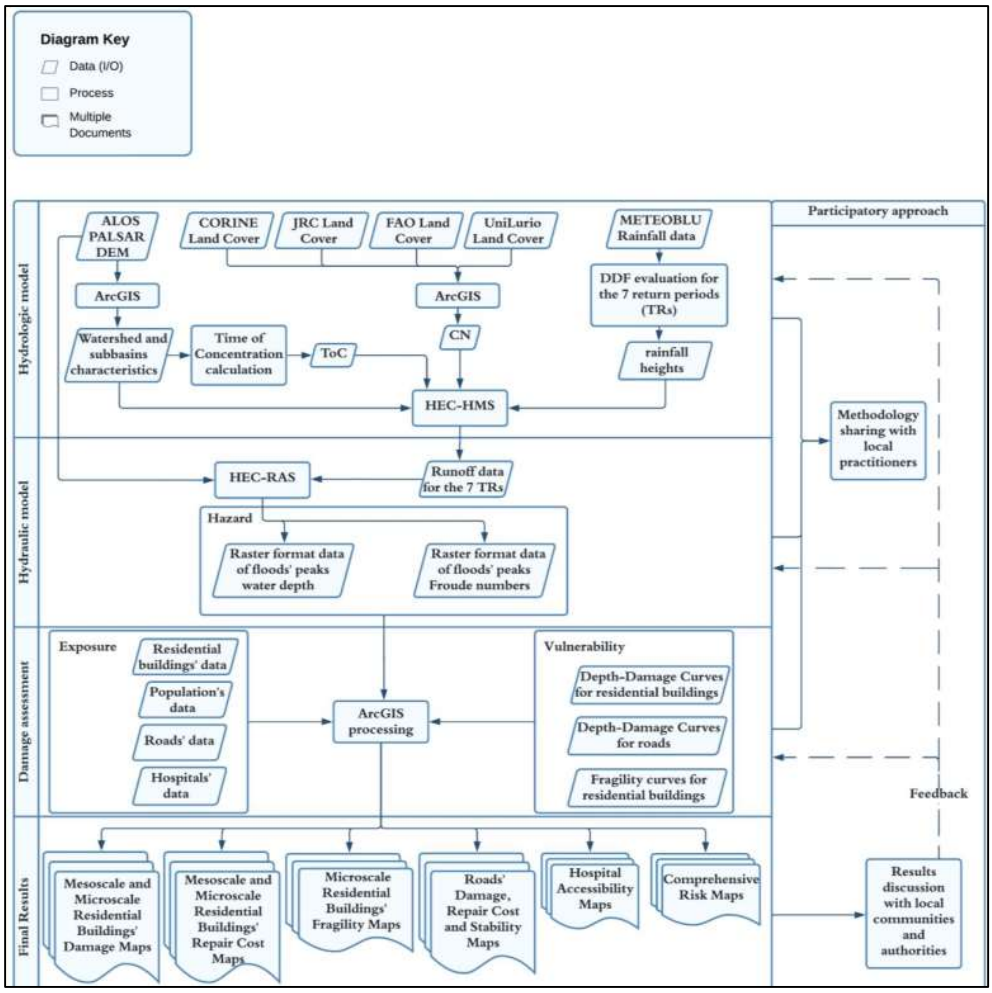

Figure 1-9: The implemented framework. Source: (Paz Idarraga & Rotaru, 2023)

In their study, the flood hazard was obtained from the hydrologic and hydraulic analysis of the Rio Muaguide River. Through the statistical analysis of the precipitation data, the depth-duration-frequency (DDF) curves for seven return periods were generated. The watershed analysis was performed considering the sixteen sub-basins, and their geomorphological characteristic data were used to compute the time of concentration according to various empirical formulas. The SCS curve number method was employed as an infiltration model. After collecting the required input data for the hydrological model, the rainfall-runoff modeling was performed in HEC-HMS, considering four relatively small sub-basins to generate synthetic hydrographs that were used input data in the hydraulic model.

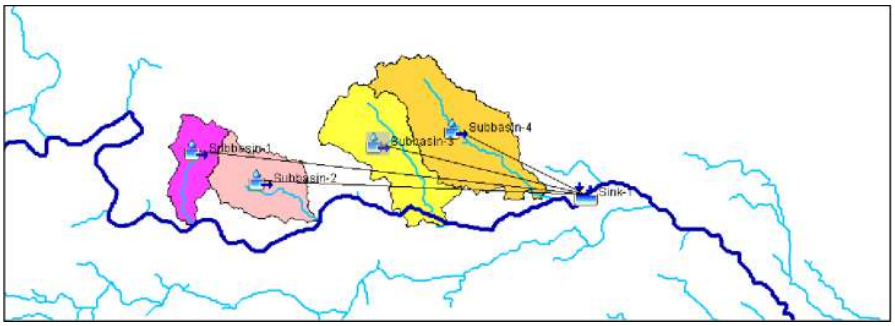

Figure 1-10: Basin model in HEC-HMS. Source: (Paz Idarraga & Rotaru, 2023)

As hydraulic modeling, the 2D unsteady flow simulations were performed by using HEC-RAS considering seven return periods. Considering the presence of culverts along the roads intersecting the village of Namuapala was identified in the previous field survey by Corti & Rrokaj (2019); in this study, these hydraulic structures were introduced in the hydraulic modeling. In particular, the introduction of these culverts was done by raising the terrain elevation of the two mentioned roads by 2 m in the DEM. The results of the hydraulic modeling were used to create hazard maps considering three target villages: Nacuta, Namuapala, and 25 de Junho. The obtained hazard maps of the Namuapala are presented below in Figure 1-12.

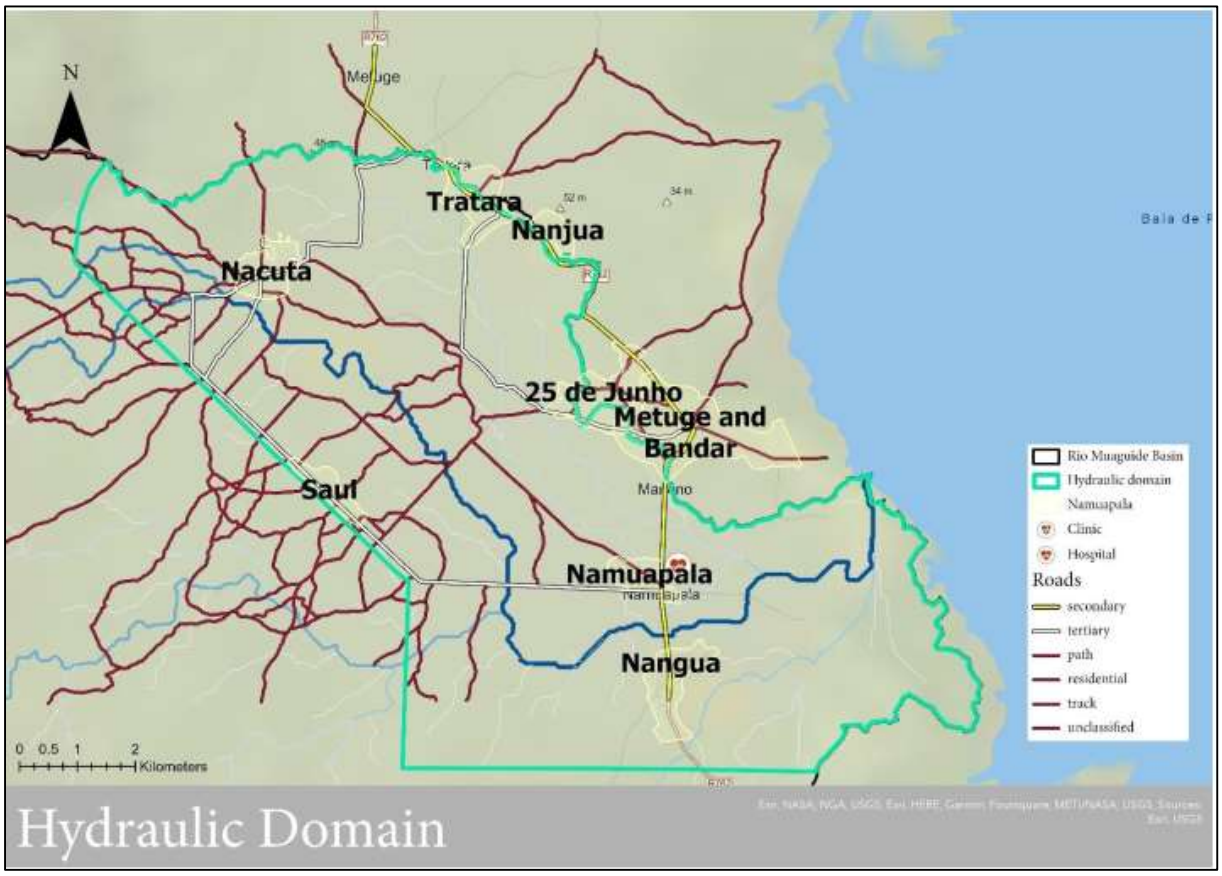

Figure 1-11: Hydraulic domain. Source: (Paz Idarraga & Rotaru, 2023)

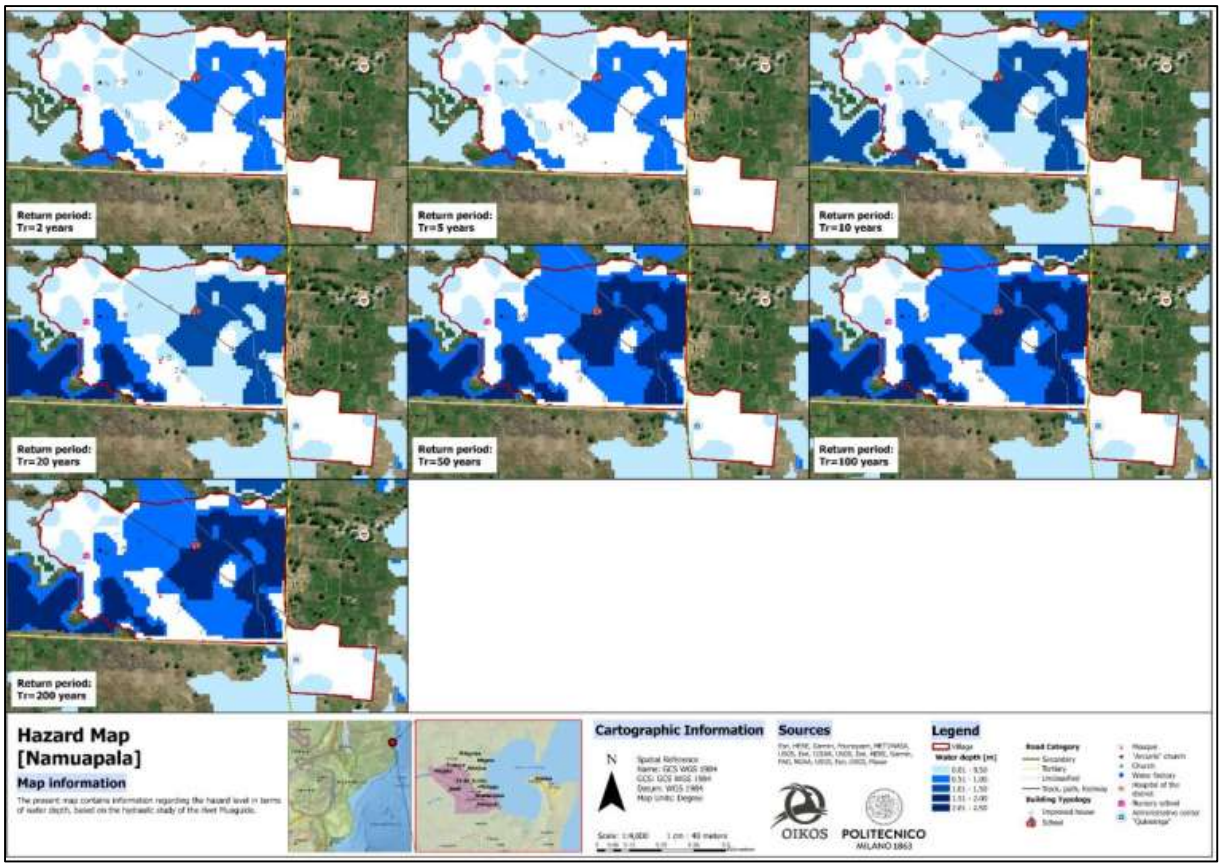

Figure 1-12: Hazard maps of Namuapala for seven return periods. Source: (Paz Idarraga & Rotaru, 2023)

The damage assessment of the residential buildings, roads, and population in the aforementioned three target villages was performed by utilizing the depth-damage curves. Additionally, a road accessibility assessment was performed, taking the physical and functional vulnerability of the road network as a basis. An analysis of the accessibility to the hospitals from different villages in the district is also presented in this study.

In general, the models employed in this study were purposely designed to be simple and easily replicated, given the limitations imposed by data scarcity. A collection of maps displaying the hazard, relative and absolute damage (micro and meso scale), road stability and accessibility, and flood risk was prepared in both English and Portuguese, and seven different return periods were used to assess flood hazard and risk. Furthermore, the Annual Average Damage (AAD) was estimated for the various exposed assets at the district level, providing a comparative analysis of the three target villages under study. As mentioned before, according to the results of the analysis, Namuapala was determined to be the village most impacted by flooding. Finally, the study also includes a participatory approach to share the results with CLGRC members of Namuapala. Through round tables and workshops, the local stakeholders were provided with a better understanding of the modeling process and requirements.

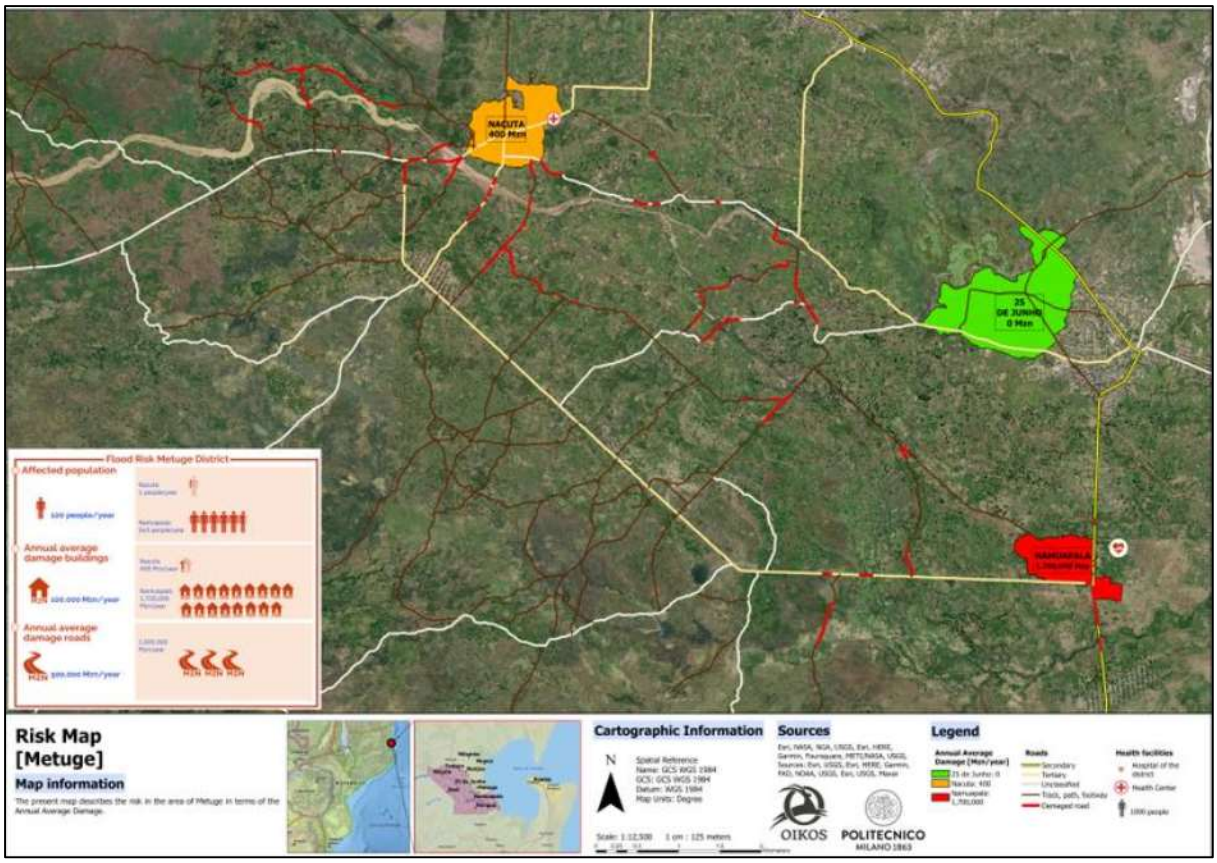

Figure 1-13: Risk Map of target villages. Source: (Paz Idarraga & Rotaru, 2023)

It is important to mention that this study represents a significant improvement over the previous study, which focused solely on the 10-year return period. Also, the hydraulic domain was extended to include strategic facilities and roads in the present study, which represents an improvement over the previous study. The domain properly describes the most affected areas in the district by covering the target villages and important facilities. The results obtained in this study represent a substantial upgrade of the risk knowledge that was previously available for the same area. The study also enabled the understanding of the current flood risk awareness and preparedness status and provided an overview of possible measures suitable for the region, addressing the current weaknesses and needs of the community.

1.2 Problem Statement

It was noticed that there were some uncertainties arising from previous studies regarding the flood hazard and damage estimations regarding the Namuapala village in Cabo Delgado province. For instance, in the thesis of Corti &Rrokaj (2019), a 2D hydraulic modeling approach was employed to assess the impact of flooding, revealing that the villages of Nacuta and Namuapala were the most severely affected. However, it is notable that their computational domain did not fully encompass the entirely of Namuapala village, nor did it include the Metuge district hospital, which is situated within the confines of Namuapala. Additionally, in their study, only a 10-year return period was considered for the hydraulic modeling approaches; thus, this left gaps in understanding the risk for other return periods. Importantly, the study did not provide any information regarding damage estimation resulting from flooding impact within the region. These gaps were addressed in the thesis of Paz Idarraga & Rotaru (2023) by introducing a more comprehensive modeling chain, including the production of hazard maps corresponding to seven different return periods. Also, the hydraulic domain was extended by incorporating the villages of Namuapala, Nacuta, and 25 de Junho and the

hospital in the Metuge District. Additionally, they implemented the physical vulnerability and damage assessment considering the residential buildings, roads, and population while incorporating a participatory methodology to ensure the robustness and reliability of the findings obtained from the site.

However, during the participatory meeting, members of the CLGRC pointed out that the safe zones in Namuapala village, as indicated by the modeling results, were found to be overestimated when compared to actual conditions experienced during previous flood events. The obtained water depth values and flooding extent in the village derived from the hydraulic modeling outcomes did not accurately reflect the conditions of the actual event. Therefore, this discrepancy between the modeling results and the comments of CLGRC members was attributed to the fact that the water volume obtained from the rainfall-runoff modeling was insufficient to show the flood impact in the village according to the hydraulic model results. The main reason for this insufficiency was considered to be the flow discharges obtained from the selection of four small sub-basins in the hydrological modeling. Furthermore, according to the later conducted ad hoc surveys of local technicians, it became understood that the elevation of the roads in the Namuapala village did not differ from the surrounding area. On the other hand, in hydraulic modeling, it has been noticed that raising the elevation of the relevant roads in the terrain geometry may lead to some inconsistencies regarding hazard and damage assessment results.

The previously mentioned inconsistencies in modeling results regarding the Namuapala village highlight the need for a flood hazard modeling approach taking these aspects into account. In summation, prior investigations in the Metuge District have unequivocally identified Namuapala as the most severely impacted village in the region. However, it is important to acknowledge that the initial thesis fell short of encompassing the village entirely, and the subsequent thesis inadequately captured real-world conditions, including critical factors such as variations in water depth and the extent of inundation within the village.

Such improvements are not only essential to our scientific understanding but are instrumental in equipping the community with more effective tools for flood risk management.

1.3 Research Objectives

As previously explained, the results of the participatory approach have illuminated specific aspects that require improvement within the existing framework of flood hazard and damage modeling. Recognizing these aspects, the primary goal of this research is to refine hazard and damage modeling by incorporating diverse assumptions related to hydrological factors and local terrain geometry in hydraulic modeling. Considering that the information gathered from participatory meetings was conveyed orally by local residents, uncertainties and concerns regarding the reliability of this information make the unavailability of performing validation of models. Due to the absence of a robust validation process, the second objective of this study is to conduct a sensitivity analysis focusing on the hazard parameter, which is the water depth level. This analysis aims to discern the impact of various assumptions used in modeling on hazard assessment results.

Lastly, to comprehensively grasp how uncertainties in the modeling process may influence also damage estimations, the last objective is to scrutinize the sensitivity of annual average damage concerning modeling assumptions for elements such as residential buildings, population, and roads.

Chapter 2: Methodology

The methodology used in this study basically consists of a comprehensive hydrological, hydraulic, and damage modeling chain considering various return period scenarios. The modeling has been performed several times within a sensitivity analysis to different choices for input data and assumptions. The comparison between the results was carried out at the three rings of the chain, namely the hydrological, hydraulic, and damage assessments.

2.1 Input Data

The lack of available information on the area of interest made the use of global databases necessary for hydrologic and hydraulic modeling. Generally, the data used in the present thesis are the same ones retrieved in prior studies of Corti & Rrokaj (2019) and Paz Idarraga & Rotaru (2023).

Input rainfall data with one-hour temporal resolution for the period of 1985 to 2018 were bought from Meteoblue, a meteorological service created at the University of Basel, Switzerland, in 2002. Meteoblue produces, manages, and provides high-precision weather and environmental data for the entire world, using observation data, high-resolution Numerical Weather Forecasts (NWP), and specialized data output methods tailored to the needs of different user groups.

For the topographic data, the ALOS PALSAR Digital Elevation Model (DEM), with a spatial resolution of 12.5 meters, was used to analyze the watershed characteristics and to provide a geometry to be used in the hydraulic simulations. It is a product derived from the data collected by the Japanese satellite ALOS (Advanced Land Observing Satellite) equipped with the PALSAR (Phased Array type L-band Synthetic Aperture Radar) sensor. (© JAXA/METI, 2019)

To gather land cover information, data was utilized from a variety of reputable sources. These sources include the 2021 CORINE Land Cover dataset produced by the Copernicus Land Monitoring Service and European Environment Agency (EEA), the JRC Land Cover Map of Africa created by the European Commission and JRC, the FAO's 2021 land cover classification map, and the Land Cover Map provided by the Lurio University.

The information on residential buildings and population was gathered from satellite imagery and local authorities. A field survey was conducted to determine the vulnerability parameters of existing buildings, which were grouped into “traditional” and “improved.” The former relates to buildings built with wood/bamboo and mud structures, while the latter is for brick buildings.Lastly, data on the roads was obtained from both field surveys and OpenStreetMap (OpenStreetMap contributors, 2022)

2.2 Hydrological Modelling

Hydrological modeling was used to obtain synthetic hydrographs for selected return periods for the Rio Muaguide River. Synthetic hydrographs are in fact needed to provide the boundary conditions for hydraulic models in the subsequent step. This process requires information on topography, land use, rainfall data, and characteristics of a selected sub-basin to transform rainfall into runoff. The Hydrological Modeling System (HEC-HMS) was used to simulate the rainfall-runoff processes of the drainage basin, as described below. To carry out this assessment, rainfall, topographic, soil, and land use data as well as the basin selection and characteristics of the selected basin, are required.

2.2.1 Depth-Duration-Frequency curves

Depth-Duration-Frequency (DDF) curves, which are a graphical representation of the relationship between the depth, duration, and frequency of precipitation for a specific location or region, have been built by Corti & Rokaj (2019) using the rainfall data from Meteoblue (for the period from 1985 to 2018). Annual maxima extracted from the time series were analyzed assuming The Gumbel

distribution (Extreme Value Type I), determining the distribution parameters using the methods of moments. As an example, Figure 2-1 shows the DDF curves for return periods between 2 and 100 years and durations from 1 to 24 h.

	T=2 yrs	T=10 yrs	T=50 yrs	T=100 yrs
Durations(t)	Rainfall Depth [mm]			
1 h	5.69	10.44	14.61	16.37
3 h	15.16	29.13	41.37	46.55
6 h	25.77	51.51	74.08	83.62
12 h	37.1	79.85	117.33	133.17
24 h	49.03	117.58	177.68	203.09

Figure 2-1: Calculated rainfall depths for the five different durations and four different return periods. Source: (Paz Idarraga & Rotaru, 2023)

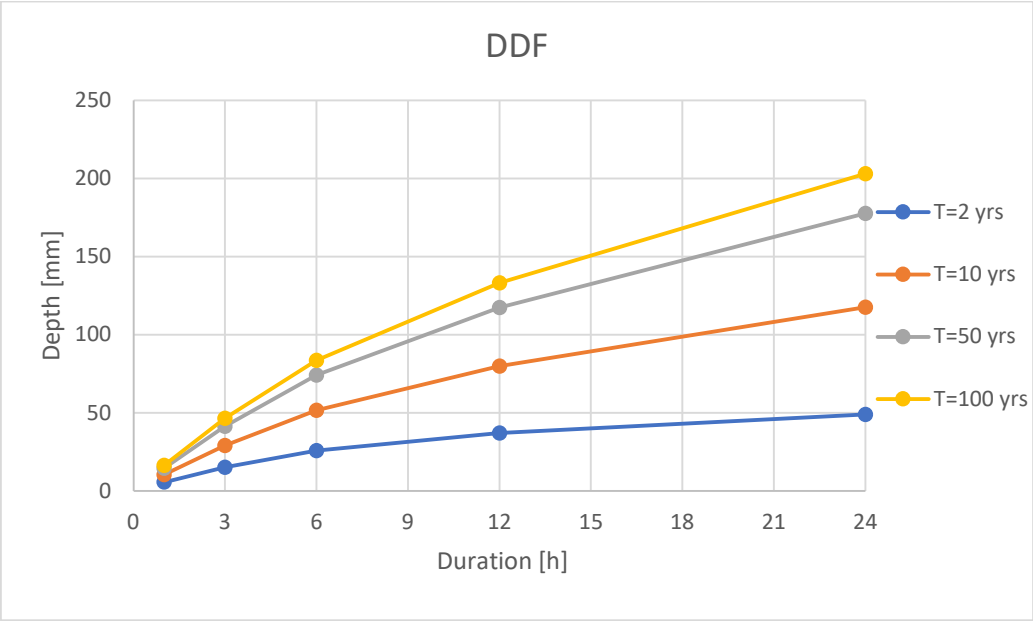

Figure 2-2: Depth-duration frequency curves. Source: (Paz Idarraga & Rotaru, 2023).

2.2.2 Watershed Analysis

The ALOS PALSAR DEM was processed to transform the drainage paths and watershed boundaries into a hydrologic data structure that could represent the watershed response to rainfall.

In terrain pre-processing in, the DEM raster file was clipped based on the Rio Muaguide River basin. Furthermore, the sinks in the DEM were filled as, sometimes, big raster datasets could have errors in the representation; therefore, removing the numerical errors such as sinks is necessary to obtain a digital elevation model without depression to continue the upcoming analysis.

A Flow Direction tool was used to determine how water would move over the terrain, which is essential for accurate runoff and streamflow simulations and to establish the flow paths and connectivity within a watershed. This tool creates a raster of flow direction from each cell to its downslope neighbor, or neighbors, using an adjacency criterion based on eight neighboring cells.

Basically, it identifies the direction that a hypothetical drop would take to flow downstream. After this step, the Flow Accumulation tool was used by the Flow Direction as an input raster data. This tool allows to identify basins and measures how much water flows to different locations. By accumulating runoff in each cell, one can identify areas that contribute to specific points within the basin, thus enabling the boundaries and characteristics of sub-basins to be determined.

Defining the spatial extent of the Rio Muaguide River basin and identifying its boundaries, watershed delineation, and choosing a sub-basin is fundamental for any further calculations and hydrological analysis. For the delineation of watersheds, one needs the Flow Direction input raster and input raster of pour point data. A pour point is a specific location within a watershed where flow from contributing areas converges and exits as runoff into a stream. This point was chosen as the location of the flow corresponding to the upper left part of the domain that would be later used for the hydraulic modeling, and, as a result, a sub-basin was obtained (Figure 2-3). Then, its geomorphological characteristics (area and average slope) and its mainstream characteristics (length, average mainstream slope, and maximum and minimum elevation) were determined for further calculations.

2.2.3 Determination of the Time of Concentration

The calculation of time of concentration is a critical component of this process and has a direct impact on the generation of synthetic hydrographs. As known, the time of concentration measures the response of a basin to a rain event. It is defined as the time needed for water to flow from the most remote point in the catchment-to-catchment outlet. There are several empirical formulas to determine the time of concentrations in hours as a function of some parameters. These equations have been derived through experimental and analytical approaches, and they originate from various field studies adapted based on local hydrological features and physical conditions. Nonetheless, these equations prove beneficial in determining the time of concentration within specific basins (Almeida et al., 2014). After reviewing the literature on formulas suitable for the characteristics of the basin, four formulas deemed appropriate were chosen. The equations selected are the following:

- Chow- calibrated for rural basins in the USA (0.01-18.5 km^2) and slight slopes (0.005<S<0.09):

$$T_c = 0.1602 L^{0.64} S^{-0.19} \quad (1)$$

- Corps of Engineers- calibrated for rural basins in the USA:

$$T_c = 0.19 L^{0.76} S^{-0.19} \quad (2)$$

- Dooge - calibrated for rural basins in Ireland (145-948 km^2):

$$T_c = 0.365 A^{0.41} S^{-0.17} \quad (3)$$

- Johnstone – calibrated for rural basins in the USA (64.8-4206.1 km^2):

$$T_c = 0.4623 L^{0.5} S^{-0.25} \quad (4)$$

Where L is the flow path length, A is the area of the watershed, and S is the flow path of the slope. The values calculated for each formula and the final time of concentration value obtained by averaging these values in terms of hours.

2.2.4 SCS Curve Number Calculation:

Infiltration losses were determined using the SCS-CN method developed by the Soil Conservation Service (SCS) to estimate total runoff from agricultural watersheds. The method assumes that part of a rainfall will contribute to surface storage interception while another part will be initial abstraction, and direct runoff will be generated only after initial abstraction or surface storage are completed. The SCS equation for calculating excess rainfall is the following:

$$P_{e=}\frac{(P-I_a)^2}{P-I_a+S}=\frac{(P-0.2S)^2}{P+0.8S} \quad (5)$$

where P is cumulative rainfall, $I_a$is initial abstraction, S is maximum soil retention and P_e is excess rainfall. About this expression, if the cumulative total rainfall is less than the initial abstraction then there is no direct runoff and this formula is not applicable.

In this equation, S is an unknown parameter depending on the soil properties. The ability of a soil to store water is quantified by a parameter called the curve number (CN); the higher the curve number the direct runoff will be obtained for a certain rainfall, and vice versa. The relationship between the curve number and the maximum soil retention is expressed by this formula:

$$S=\frac{25400}{CN}-254\ [mm] \quad (6)$$

The curve number can be chosen from a table where it is a function of the hydrologic soil group as four groups (A, B, C, D) according to the underlying lithology, and the land cover. Furthermore, the curve number and maximum soil retention depend on antecedent moisture conditions. So if the land use, hydrologic soil group, and antecedent moisture condition are known or assumed for the watershed, the curve number can be obtained.

Cover description		Curve numbers for hydrologic soil group			
Cover type	Hydrologic condition	A	B	C	D
Pasture, grassland, or range—continuous forage for grazing. 2/	Poor	68	79	86	89
	Fair	49	69	79	84
	Good	39	61	74	80
Meadow—continuous grass, protected from grazing and generally mowed for hay.	—	30	58	71	78
Brush—brush-weed-grass mixture with brush the major element. 3/	Poor	48	67	77	83
	Fair	35	56	70	77
	Good	30 4/	48	65	73
Woods—grass combination (orchard or tree farm). 5/	Poor	57	73	82	86
	Fair	43	65	76	82
	Good	32	58	72	79
Woods. 6/	Poor	45	66	77	83
	Fair	36	60	73	79
	Good	30 4/	55	70	77
Farmsteads—buildings, lanes, driveways, and surrounding lots.	—	59	74	82	86

Figure 2-3 :CN values. Source :(United States Department of Agriculture (USDA), 1986)

Regarding the sub-basin selected in this study, a significant limitation was represented by the scarcity of readily available data on lithology and soil type for this region. Consequently, it was necessary to rely on assumptions based on broader regional or global knowledge. The assumptions made in the prior studies were that the soil type belongs to the hydrologic soil group C which has a slow infiltration rate when it is thoroughly wet; furthermore, the antecedent moisture condition AMC II was chosen, corresponding to an intermediate average soil moisture. For the land cover data, the four different sources (CORINE, JRC, FAO, and UniLurio Land Cover Maps) were used to evaluate the Curve Number. The data coming from the different sources were separately analyzed with the help of the tables from the TR-55 report (United States Department of Agriculture (USDA), 1986). After obtaining the spatially average curve number for the sub-basin for four different, as a weighted average (based on the area with any certain coverage).

2.2.5 Rainfall-Runoff Model

Rainfall-runoff transformation was performed using HEC-HMS developed by the US Army Corps of Engineers. HEC-HMS utilizes various model components to simulate the hydrologic response within a watershed. These components include basin models, meteorological models, control specifications, and input data. The simulation utilizes input from the meteorological model to calculate the precipitation-runoff response in the basin model. The control specifications define the time period and time step of the simulation run. Input data components, such as time-series data, are necessary as parameters or boundary conditions in the basin and meteorological models.

Only one sub-basin was considered in the calculations. The basin model required the input data, such as the watershed area, the value of the curve number, and the lag time (60% of the time of concentration) obtained in the previous steps. Then, the SCS curve number was chosen as the loss method, and the SCS Unit Hydrograph was chosen as the transform method. For the second step, the meteorological model was created using the Specified Hyetograph as a precipitation method. The Time-Series Data component was used for the purpose. To simulate rainfall events of 12 hours for all four return periods, precipitation data was introduced into the model extracting the computed precipitation depths for a 12-hour duration from the DDF curves. From the control specifications, the time span of a simulation run was set as two days and the time interval was decided as 30 minutes. After running the simulations, the final synthetic hydrographs were obtained to be used in the hydraulic modeling.

2.3 Hydraulic Model

To obtain flood hazard maps of the Metuge District, hydraulic simulations for different return periods were conducted by using HEC-RAS. The Hydrological Engineering Center's (HEC) River Analysis System (HEC-RAS) software, also developed by the US Army, provides the user with two-dimensional (2D), unsteady flow river calculations. Required input data are flood hydrograph, topographic data, terrain roughness, and data regarding the hydraulic structures.The output of the modeling is a set of flood hazard maps displaying the extent of the flooded area with hazard components such as water depth or velocity.

2.3.1 Hydraulic Domain

The choice of a hydraulic domain specifies the area where flow computations are performed in hydraulic modeling. The hydraulic domain was obviously chosen to include the area of the Metuge District, which is prone to flood during the rainy seasons, and it includes the focused village of Namuapala within the borders. The upstream boundary of the modeling area was placed upstream of the locations where the Muaguide starts to divide into different branches (Figure 2-4), in order to simplify the treatment of an upstream boundary condition.

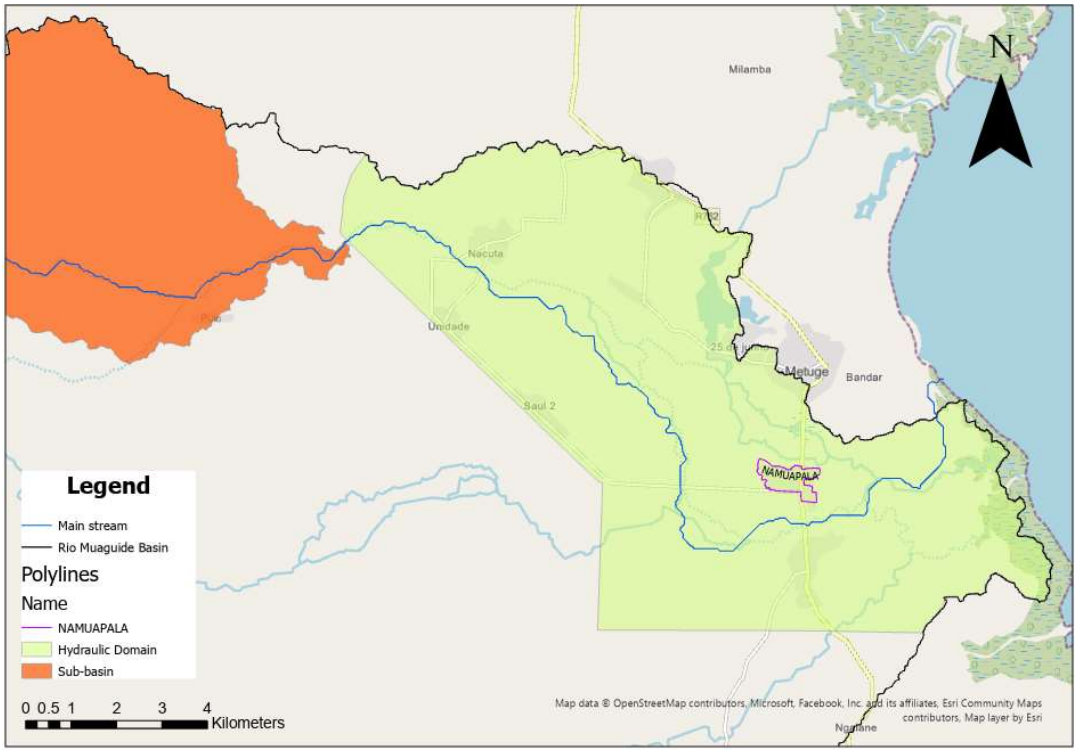

Figure 2-3: Hydraulic Domain.

2.3.2 Computational Mesh and Surface Roughness

The terrain model corresponded to the topographic data of the ALOS PALSAR Digital Elevation Model (DEM) with a 12.5-meter resolution mentioned above. A computational mesh was created starting with a cell size of 50 m and applying mesh refinement (cell size of 15 m) in an area of larger interest, encompassing the village of Namuapala and the upper section of the domain (Figure 2-4). The final mesh included a total of 146,055 cells. As 2D surface roughness data, a Manning's roughness coefficient value of 0.04 $s/\sqrt[3]{m}$ was considered for the entire domain.

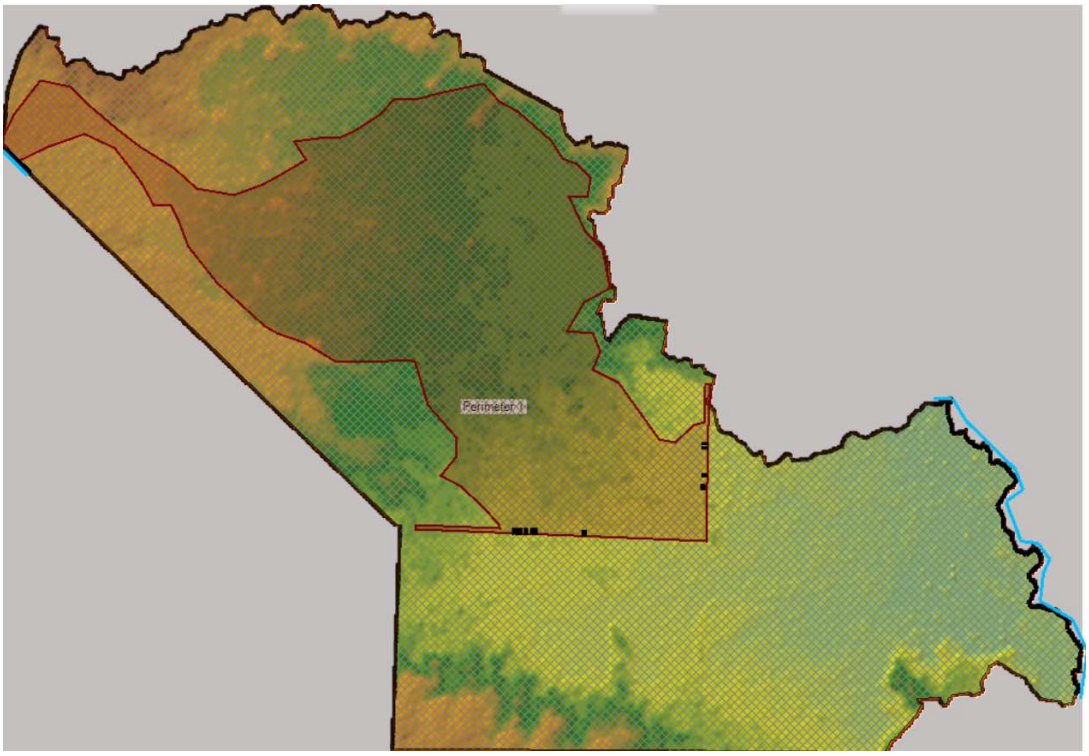

Figure 14 :Mesh and refinement region.

2.3.3 Incorporation of Hydraulic Structures

According to the findings of the field survey conducted earlier by Corti & Rrokaj in 2019, the culverts on the road R762 and its intersecting road in Namuapala were accurately introduced (Figure 2-5). Additionally, the DEM was updated to reflect the elevation of both roads by increasing the terrain elevation by 2 m. Hydraulic structures like culverts were added to the geometry of the terrain.

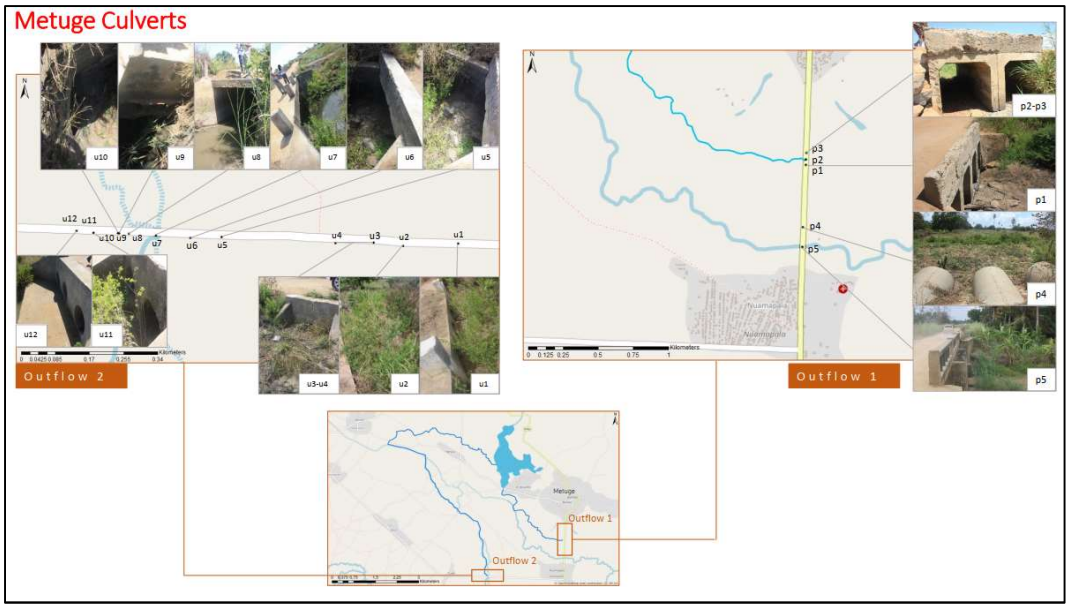

Figure 15: Culverts in the Metuge District

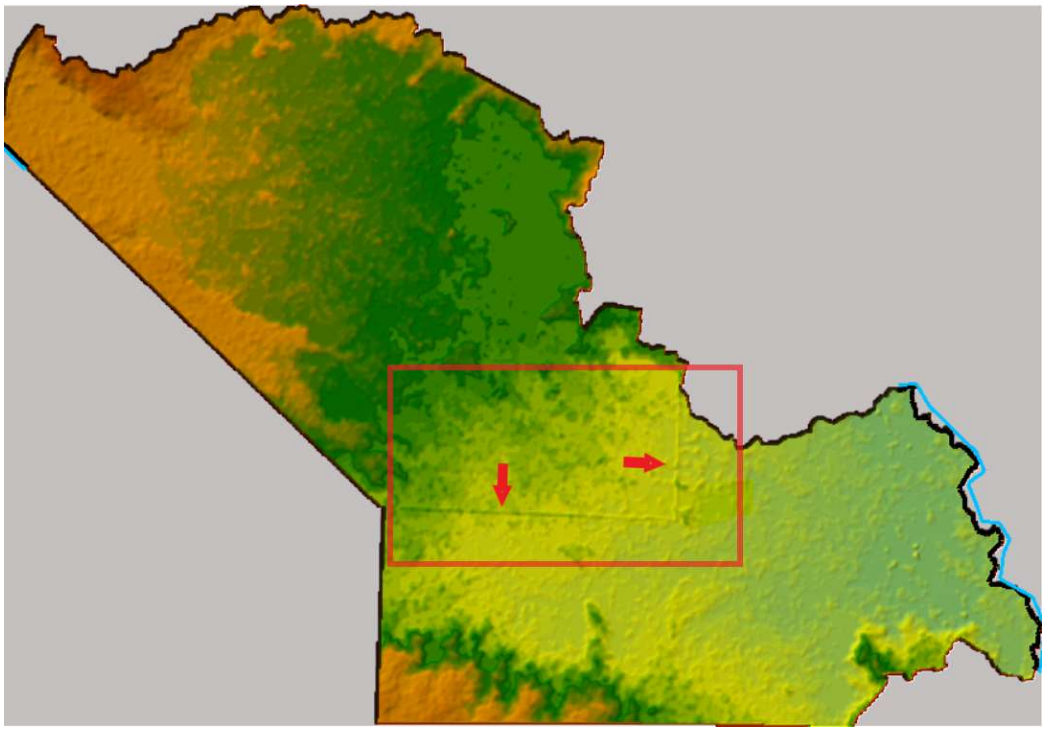

Figure 16: Elevated roads in DEM.

2.3.4 Boundary Conditions

The boundary condition lines were drawn for the upstream location where the Muaguide River meets the domain, while the downstream location was determined as the location of the coastline. For the upstream boundary condition, the synthetic hydrographs obtained from the hydrologic model were used as time series data input, while regarding the downstream boundary condition a normal depth was selected. It is noted here that a boundary condition corresponding to the sea level would have been conceptually more appropriate, but it could not be used because it determined the crash of the

numerical simulations. However, the downstream boundary condition was placed sufficiently far from the villages of the district to avoid its influence on the hazard modeling results.

2.3.5 Simulations and Result Extraction

The duration of the simulation period was set to 6 days. The typical results of a simulation were a set of maps with water depth, water surface elevations, flow velocities, and flood extent as in raster format (Figure 2-7 shows an example). These results were critical for the creation of flood hazard maps, particularly for extracting maximum water depth raster layers for each return period, which served as the foundation for further analyses and assessments.

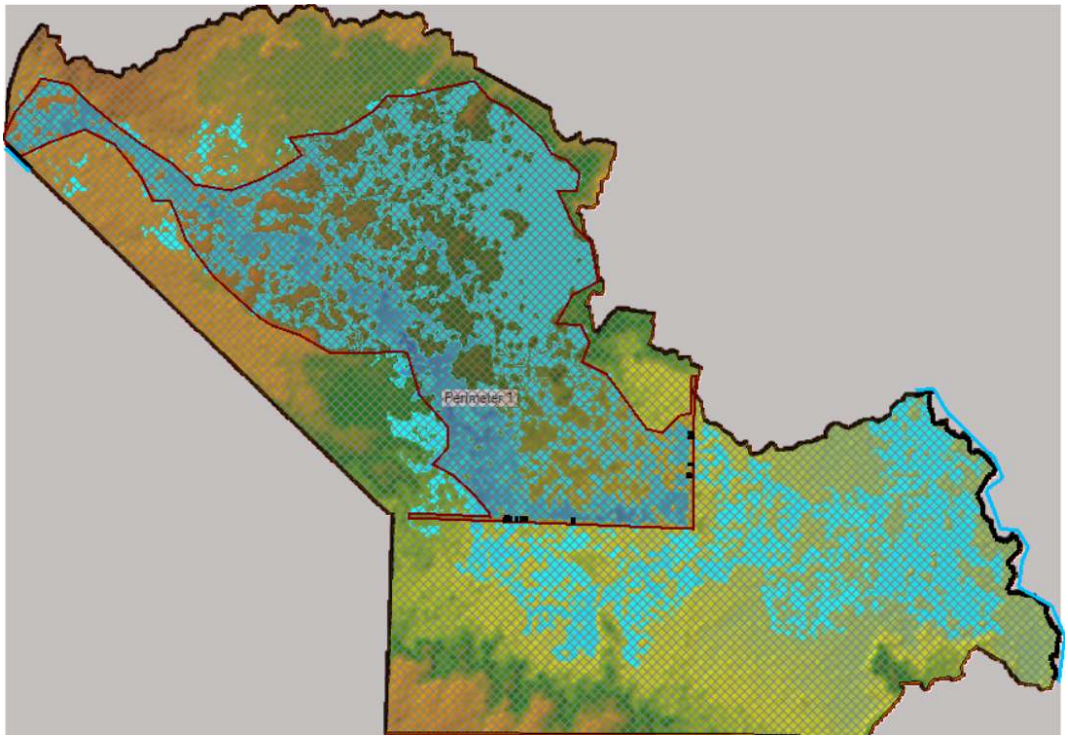

Figure 17: The output of hydraulic simulation.

2.4 Damage Modeling

The damage assessment was generally carried out by using depth-damage curves for exposed elements. These curves provide a quantitative relationship between flood hazard components such as water depth and estimated economic damage to structures or assets. The expected damage induced by hazard factors is typically represented by a damage ratio value ranging from 0 to 1 for exposed elements like buildings and roads. Then, absolute damage is obtained by multiplying the relative one by the repair cost.

2.4.1 Depth-Damage Curves for Residential Buildings

The residential buildings present in the Metuge district can be roughly classified into two categories as traditional and improved (or semi-permanent), as shown in Figure 2-8. The buildings are geolocated, and the traditional houses were reproduced by satellite image (Istituto Oikos, 2023). According to the field survey performed in prior studies, and considering, for example, the target village of Namuapala that will also be mostly accounted for in this thesis, out of 361 residential

buildings present in the village, 329 are classified as traditional houses while the remaining 32 are classified as semi-permanent houses.

Figure 2-8: Traditional House (on the left) & Semi-Permanent House (on the right).

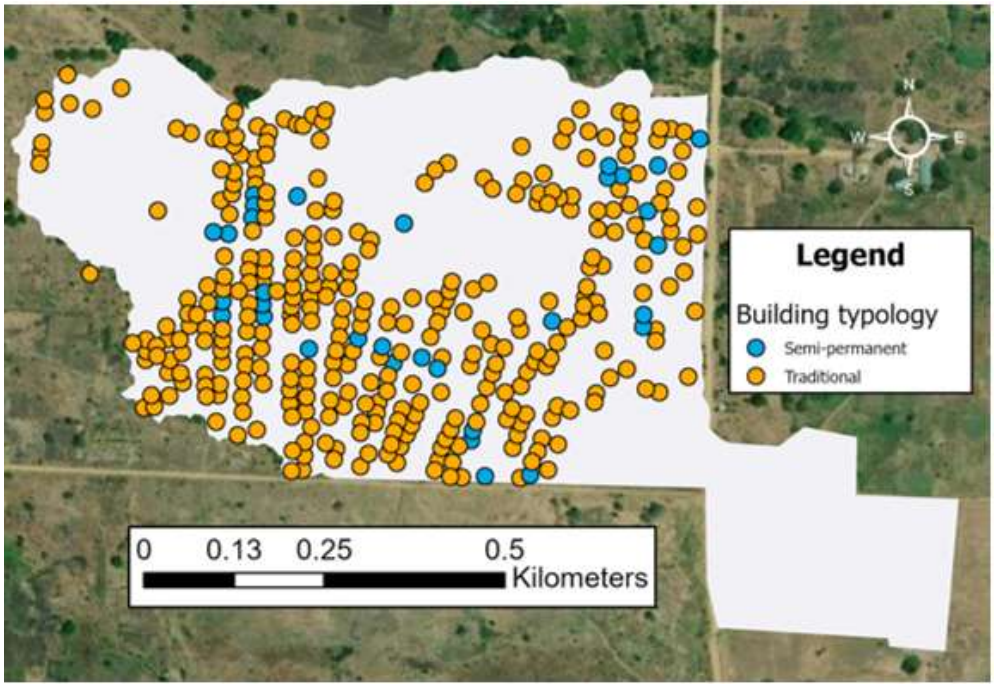

Figure 2-9: Building exposure map of Namuapala. Source: (Istituto Oikos, 2023)

Three different depth-damage curves were used by Paz Idarraga & Rotaru (2023) as they were considered suitable for the building typologies present in the district to estimate relative damage.

The first curve is from Englhardt et al., (2019), who introduced four vulnerability classes and associated curves depending on the construction types and building materials of residential buildings in Ethiopia. According to the study, two types of building classes were found suitable, Building Class I consisted of non-engineered buildings built with materials such as compacted mud and traditional materials found in the natural environment; they can disintegrate and collapse easily when impacted by flood waters. Building Class III consisted of unreinforced masonry/concrete buildings with walls of burnt bricks or stone or concrete blocks. In this thesis, the developed curve for Class I was used for the traditional buildings while the curve developed for Class III was used for the semi-permanent houses in the village of Namuapala. According to the formulation of both curves, the damage ratio

was considered zero in cases where the water elevation was less than 0.15 m. In the formula applied to traditional buildings, the damage ratio is equal to 1 for water elevation of 1.2 m and more, while in the formula applied to semi-permanent buildings, the damage ratio is determined as 1 if the water elevation is more than 2.5 m.

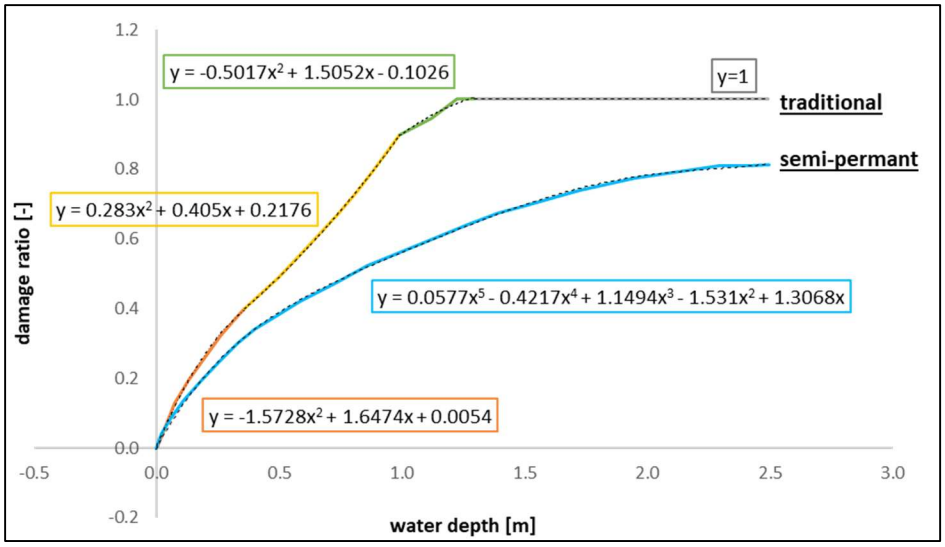

Figure 2-10: Damage models for Traditional and Semi-permanent Houses. Source:(Englhardt et al., 2019)

The second source used in this study focused just on traditional buildings. Thapa et al. (2020); developed a depth-damage curve for wattle and daub types of houses in Nepal, which were found to have similar characteristics to the traditional building typology observed in the village of Namuapala. The damage ratio for traditional buildings was considered zero, where the water elevation was below 0.15 m, as in the previous case. On the other hand, when the water elevation exceeded 1.8 m, the damage ratio was set to 1.

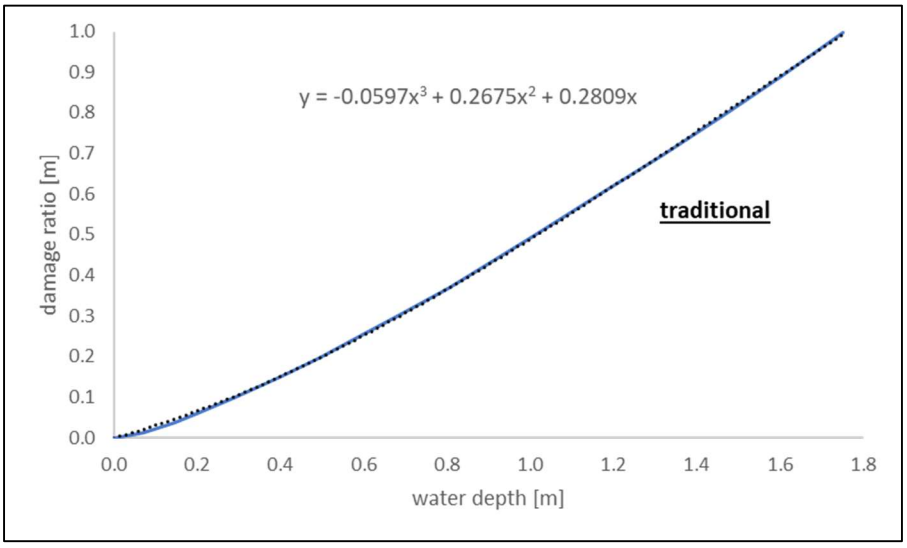

Figure 2-11: Damage model for Traditional Houses. Source: (Thapa et al., 2020)

The third source utilized in this study was Wouters et al., (2021). They created a flood damage model based on the automated recognition of buildings and their characteristics through UAV image

processing for various building types, including permanent, semi-permanent, and traditional structures in southern Malawi. Specific vulnerability functions were extracted to determine the damage estimation of these buildings. Traditional and semi-permanent functions were applied to the same type of buildings found in Namuapala village. Also, in this model, the damage ratio was set to zero when the water elevation to buildings was below 0.15 m. For traditional buildings, a damage ratio of 1 occurs when the water elevation exceeds 1.8 m, while for semi-permanent buildings it happens at a water elevation above 2.5 m.

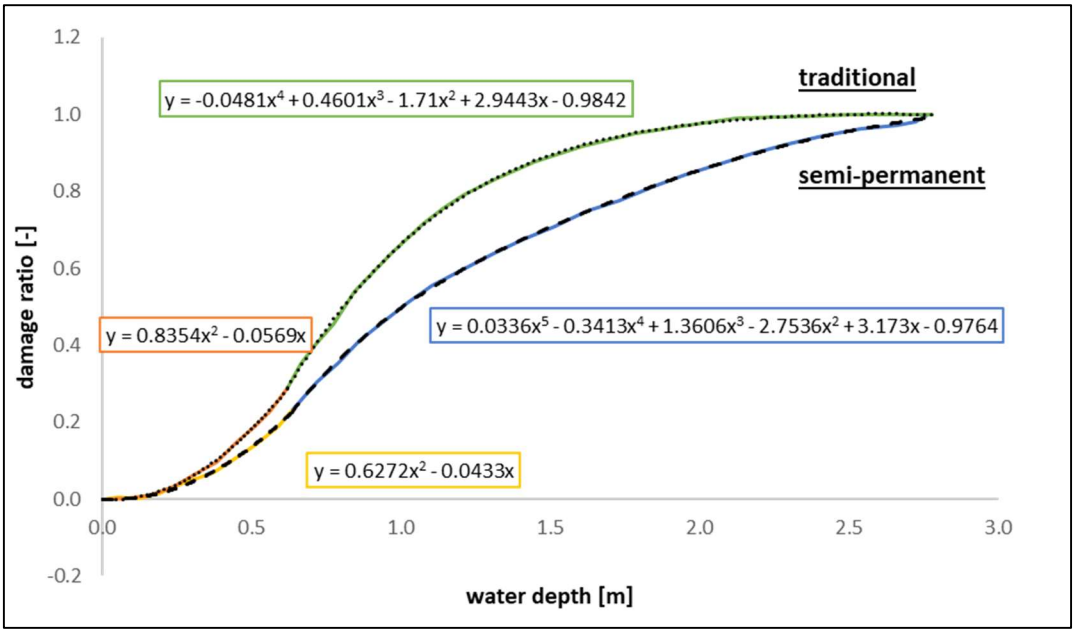

Figure 2-12: Damage Models for Traditional and Semi-Permanent Houses. Source:(Wouters et al., 2021)

Once the depth-damage curves were selected, the shape file of the residential buildings in Namuapala village and the raster files of water depth values obtained from hydraulic modeling for each return period were combined to generate the water elevation to which each building was exposed. Then, the damage ratio for each building was calculated using three depth-damage functions based on the building typology. The final damage ratio value was determined by taking the average of these ratios, which were calculated for each return period. In this way, the relative damage to each building was obtained in terms of damage ratio for 2,10,50, and 100-year return periods. Ultimately these relative damage values were used to calculate the absolute damage by multiplying the relative damage values by the construction costs of the buildings. According to the retrieved information, traditional houses in Metuge District have a construction cost of 30,000 MZN (Mozambique Metical), while semi-permanent houses cost 50,000 MZN. The quantitative direct damage estimation for residential buildings was finally completed by summing up the calculation of the total repair cost of the residential buildings for all four return period scenarios.

Furthermore, to assess the relative damages qualitatively, the damage ratio values from 0 to 1 were divided equally into four classes for which damage grading was named as Low, Medium, High, and Very High, depending on their corresponding damage ratio value.

	Damage Ratio	Damage Grading
Threshold 1	0.00 - 0.25	Low
Threshold 2	0.25 - 0.50	Medium
Threshold 3	0.50 - 0.75	High
Threshold 4	0.75 - 1.00	Very High

Table 2-1: Damage Level Grading

2.4.2 Calculation of Affected Population

The estimate of affected population was determined by considering the number of residential buildings flooded and the average number of residents per household, for each damage level and return period. According to the information obtained from the field survey, a total of 2368 inhabitants were present in Namuapala while the number of houses was 361 so it was assumed that 6 people could be present in each household.

2.4.3 Depth-Damage Curves for Roads

The model used to evaluate the relative damage to roads in the Metuge District was that of Ghimire et al. (2021). The function is derived from the analysis of damage observed in past flood events on unpaved roads in western Georgia:

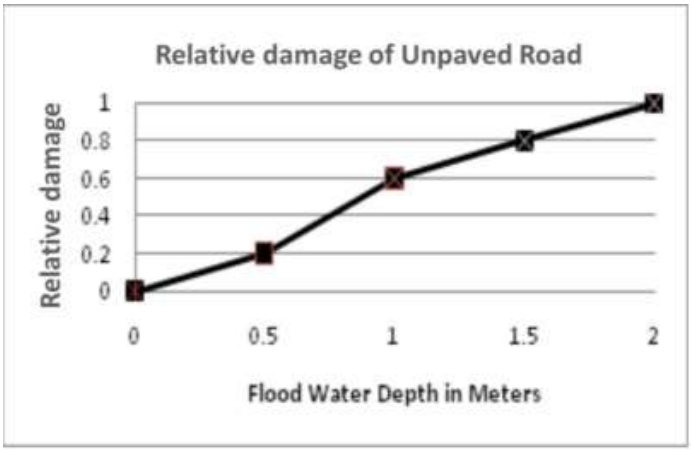

Figure 2-13: Damage model for unpaved roads. Source: (Ghimire et al., 2021)

Vulnerability scale	Description
0	- No damage.
0.2	- Very low damage and only small holes or pits formed in the road. - Repairing cost is also low.
0.5	- Partly damage in the roads i.e. some part of the roads washed out and the holes or pits get larger. - No need of replacement but the repairing cost is high.
1	- Completely damaged - Need full replacement with high cost

Table 2-2: Damage grade description. Source: (Ghimire et al., 2021)

To assess the relative damage to the roads, it was first necessary to process the Metuge District's road network shape file obtained from OpenStreetMap and field surveys and the water depth raster files obtained from hydraulic modeling results. Initially, by using the Generate Points Along Lines tool from the Data Management Toolbox, points were generated along the roads at a resolution of 12.5 meters, which matched the DEM used in hydraulic modeling. The water height for each point was extracted by using the Extract Multi Values to Points from the Spatial Analyst Toolbox and using raster files from hydraulic modeling results. Subsequently, the roads were split into segments every 12.5 meters to generate damage values for each segment by using the Split Line at Point tool from the Data Management Toolbox. As the last step of this procedure, the formulation of the damage curve was applied by using the Field Calculator for each return period and the damage ratio was obtained for each segment of the road. To obtain absolute damage in terms of repair cost, every damage ratio assigned to each segment was multiplied by the length of the segments and the repair cost of the roads. According to the Istituto Oikos (2023), the estimated cost of constructing this type of road in Mozambique is 1500Mzn/m. The total repair cost of roads was calculated for each of the four return period scenarios to estimate the absolute damage.

2.4.4 Calculation of Annual Average Damage

Flood risk is often expressed in terms of annual average damage (AAD), which is commonly used as a convenient measure of the expected average damage each year. It is important to note that the damage caused by natural hazards can vary from year to year. While some years may result in high damage, others may have minimal damage. However, over time, there will be a monetary impact that one should expect to incur.

In this study, the economic and social risks were evaluated for residential buildings, roads, and the population. The economic risk was assessed based on the monetary damage for four exceedance probabilities, while the social risk was assessed based on the annual average affected people for the same probabilities. Exceedance probability is referred to as the probability that a certain value will be exceeded in a predefined future time period, so basically, it is the inverse of the return period.

To calculate annual average damage, damage-probability curves were plotted by using the expected damage against its exceedance probability. The area under this curve, simply computed by numerical integration, represents the risk called ''the annual average damage".

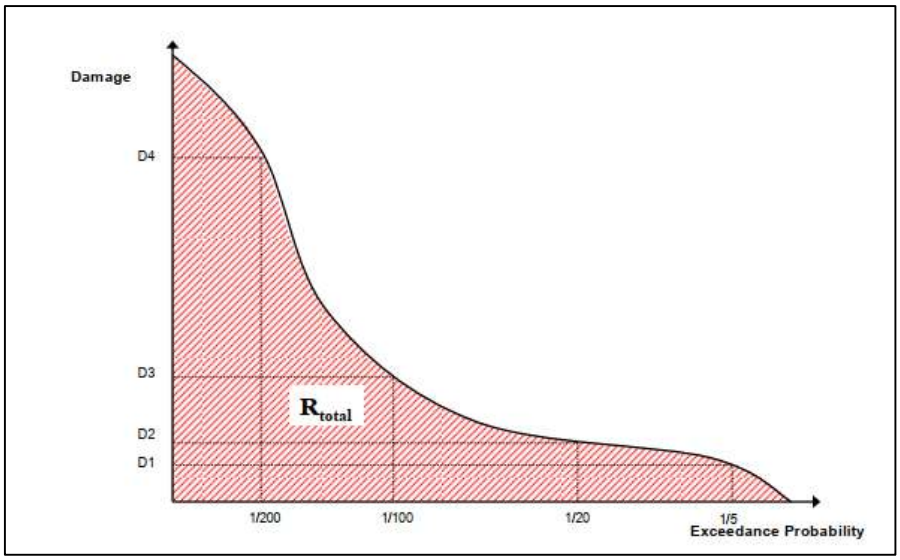

Figure 2-14: Damage-probability curve. Source: (Meyer et al., 2007)

The curves were created by using the absolute damages calculated from the depth-damage curves for residential buildings and roads. The curve for the population was obtained considering the total number of people directly affected due to the degree of loss of their homes. The integral was calculated using the trapezoidal rule, which involves summing the areas of the trapezoids formed by the corresponding damage probability pairs. Hence, the formulation can be represented as follows (Lugeri et al., 2010):

$$AAD = \frac{1}{2} \cdot \sum_{n=0}^{N-1} (D_n + D_{n+1}) \cdot (P_n - P_{n+1}) \tag{7}$$

where $D_0 = 0,\ D_n = D_\infty\ and\ P_n = 0.$

2.5 Models Adopted Based on Prior Studies

The creation of the additional model sets has been decided, depending on their hydrological modeling and terrain geometry input parameters, to conduct a sensitivity analysis of results. To accomplish this, input parameters and models were obtained from two prior studies conducted for the Rio Muaguide basin. This section will provide details on how the obtained parameters and models were utilized to create diverse sets of models, along with an explanation of the procedure that was followed. Additionally, a table will be shown summarizing all the models obtained in this study, along with their respective characteristics.

2.5.1 Models from the SIXHIARA Project

The peak flow discharge values corresponding to the return periods of 10, 50, 100, and 500 years for the lower reaches of the Rio Muaguide River were derived from the SIXHIARA Project (iCarto & ARA-NORTE, 2017). The values were used to analyze the impact of peak flow discharge values on hydraulic modeling results. The table below presents the peak flows used for a hydraulic analysis in subsequent stages:

ID	Rio	Ac, km^2	Qo, m^3/s	Q_{500}, m^3/s	Q_{100}, m^3/s	Q_{50}, m^3/s	Q_{10}, m^3/s
1	Muaguide	1415.9	191.4	763.8	593.4	522.6	361.8

Table 2-3: Peak Flow Values of Rio Muaguide River. Source :(iCarto & ARA-NORTE, 2017)

The hydrograph data of the peak flow values obtained in the SIXHIARA Project were unavailable. It was decided to create synthetic hydrographs for peak flow values to facilitate hydraulic modeling simulations, as the modeling process requires input hydrographs as boundary conditions. To do this, the Hydrograph Scaling Approach was utilized, and synthetic hydrographs and time series data for the 2,10,50 and 100 years return periods considering the large sub-basin in the HEC-HMS model were taken as reference hydrographs. However, incorporating peak flow values from another source using the hydrograph scaling approach is a simplified method that relies on assumptions about the shape and duration of hydrographs. Despite this, the method can be considered justifiable, given the comprehensive hydrological study that was previously developed and used as a reference. This approach was aimed at ensuring data consistency and enabling sensitivity assessments.

The Hydrograph Scaling Approach requires the calculation of the scaling factor as a ratio between the two peak flow values. The calculation of the scaling factor was done by dividing the peak flow values obtained from HEC-HMS modeling results by the peak flow values obtained from the SIXHIARA Project for the same return periods. It is worth adding that there was no peak flow value in the HEC-HMS model with a return period of 500 years, so the scaling factor for this return period was obtained using the peak flow value with a return period of 100 years. Each time series data of the HEC-HMS model was multiplied by a corresponding scaling factor to obtain a new time series. Table 2-4 shows the scaling coefficients used while the obtained hydrographs corresponding to 10,50,100 and 500-year return periods are represented in Figure 2-15.

	Qpeak[m3/s]		
Return Period[years]	HEC-HMS	SIXHIARA	Scaling Coefficient
TR 2	147.5	-	-
TR 10	735.5	361.8	2.033
TR 50	1364.2	522.6	2.610
TR 100	1644.5	593.4	2.771
TR 500	-	763.8	2.153

Table 2-4: Scaling Coefficients

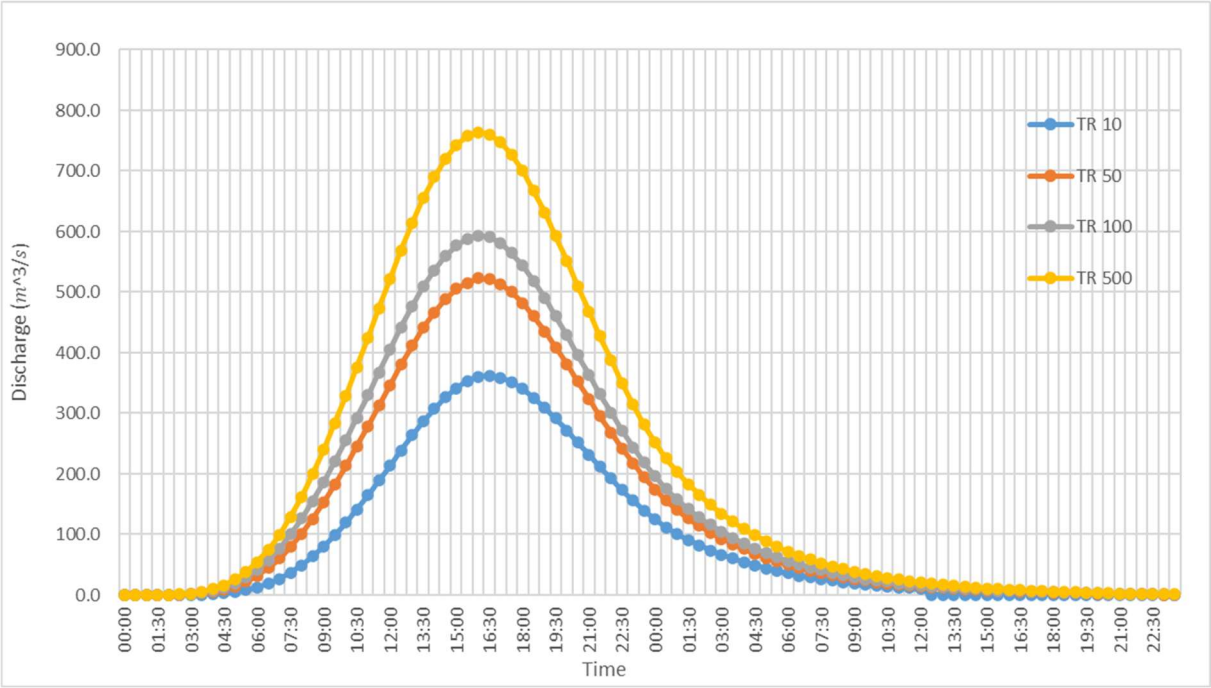

Figure 2-15: The derived hydrographs for peak flow values of the SIXHIARA Project

This set of hydrographs was utilized to re-run the hydraulic simulations to assess the effect of peak discharge values on flood hazard modeling outcomes for the Metuge District, focusing on Namuapala village. The simulation methodology, along with other input parameters, was the same as that previously described.

2.5.2 Models from Paz Idarraga & Rotaru, 2023

Additional input hydrographs and hydraulic modeling results were included from a prior study of Paz Idaragga& Rotaru (2023). In their analysis, the same methodology was followed as in the current research but with different sub-basin selections as input data for rainfall-runoff modeling. They considered four relatively small sub-basins, as shown in Figure 2-16, within the Rio Muaguide catchment and developed hydraulic models corresponding to seven different return periods. To compare how the selection of sub-basins in hydrological modeling and geometric input data in hydraulic modeling affect the results in terms of flood extent, water depth, and damage, their input hydrographs were used to repeat the simulations by only modifying the DEM used in hydraulic simulations. On the other hand, the result of the hydraulic simulations, as shown in Figure 2-17, which corresponds to the return periods of 2,10,50, and 100 years, were used to compare with the outcomes of the other models.

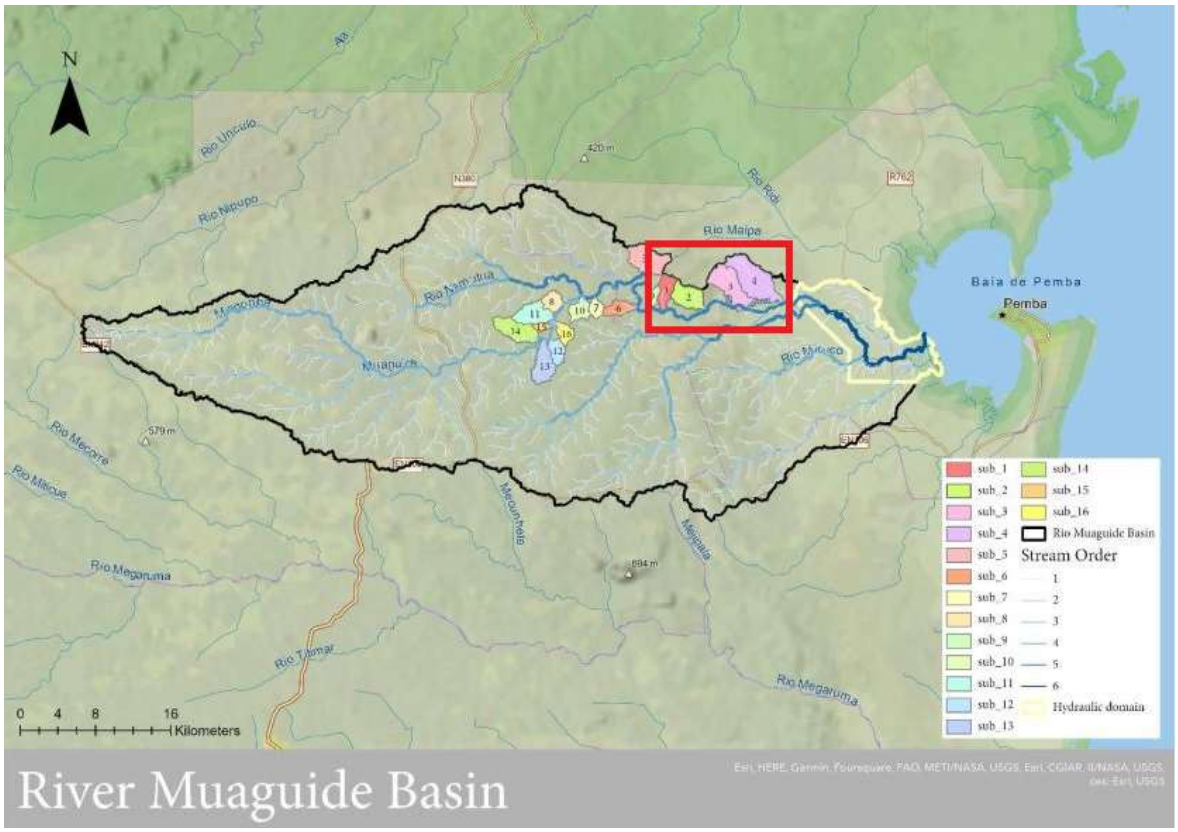

Figure 2-16: Four sub-basin selections in hydrological modeling. Source:(Paz Idarraga& Rotaru, 2023)

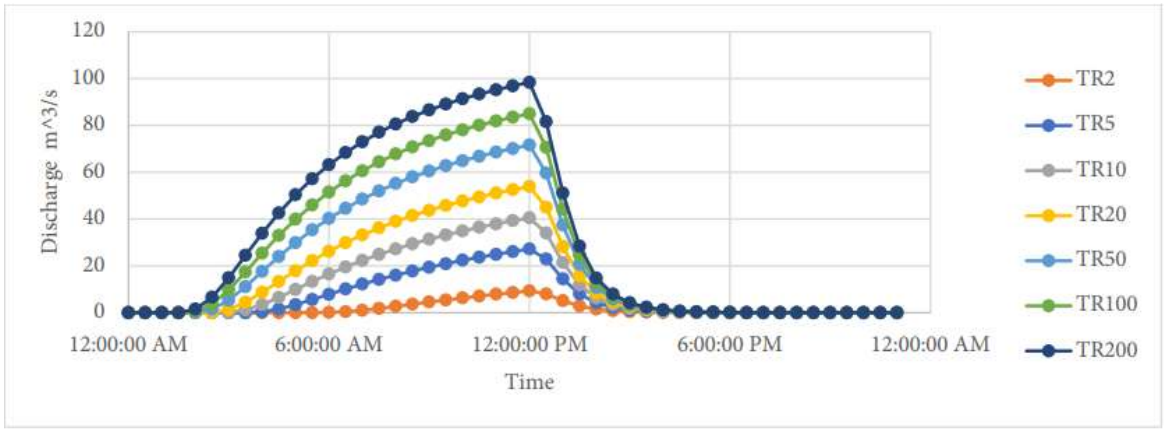

Figure 2-17: Input hydrographs. Source:(Paz Idarraga& Rotaru, 2023)

To assess the impact of the topographic input data on the hydraulic modeling results, adjustments were made to the digital elevation model (DEM) by removing the culverts and elevation of the roads in the hydraulic modeling. This allowed for repeated hydraulic simulations, along with subsequent damage assessment and annual average damage calculations for residential buildings, roads, and the population. Maintaining consistency in the modeling chain was considered essential for accurate comparative analysis, as it helps to isolate the effects of changes in specific modeling choices.

2.6 Summary of Simulation Runs

This section summarizes the hydraulic model sets created and/or used based on the methodology explained earlier. Each model set consists of four models, and each model corresponds to a return period. To simplify the explanations, a naming convention has been implemented. The models used in the study have been classified as follows: L-R for models that used the large basin in the hydrological model and where the height of the roads was elevated in the hydraulic modeling. L-NR for models that used the large basin in the hydrological model but where the height of the roads was not elevated in the hydraulic modeling. S-R for models implemented from the SIXHIARA Project using peak flow values and the height of the roads was elevated. P-R for models obtained from a prior study (Paz Idarraga& Rotaru, 2023) that used the four small sub-basins in the hydrological model and where the height of the roads was elevated in the hydraulic modeling. These models (P-R) were used to compare results, and no changes have been made to them. P-NR for the models referring to the small basins of Paz Idarraga & Rotaru (2023), but where the height of the roads was not elevated in the hydraulic modeling.

Simulations	Peak Discharge [m3/s]	Performed/Used
L2-NR	147.5	Performed
L10-NR	735.5	Performed
L50-NR	1364.2	Performed
L100-NR	1644.5	Performed
L2-R	147.5	Performed
L10-R	735.5	Performed
L50-R	1364.2	Performed
L100-R	1644.5	Performed
S10-R	361.8	Performed
S50-R	522.6	Performed
S100-R	593.4	Performed
S500-R	763.8	Performed
P2-NR	9.3	Performed
P10-NR	40.5	Performed
P50-NR	71.6	Performed
P100-NR	85	Performed
P2-R	9.3	Used
P10-R	40.5	Used
P50-R	71.6	Used
P100-R	85	Used

Table 2-5: Summary of the models

Chapter 3: Results

3.1 Results of the Hazard Assessment

The present sub-chapter systematically presents the results of each crucial component of the modeling chain described in Chapter 2, starting with the hydrological modeling outcomes in Section 3.1.1. Subsequently, Section 3.1.2 delves into the hazard maps generated based on the hydraulic modeling results for various model scenarios. Lastly, Section 3.1.3 presents the conducted sensitivity analysis focusing on the impact of sub-basin selection and terrain geometry on hydraulic modeling results for each model scenario.

3.1.1 Results of Hydrological Model

In this study, the developed hydrological model considering a large sub-basin in Rio Muaguide Catchment was used as input data in the hydraulic modeling to create the model sets of L2-NR, L10-NR, L50-NR, L100-NR, and L2-R, L10-NR, L50-NR, L100-NR. The selected sub-basin within the watershed analysis is represented in Figure 3-1, while Table 3-1 provides the sub-basin geomorphological features, including its area and average slope, as well as information about its mainstream characteristics, such as length, average mainstream slope, and maximum and minimum elevation.

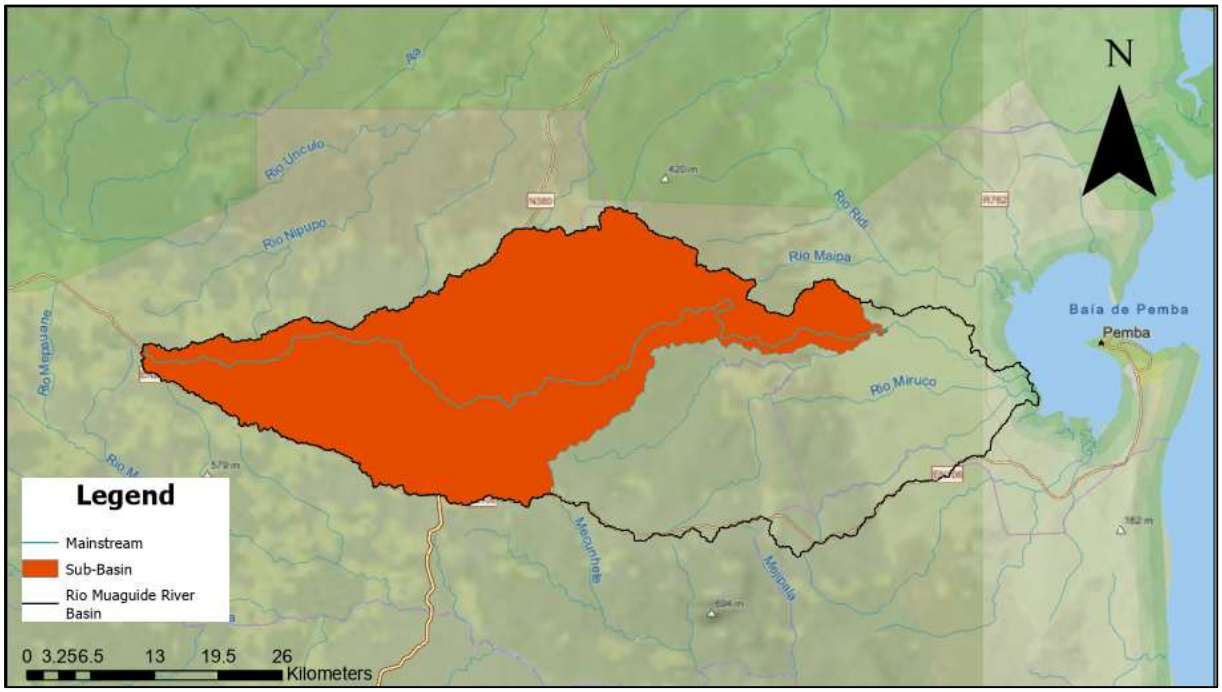

Figure 3-1: The selected sub-basin for the L-NR and L-R model sets in Rio Muaguide Catchment.

.

Basin			Main Channel				
Area [km2]	**Slope [°]**	**Slope[-]**	**L[km]**	**Hmax[m]**	**Hmin[m]**	**Mean Slope [°]**	**Mean slope[-]**
993.41	3.259	0.0569	109.28	652	40	1.123	0.0196

Table 3-1: The geomorphological characteristics of sub-basin.

The calculation of the time of concentration for the selected sub-basin was carried out using the four formulas explained above, and the final value of time of concentration was obtained as 12.62 h, shown in Table 3-2, by averaging the results of all the formulas.

Time of Concentration [h]				Final ToC [h]
Chow	CorpsofEngineers	Dooge	Johnstone	Mean
11.37	14.28	11.9	12.92	12.62

Table 3-2: The results of the formulas used and the final value of time of concentration for the selected sub-basin.

Determining the curve number for the sub-basin was completed by using the four different land cover data with the assumptions made on the hydrological soil type and antecedent moisture condition explained earlier. Table 3-3 displays the obtained curve number values for the four different sources, and the final value was obtained as 79 by performing the weighted average of the results.

Curve Number Values				Final CN
Copernicus	Unilurio	FAO	JRC	Mean
80.08	75.6	80.1	80.4	**79.05**

Table 3-3: The curve number values.

The rainfall-runoff modeling was carried out using the HEC-HMS model, and Figure 3-2 displays the obtained final synthetic hydrographs considering the 2,10,50 and 100-year return periods. These synthetic hydrographs were used as input data in the hydraulic simulations for the model set of L-R and L-NR, and it was also used as a reference to obtain time series data for the set of model S-R.

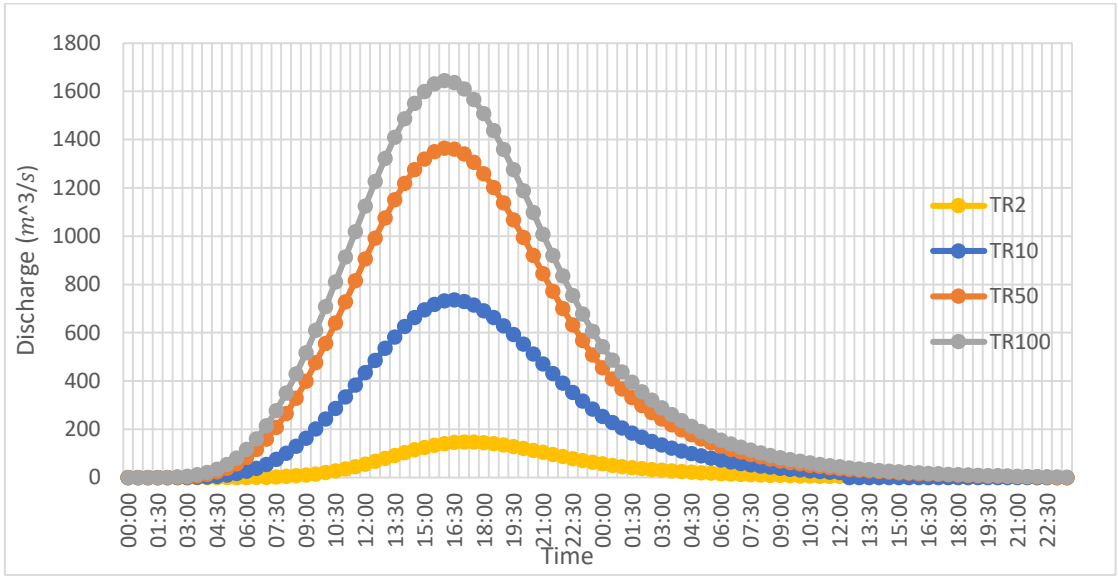

Figure 3-2: Obtained Synthetic Hydrographs from HEC-HMS model.

3.1.2 Hazard Maps

The hydraulic modeling results for each created set of models (L-NR, L-R, S-R, P-R, and P-NR) were processed in ArcGIS Pro to generate hazard maps at the district level. The hazard maps display the extent of flooded areas within the study domain and were presented for each corresponding return period of the model sets. The water depth is represented in shades of blue, with intervals of 1.50m, and this representation was kept constant for all the hazard maps to simplify the process of comparing results obtained using different sets of models, which significantly increases the ease of interpretation and analysis of the maps. Upon examining the hazard maps of the district, it is evident that the area prone to flooding is primarily concentrated around the main path of the river, and in general, the depth of the flooding is considerably high at the outlet boundary.

3.1.2.1 Results of L-NR Models

The hazard maps of the L-NR model set were generated from outcomes of the hydraulic simulation process by removing the culverts and the elevation of roads in DEM and considering a large sub-basin in the hydrological modeling. The maps presented in Figure 3-3, Figure 3-4, Figure 3-5, and Figure 3-6 illustrate the flooded area and the maximum water depth values, respectively 2, 10, 50, and 100-year return periods. It could be seen from the hazard maps that the highest water depths were concentrated in the central part of the area. According to the results, while the hazard maps of the L50-NR (Figure 3-5) and L100-NR models (Figure 3-6) are more similar to each other in terms of water depth levels, the L2-NR model stands out with the lowest water depth among all results. Also, it can be noticed that the flow path of the river is not very visible, but this could be expected considering the lack of river cross-section data and the poor resolution of the DEM data.

In Table 3-4, the areas affected by flooding regarding different return periods were displayed. It can be observed that the extent of the flooded area varies between 30.5 km² for a return period of 2 years and 50.2 km² for a return period of 100 years.

Models	Peak Discharges [m3/s]	Area[km2]
L2-NR	147.5	30.5
L10-NR	735.5	43.6
L50-NR	1364.2	48.81
L100-NR	1644.5	50.2

Table 3-4 : Areas of flooding extent in the Rio Muaguide River for the model set of L-NR.

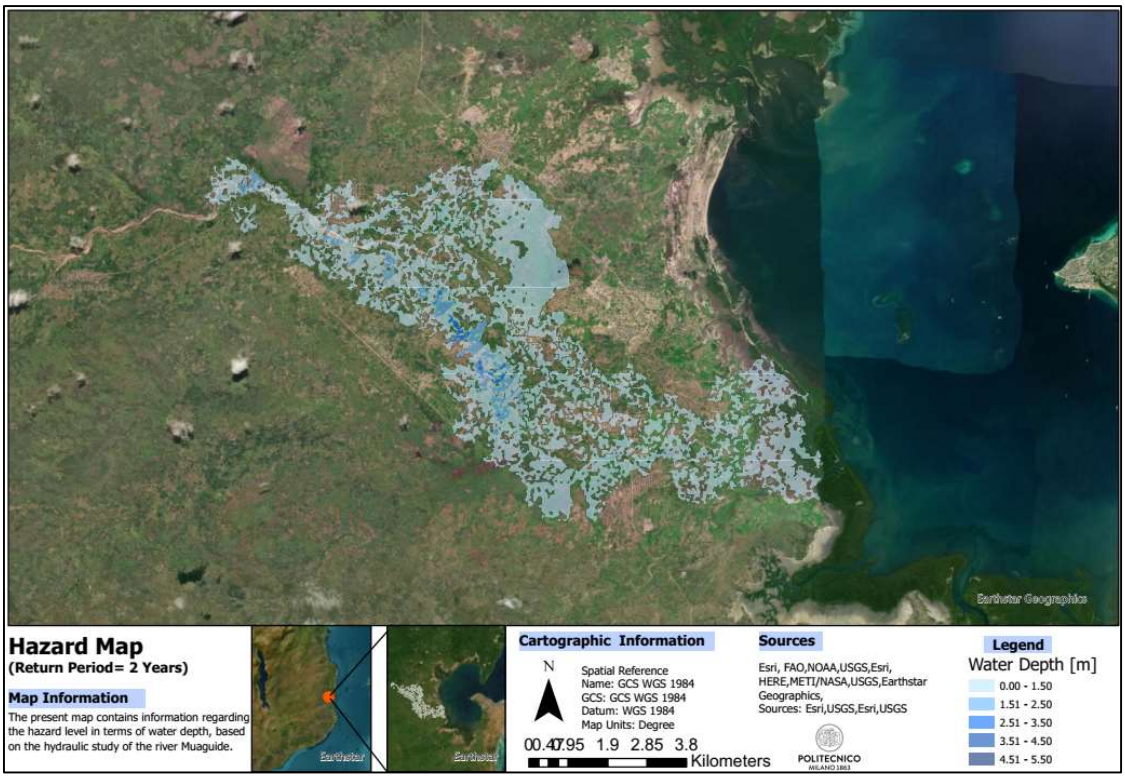

Figure 3-3: The hazard map of model L2N-R corresponds to the 2-year return period.

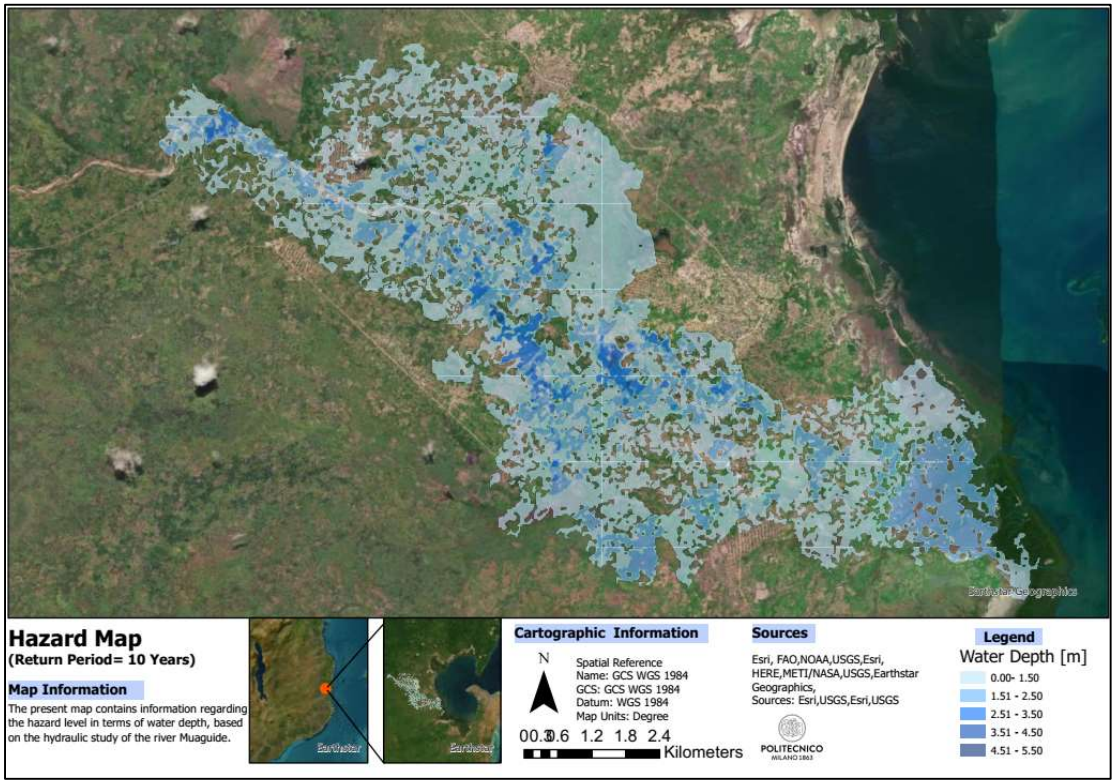

Figure 3-4: The hazard map of model L10N-R corresponds to the 10-year return period.

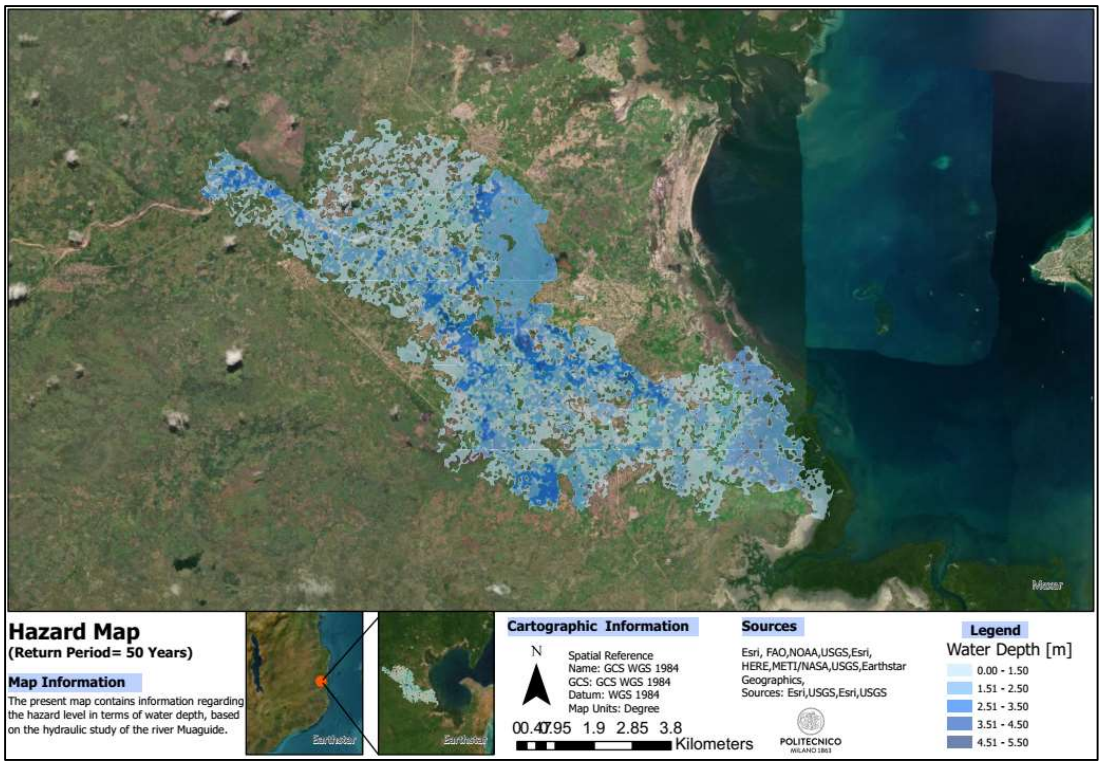

Figure 3-5: The hazard map of model L50N-R corresponds to the 50-year return period.

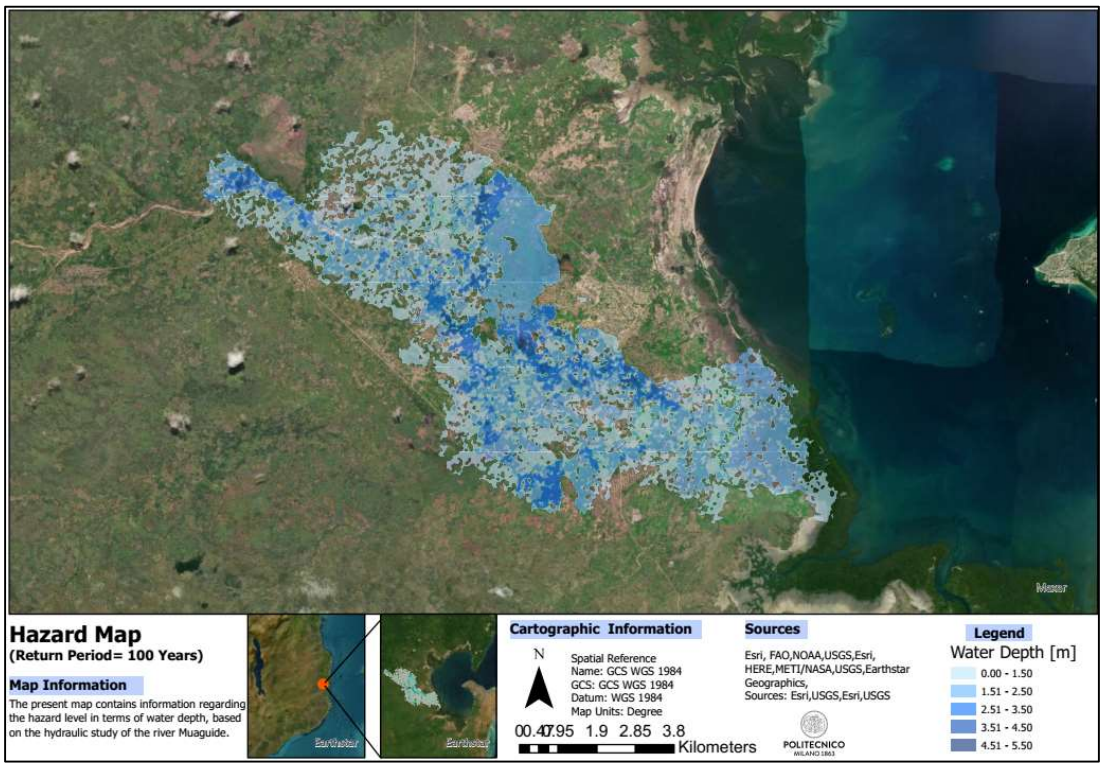

Figure 3-6: The hazard map of model L100N-R corresponds to the 100-year return period.

3.1.2.2 Results of L-R Models

The hazard maps prepared for the set of models of L-R, which consider a large sub-basin in the hydrological model and the presence of culverts and elevated roads in the DEM, were generated from the hydraulic simulation process. The presented maps in Figure 3-7, Figure 3-8, Figure 3-9, and Figure 3-10 portray the boundaries of the flooded areas corresponding to the return periods of 2, 10, 50, and 100 years as well as the water inundation depths. From Figure 3-7, it was possible to see the effect of elevated roads due to the higher water depth concentration in the lower center part of the area when compared to the hazard map of the L2-NR model (Figure 3-3).

Table 3-5 represents the area of the flood extent associated with the return period, and it displays that the flooded area for L-R models varies from 29.1 km² to 51.13 km², depending on the return period. It could be observed that the flood extent areas in the L-R models (Table 3-5) are slightly larger compared to the L-NR models (Table 3-4) except for the 2-year return period.

Models	Peak Discharges [m3/s]	Area[km2]
L2-R	147.5	29.1
L10-R	735.5	44.5
L50-R	1364.2	49.82
L100-R	1644.5	51.13

Table 3-5: Areas of flood extent in the Rio Muaguide River for the model set of L-R

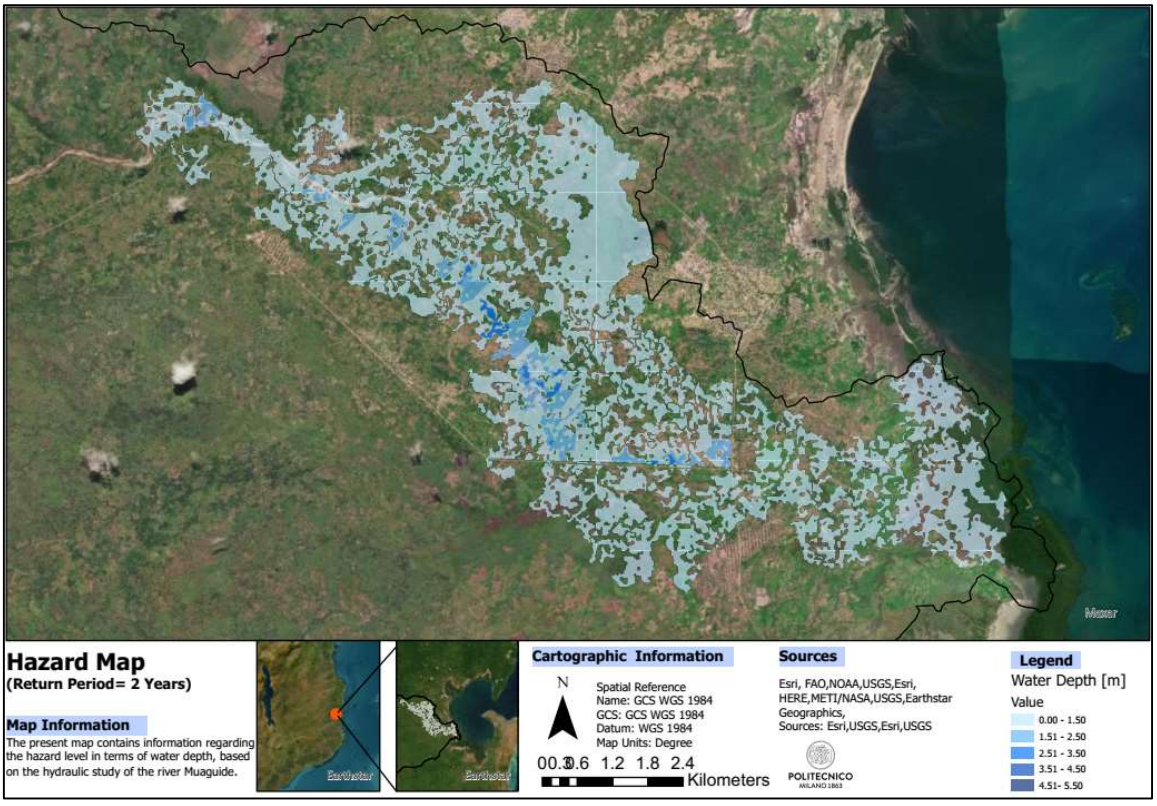

Figure 3-7: The hazard map of model L2-R corresponds to the 2-year return period.

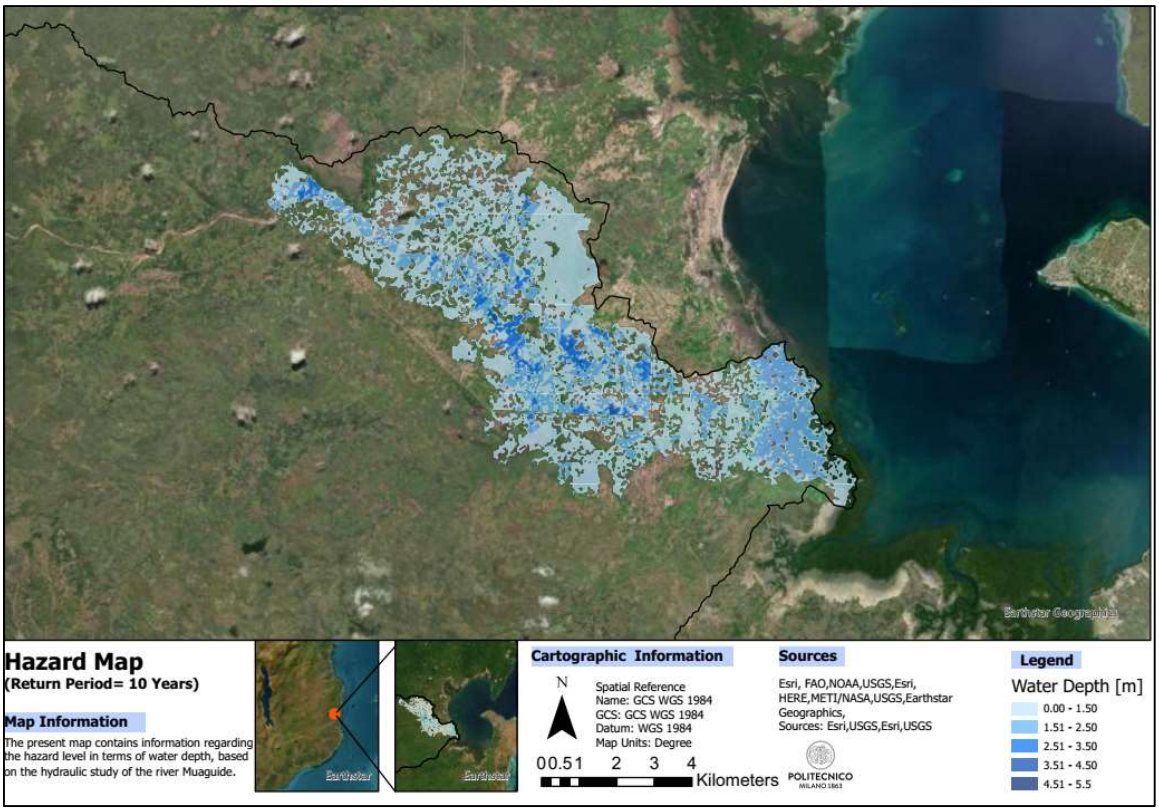

Figure 3-8: The hazard map of model L10-R corresponds to the 10-year return period.

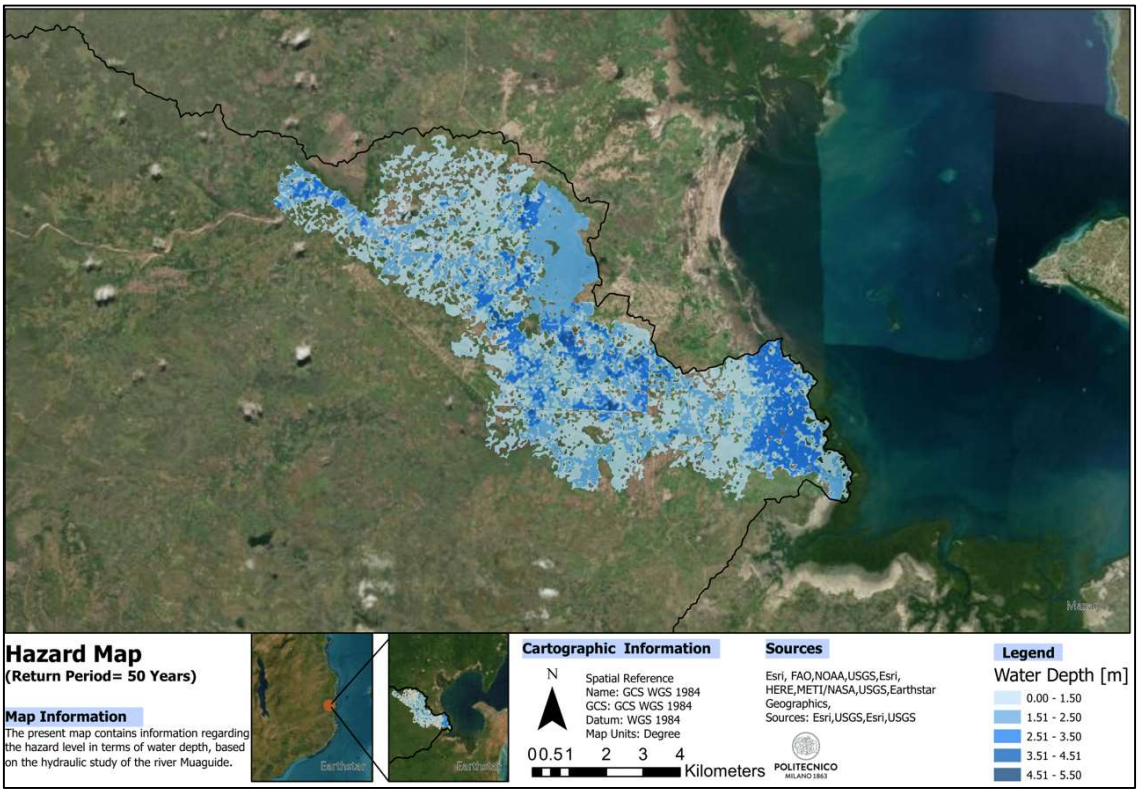

Figure 3-9: The hazard map of model L50-R corresponds to the 50-year return period.

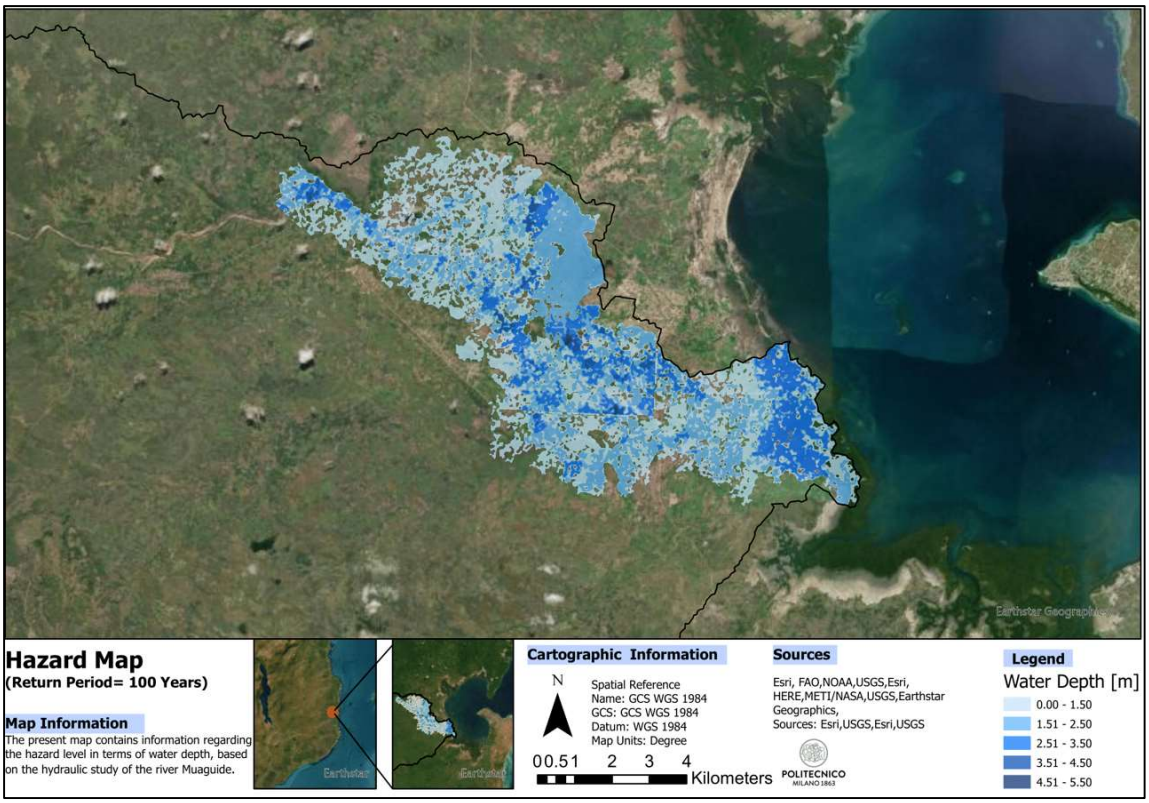

Figure 3-10: The hazard map of model L100-R corresponds to the 100-year return period.

3.1.2.3 Results of S-R Models

The hazard maps were generated for the set of models of S-R, which used the peak flow values derived from the SIXHIARA Project and incorporated the presence of culverts and the elevated height of the roads in the hydraulic simulations. As depicted in Figure 3-11, Figure 3-12, Figure 3-13, and Figure 3-14, the maps display the extent of flooded areas for the return periods of 10, 50, 100, and 500, along with water depth values. Similar to previously presented hazard maps of the L-NR and L-R models, higher water depth values are also concentrated in the central part of the flooding area. Additionally, the effect of the elevated roads could be seen as more significant in Figure 3-11 compared to Figure 3-8, even though the water depth values seem lower in those areas. As it can be seen from Figure 3-14, the water depths of the S500-R model are relatively lower than the L100-R model in Figure 3-10.

The range of the flooded extent areas varies from 38 km² for the S10-R model to 44.5 km² for the S500-R model, as shown in Table 3-6. When these results are compared with Table 3-4 and Table 3-5, it turns out that the lowest flooded area belongs to the S-R model set.

Models	Peak Discharges [m3/s]	Area[km2]
S10-R	361.8	38
S50-R	522.6	40.6
S100-R	593.4	44.3
S500-R	763.8	44.5

Table 3-6: Areas of flood extent in the Rio Muaguide River for the model set of S-R

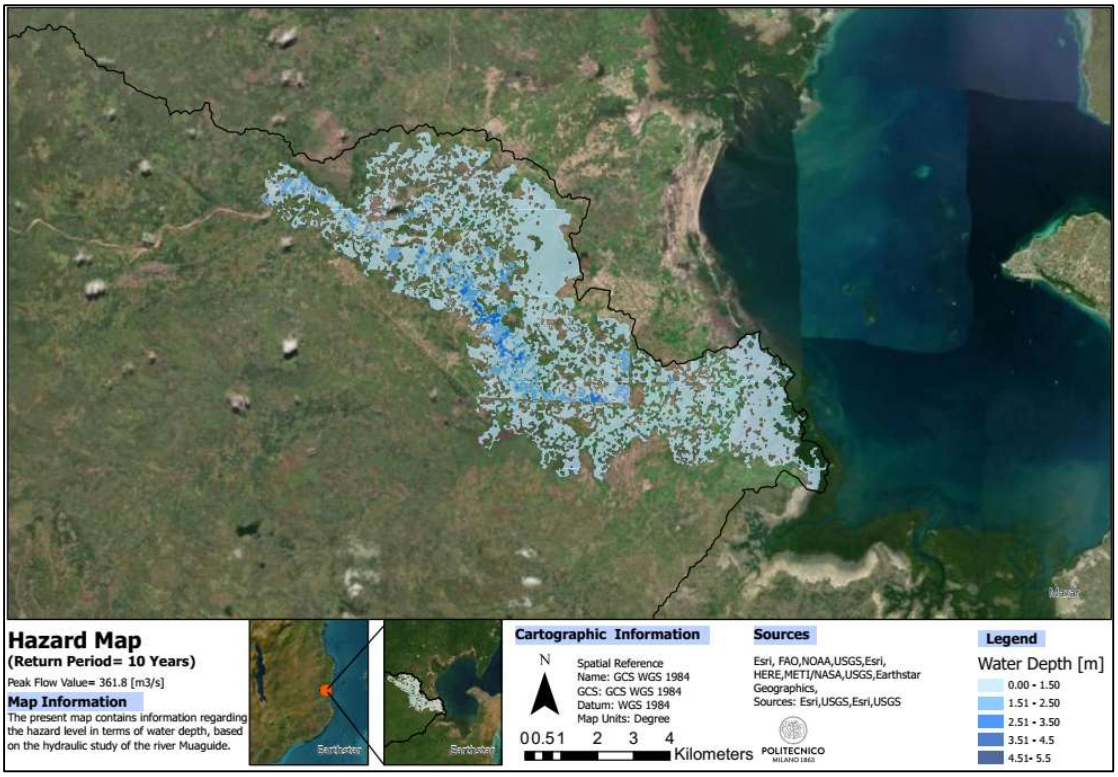

Figure 3-11: The hazard map of model S10-R corresponds to the 10-year return period.

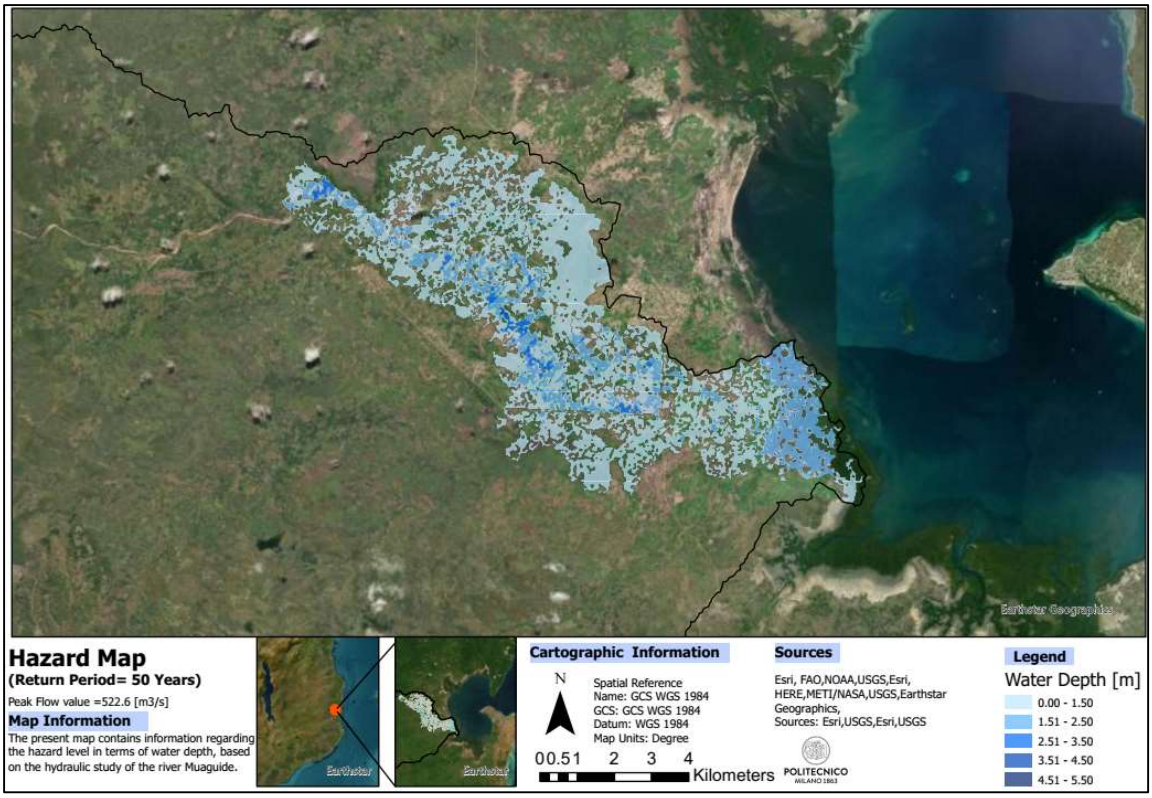

Figure 3-12: The hazard map of model S50-R corresponds to the 50-year return period.

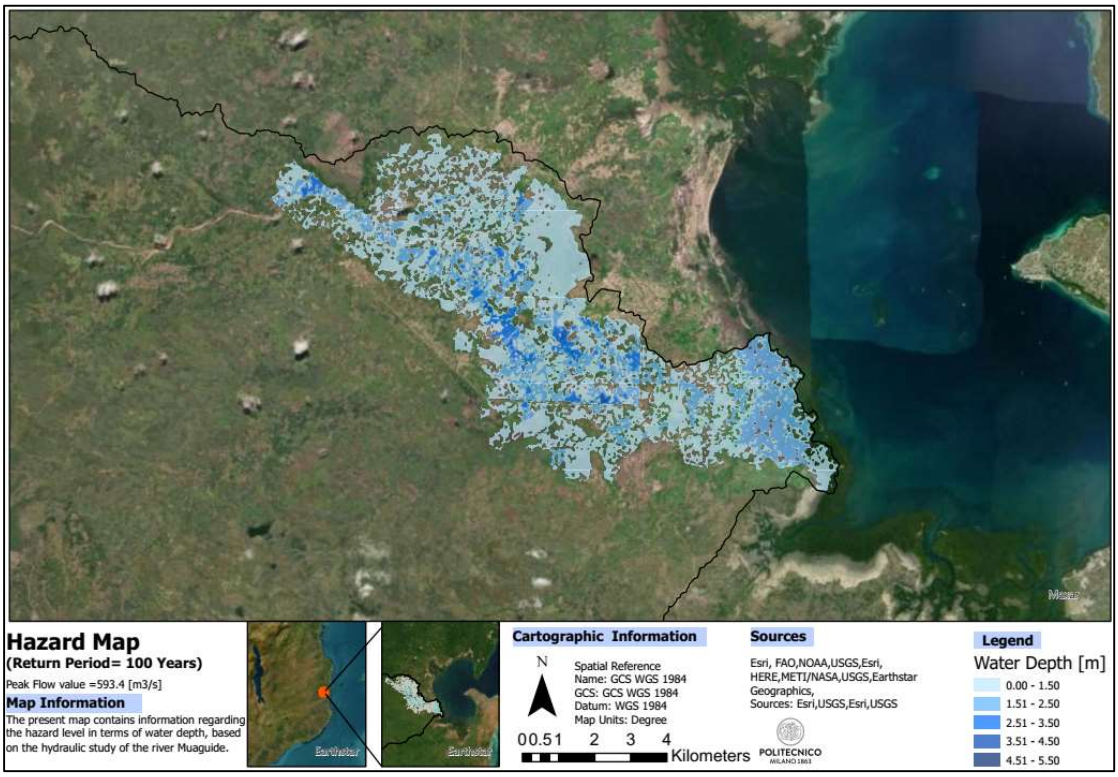

Figure 3-13: The hazard map of model S100-R corresponds to the 100-year return period.

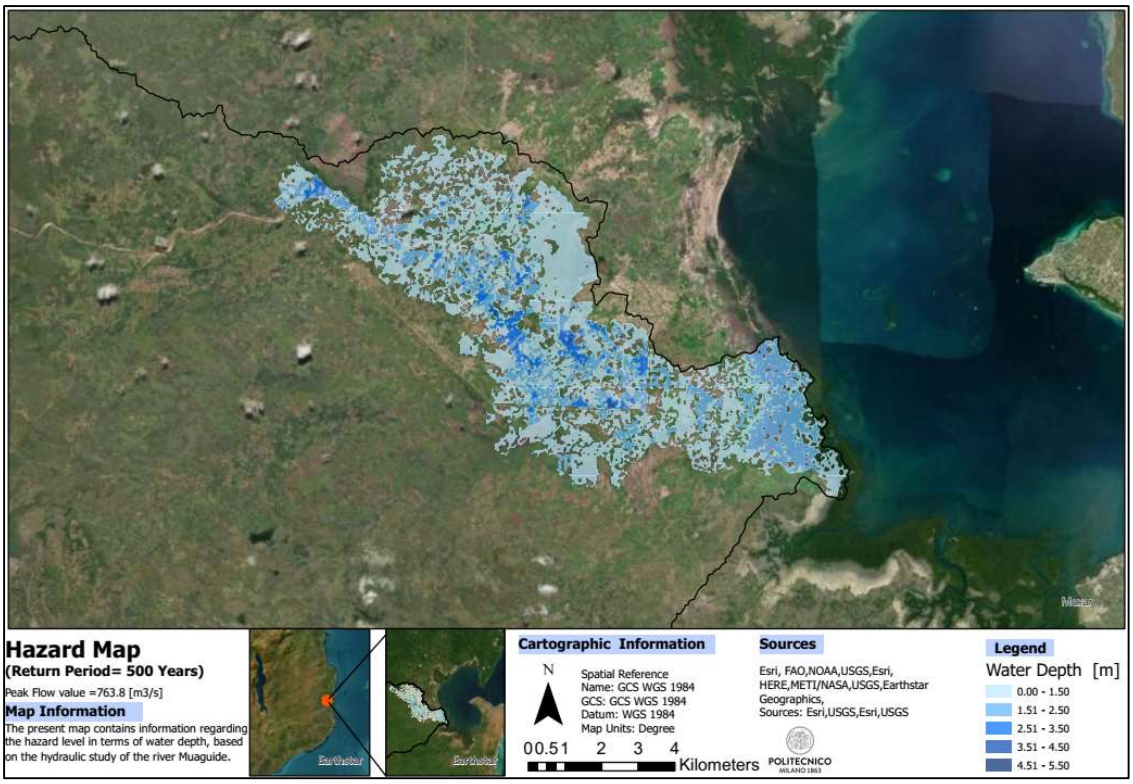

Figure 3-14: The hazard map of model S500-R corresponds to the 500-year return period

3.1.2.4 Results of P-R Models

Hazard maps of the P-R model have been reproduced to preserve the integrity of all model results. This set of models considered four small sub-basins within the hydrological model and the presence of culverts and elevated roads in the DEM.The maps presented in Figure 3-15, Figure 3-16, Figure 3-17, and Figure 3-18 show the flood water depths regarding 2, 10, 50 and 100-year return periods. The water depth levels in all return periods stand out with the lowest values compared to previously presented results of the other models. The effect of the elevated roads can be seen quite visible in Figure 3-17 and Figure 3-18 and it is noteworthy that the highest water depth levels were obtained in those areas compared to the whole area. Also, the changing dynamics of the flood area as the return period increases, which can be observed in the results of the L-NR and L-R models, cannot be observed in the results of the P-R model. Due to lower peak flow values compared to other model sets, the resulting flood areas are notably smaller, as detailed in Table 3-7. The analysis reveals a variation in flooding extent ranging from 21.47 km² to 27.3 km².

Models	Peak Discharges [m3/s]	Area[km2]
P2-R	9.3	21.47
P10-R	40.5	25.33
P50-R	71.6	26.17
P100-R	85	27.3

Table 3-7: Areas of flood extent in the Rio Muaguide River for the model set of P-R.

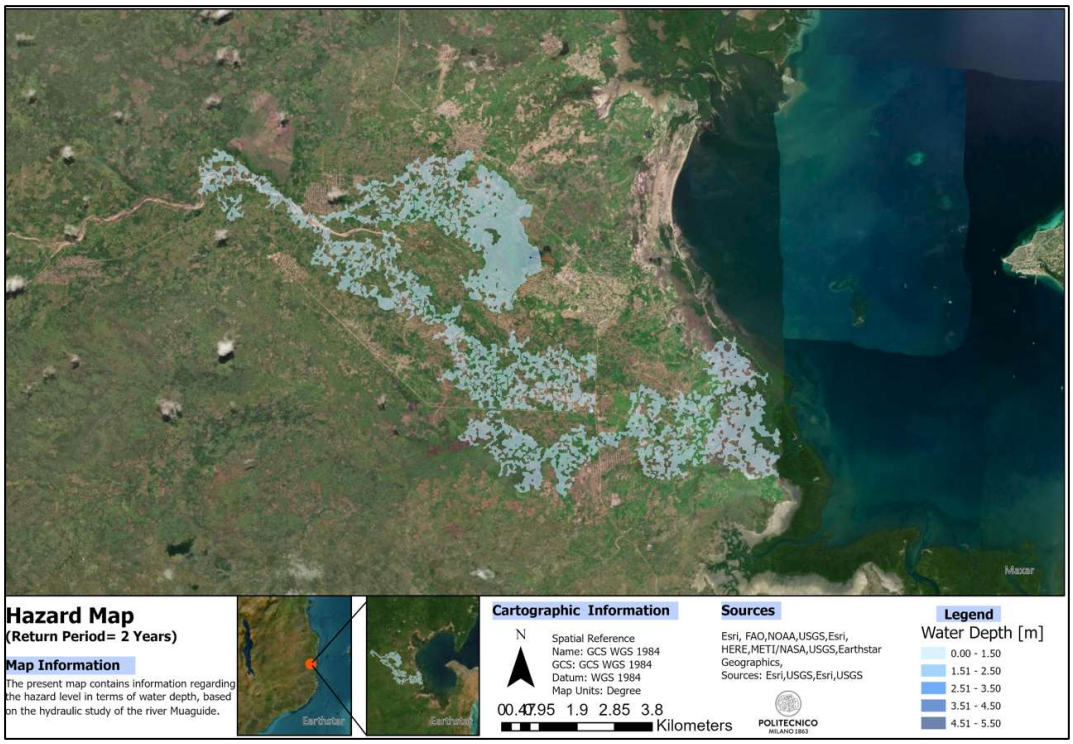

Figure 3-15: The hazard map of model P2-R corresponds to the 2-year return period.

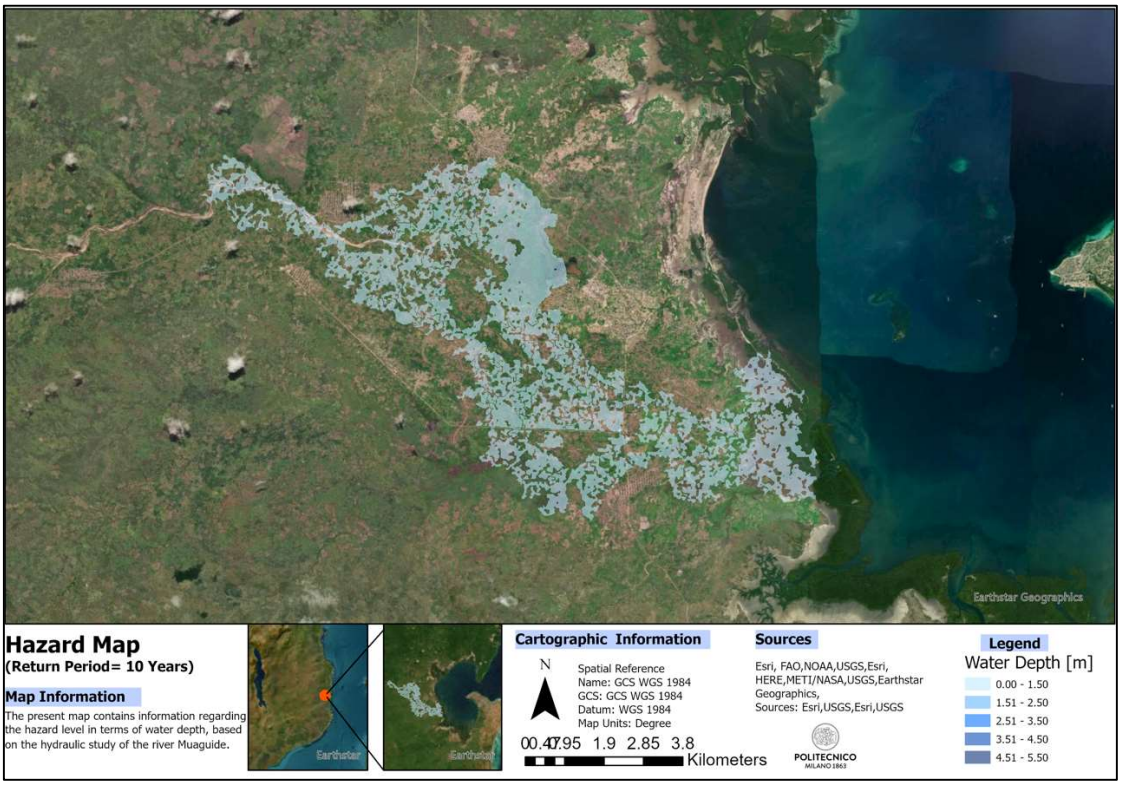

Figure 3-16: The hazard map of model P10-R corresponds to the 10-year return period.

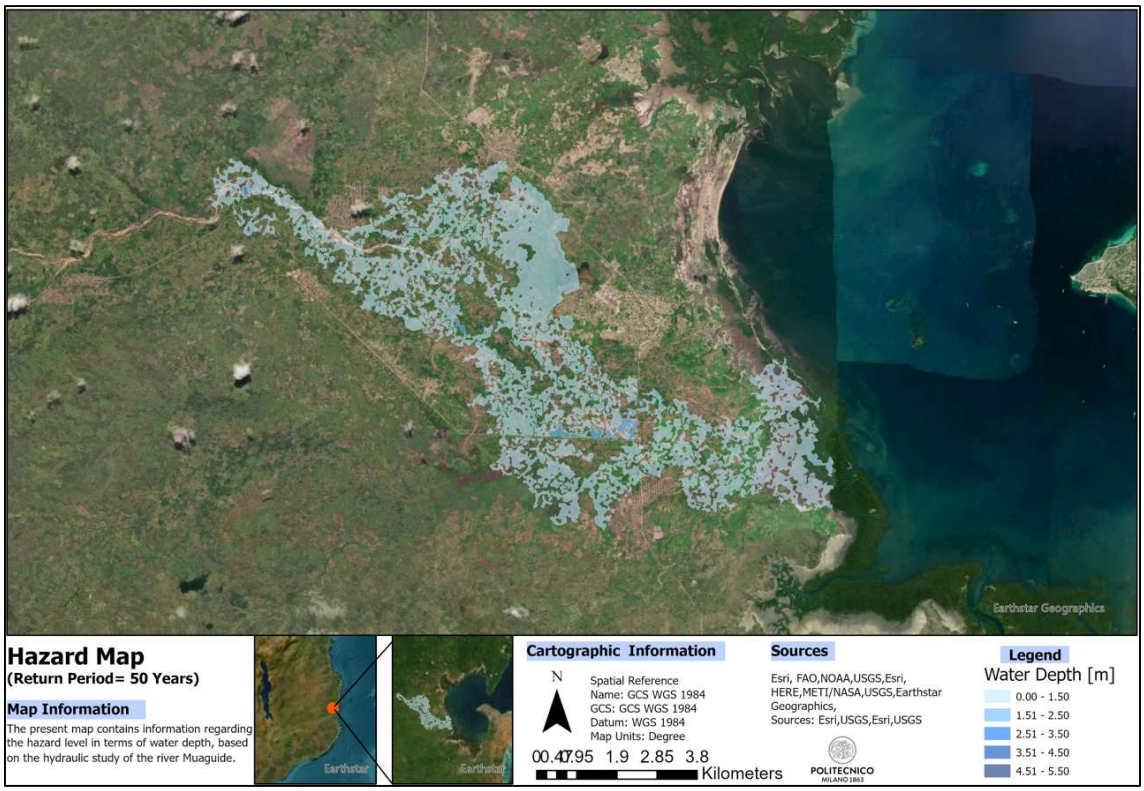

Figure 3-17: The hazard map of model P50-R corresponds to the 50-year return period.

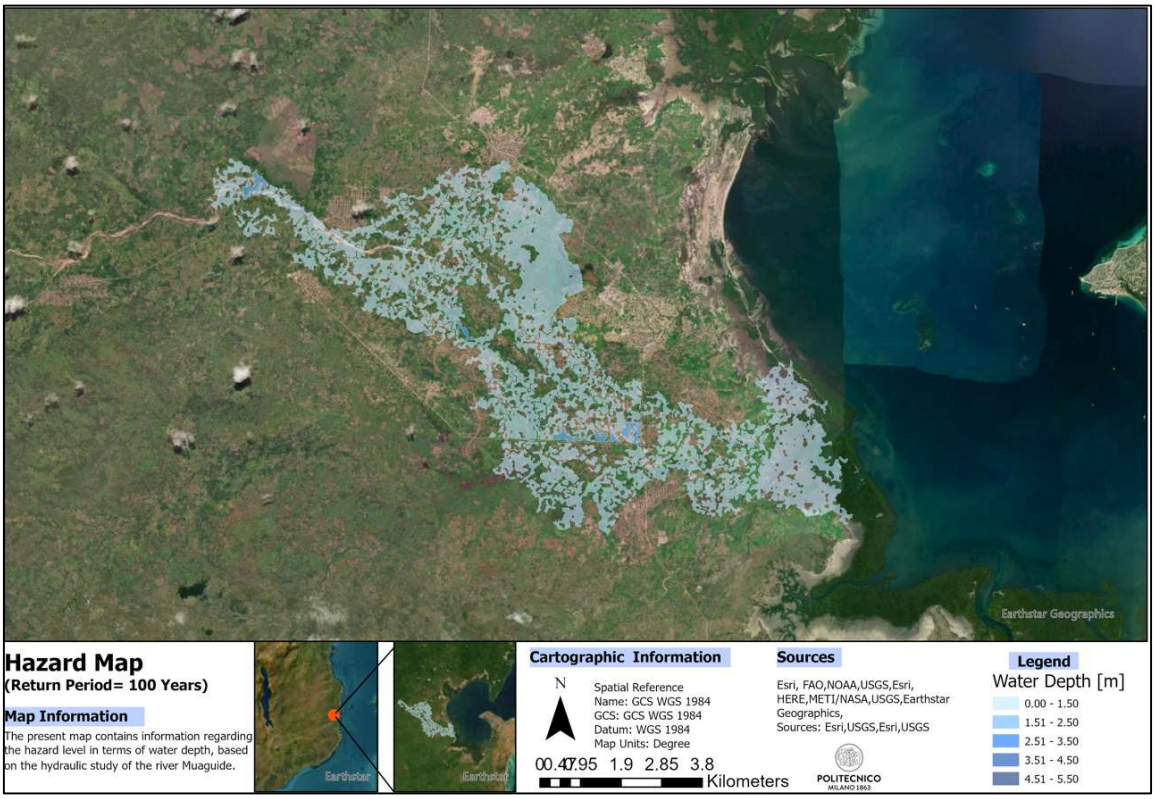

Figure 3-18: The hazard map of model P100-R corresponds to the 100-year return period.

3.1.2.5 Results of P-NR Models

The hazard maps generated for the P-NR models, illustrated in Figure 3-19, Figure 3-20, Figure 3-21, and Figure 3-22, delineate the extent of flooding and water depth values corresponding to four different return periods. These maps were developed by considering four small sub-basins in the hydrological modeling process, and the DEM used in the hydraulic modeling excluded culverts and elevated roads. The effect of excluding roads can be noticed, for example, by the fact that the accumulation of water seen in Figure 3-18 is not seen in Figure 3-22.

Reviewing the hazard maps presented for all the P-NR models, it is apparent that water depths did not even surpass 1.5 m. In contrast to the outcomes observed in other hazard maps of the L-NR, L-R, and S-R models, the flood area appears to be relatively homogeneously distributed across the region for all hazard maps of the P-NR model.

Models	Peak Discharges [m3/s]	Area[km2]
P2-NR	9.3	22.7
P10-NR	40.5	25.9
P50-NR	71.6	26.82
P100-NR	85	27.31

Table 3-8: Areas of flood extent in the Rio Muaguide River for the model set of P-NR

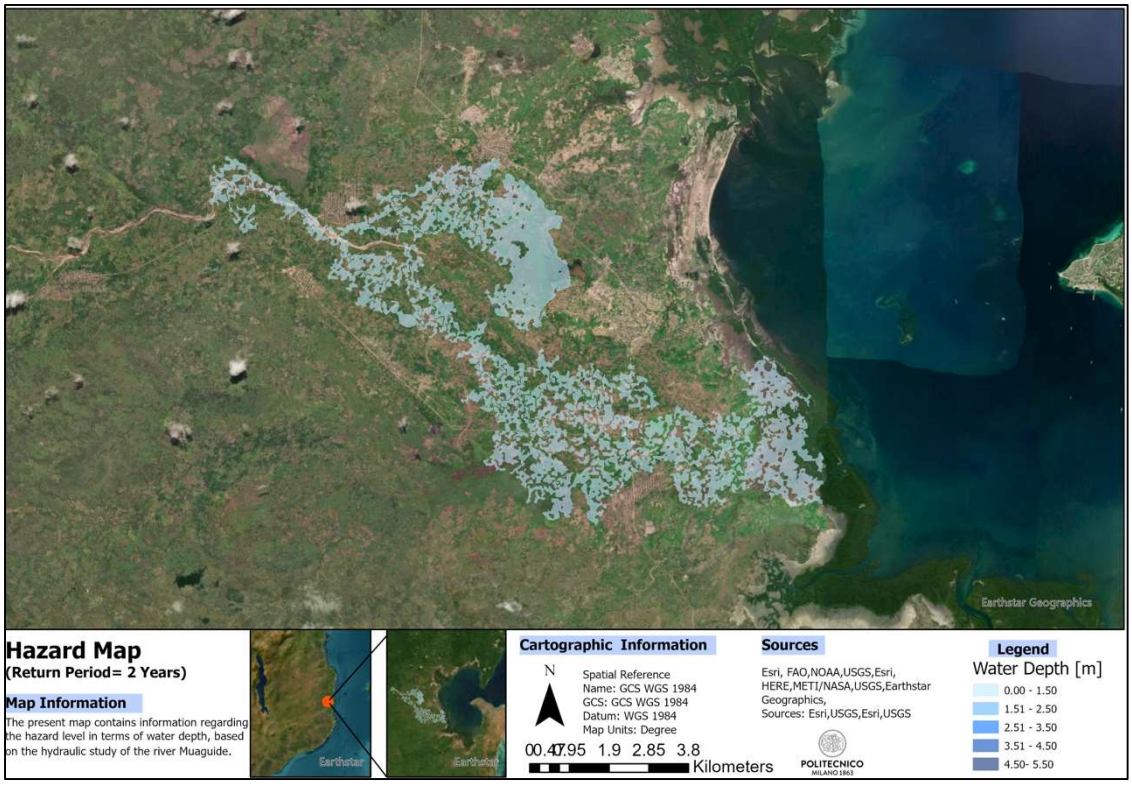

Figure 3-19: The hazard map of model P2-NR corresponds to the 2-year return period.

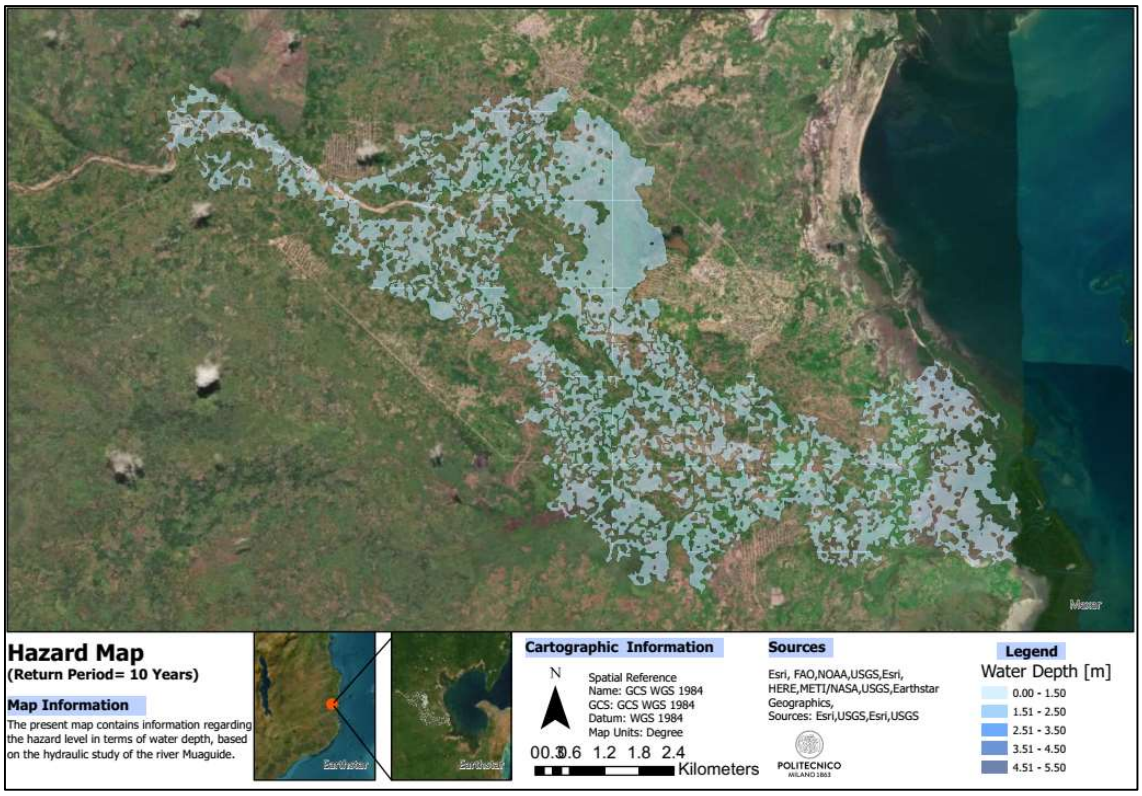

Figure 3-20: The hazard map of model P10-NR corresponds to the 10-year return period.

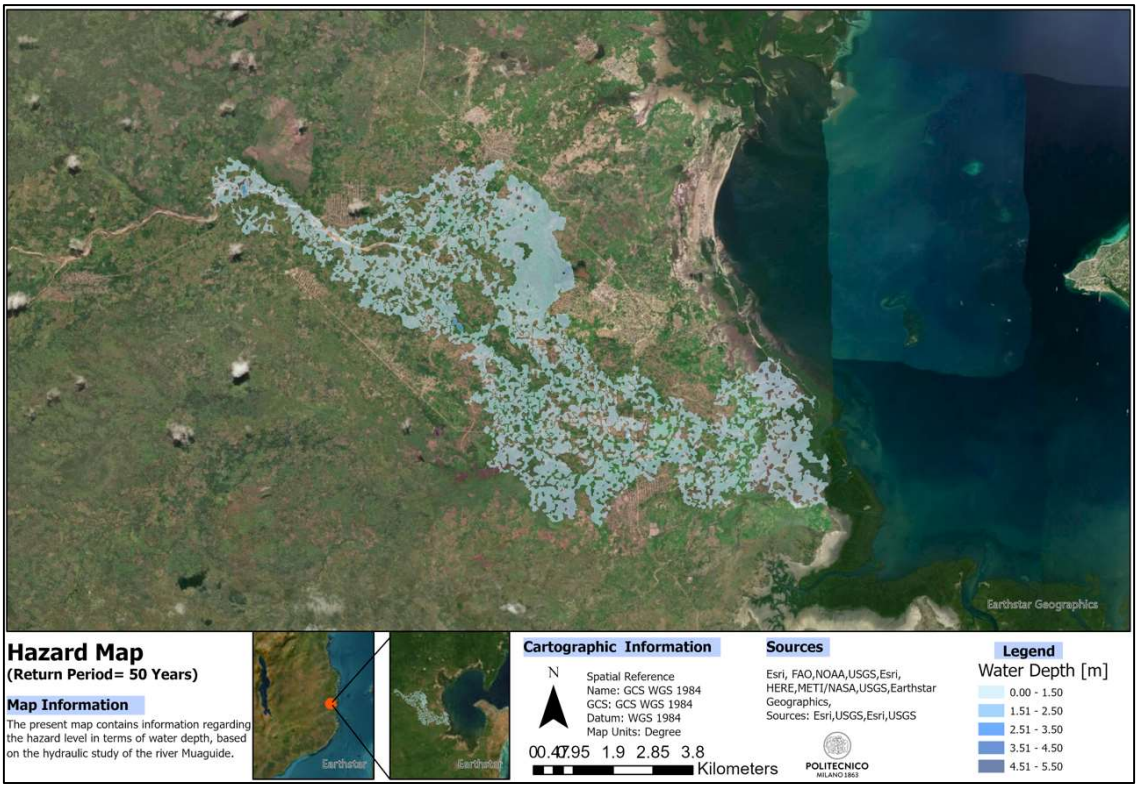

Figure 3-21: The hazard map of model P50-NR corresponds to the 50-year return period.

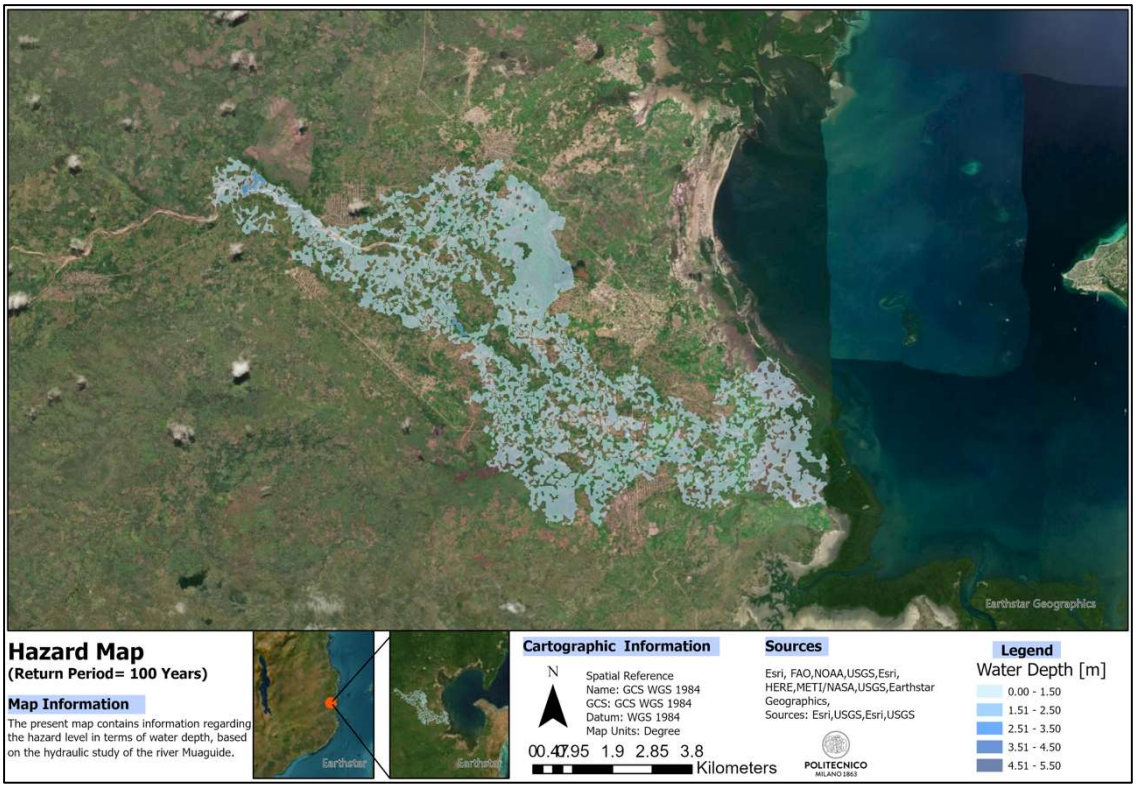

Figure 3-22: The hazard map of model P100-NR corresponds to the 100-year return period.

3.1.3 Sensitivity Analysis to Sub-Basin Selection and Terrain

The maps presented in the previous sub-sections provide a rough and reasonable view of how increasing the return period or the design discharge increases the flooded area and of how local modifications of the geometry (in this thesis, considering differently two roads) impact local maximum water depths. However, a more detailed sensitivity analysis is performed in the present sub-section by creating difference maps of the maximum water depth and by analyzing the maximum water depth values at specific locations in Namuapala. Furthermore, the impact of the sub-basin selection on the peak flow rate was analyzed.

3.1.3.1 Difference Maps

Difference maps were produced considering two pairs of model sets (L-R and L-NR, P-R and P-NR). The critical distinction between these sets lies in the inclusion or exclusion of culverts and elevated roads in the Digital Elevation Model (DEM) in hydraulic simulations, while all the other input parameters remained consistent across these model sets.

The difference maps were obtained using the Minus Tool in ArcGIS Pro. It is important to highlight that the Minus tool operates effectively when both raster layers have values in the corresponding cells. In this study, the raster values of the L10-R model were subtracted from the raster values of L10-NR. By applying this tool to the raster files of water depths from different model sets (L-R, L-NR, and P-R, P-NR) and associated return periods, difference maps were obviously obtained. However,

since the results were all similar, it was decided to show them only for the 10-year return period in this section.

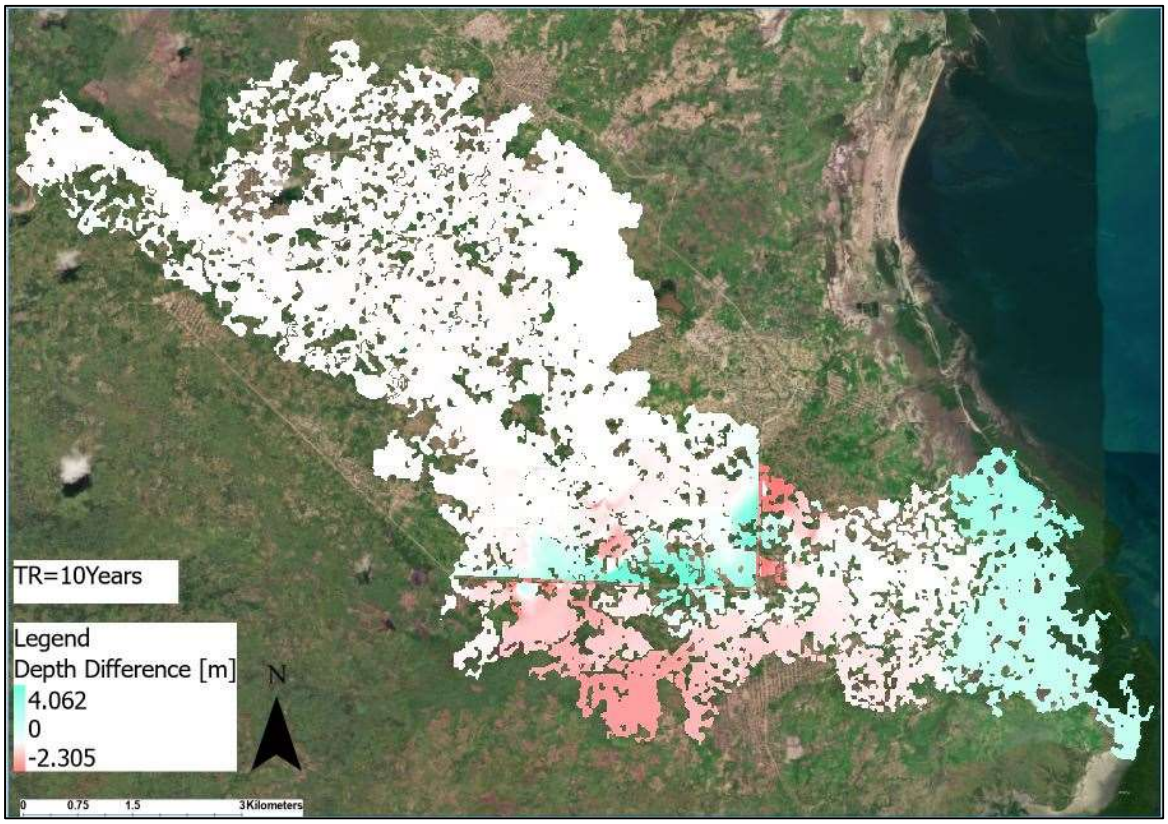

Figure 3-23: The Difference Map of the L10-R and L10-NR Model.

As shown in Figure 3-23, the depth difference varies from -2.3 m to +4 m and this underscores the large sensitivity of the models to the inclusion or exclusion of elevated roads and culverts in terrain geometry data (maximum differences are of the same order of magnitude as water depth values in the maps above). While the positive values displayed in green color refer to areas where the water depths of the L10-R model were higher than those of the L10-NR model, negative values displayed in pink color refer to water depths of the L10-NR models being higher than those of the L10-R models. The areas in white color show where the water depth values were the same in both models. According to the Difference Map, there is no water depth difference observed in the upstream part of the flooded area. In contrast, the highest difference is seen in the green areas up to 4 m in the lower center, corresponding to the location of the elevated roads in the L10-R model. This difference can be explained as the elevated roads in the L10-R model act as barriers, and when the water flow cannot pass through the roads, it causes water to accumulate in green areas, and the water depth increases. On the other hand, the negative water depth difference in the pink areas, which reached almost 2.3 m, occurred as a result of the lack of elevated roads in the L10-NR model, which did not prevent the water flow from reaching high depth in those areas. Additionally, it was observed that there was water accumulation in the green areas at the downstream location. This was not fully explained since the variations in the outflow hydrographs were not consistent with those of the water depth. However, since the focus of the study was on Namuapala village, and this issue did not have any significant impact on the other parts of the area, the unexpected behavior close to the downstream boundary was not explored further. In general, the effect of elevated roads in terrain geometry data

represents a significant impact on the water depth heights, as could be obviously expected in the Namuapala village, where it caused the accumulation of water up to 4 m compared to unelevated roads in terrain geometry data.

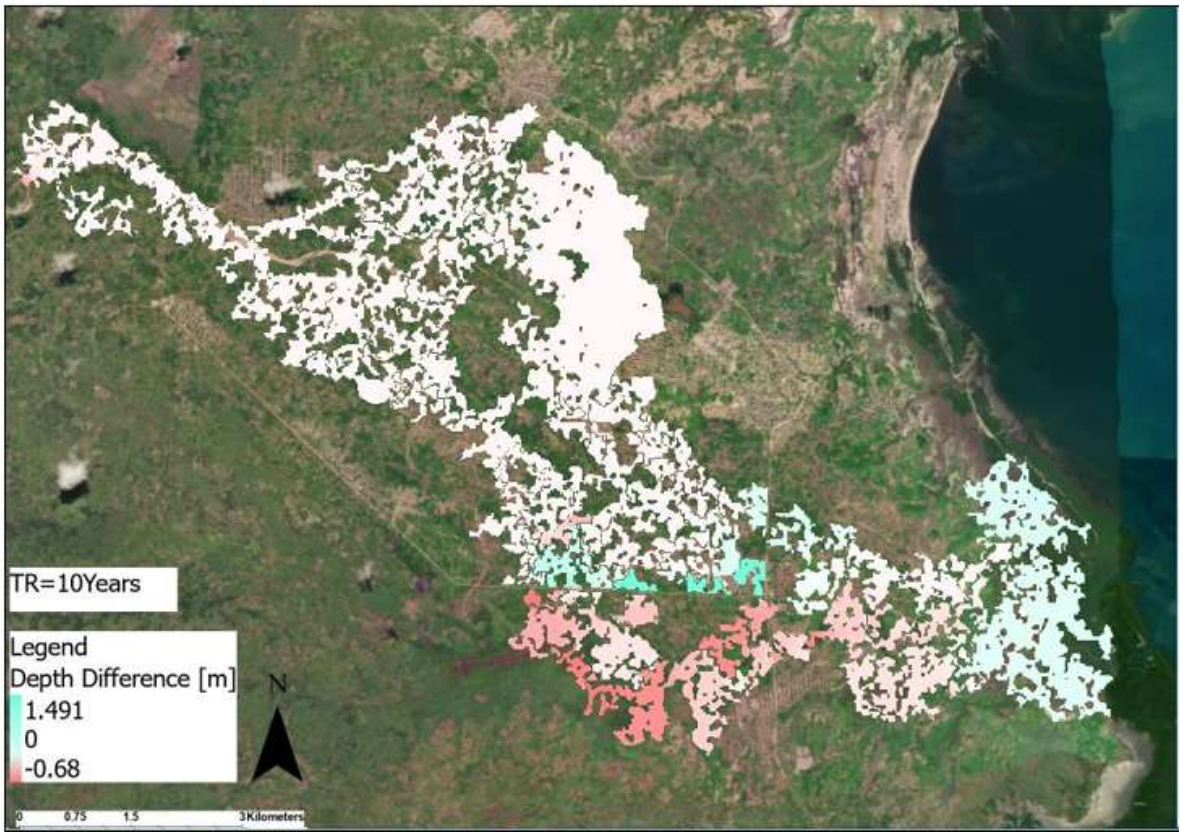

Figure 3-24: The Difference Map of the P10-R and P10-NR Model.

Figure 3-24 displays the Difference map obtained for the P10-R and P10-NR Models. The result is qualitatively similar to that for the previous comparison. The variation in water depth is smaller than in the previous case and ranges from +1.49 m to -0.68 m.

The Difference Maps presented in Figure 3-7 and Figure 3-8 show similarities in terms of results. However, as said, the water depth differences are quite higher in the Difference Map of the L-R and L-NR models than in the P-R and P-NR models. This can be attributed to the fact that terrain geometry has a more substantial impact on water depth variations in the models (L-R and L-NR) that have higher peak discharge values rather than the models (P-R and P-NR) that have relatively small peak discharge values.

3.1.3.2 Water Depth at Specific Locations

A quantitative analysis was performed across all the model results to assess the impact of sub-basin selection in hydrological modeling and terrain geometry choices in hydraulic modeling on water depth distribution within Namuapala village. Considering the subdivision of the village into six different regions shown in Figure 3-9, a total of 23 strategic points were determined, as shown in Figure 3-25. The water depth values at these points were extracted from the raster files of the results

for each set of models. To facilitate a quantitative comparison, a tabular representation of the water depth values corresponding to each point across the whole models is shown in Table 3-9.

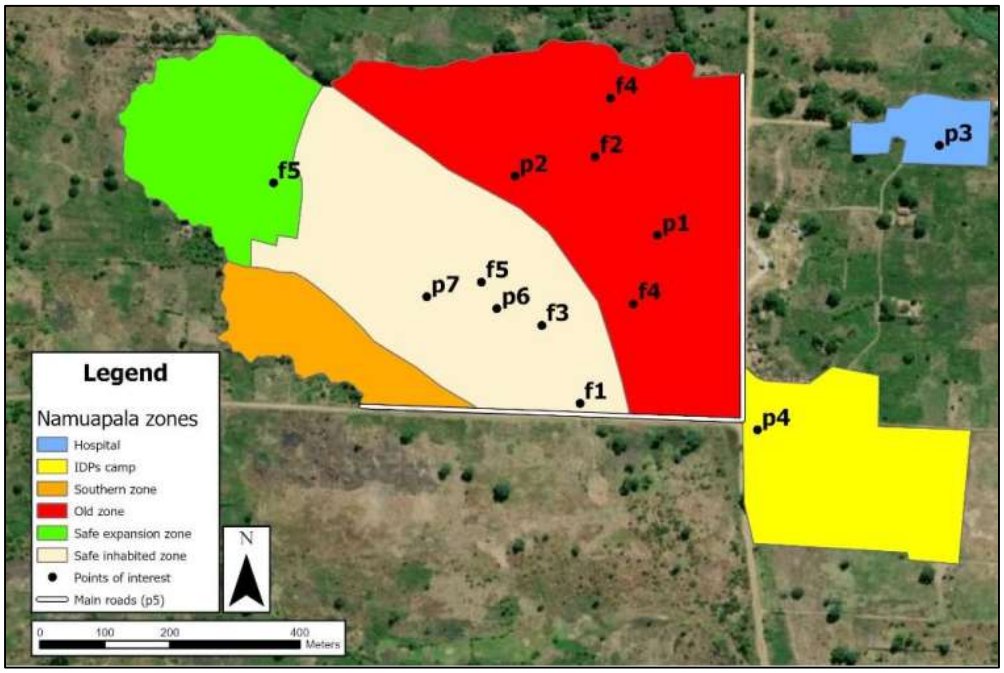

Figure 3-25: Subdivision of Namuapala in six zones. Source: (Paz Idarraga & Rotaru ,2023)

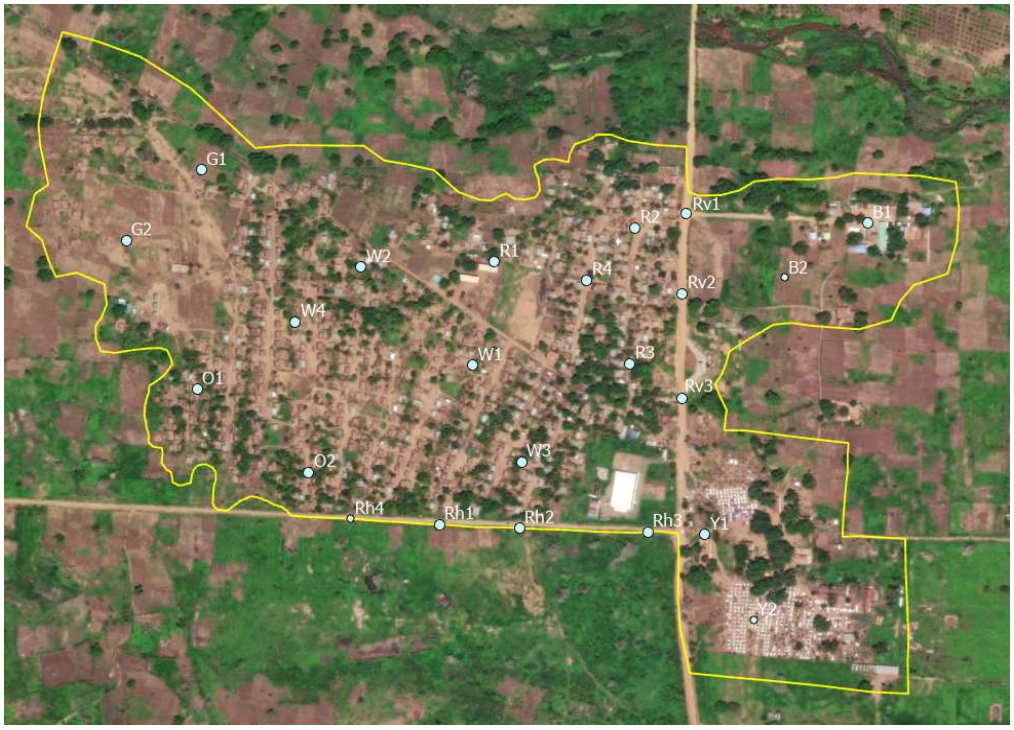

Figure 3-26: The strategic points in Namuapala.

Models	TR	Hmax [m]																						
	[years]	R1	R2	R3	R4	O1	O2	W1	W2	W3	W4	G1	G2	B1	B2	Y1	Y2	Rv1	Rv2	Rv3	Rh1	Rh2	Rh3	Rh4
L-NR	T2	0.28	0.25	0.23	0	0	0.09	0.28	0.14	0	0.14	0	0	0	0.23	0	0.16	0.24	0.24	0	0	0	0.28	0.09
	T10	1.88	1.59	1.45	0.6	0	1.41	0.28	0.14	0	1.16	0.01	0.03	0	1.14	0	0.66	1.58	1.48	0.09	0	0.31	1.17	0.96
	T50	2.06	1.83	1.72	0.83	0.44	0.97	1.84	1.43	0.8	1	0.04	0.06	0	1.41	0	0.79	1.82	1.75	0.28	0	0.56	1.4	0.67
	T100	1.97	1.88	1.8	0.9	0.45	0.99	1.93	1.32	0.8	1.3	0.04	0.09	0	1.57	0	0.95	1.83	1.8	0.64	0	0.75	1.57	0.69
L-R	T2	1.61	1.61	1.61	0.61	0.88	1.87	1.61	0.65	0.6	0.81	0	0.06	0	0	0	0	0	0	0	0	0	0.44	0
	T10	2.4	2.39	2.39	1.4	2.13	2.75	2.45	1.59	1.4	1.76	0.01	1.04	0	0.39	0	0.75	0.39	0.39	0	0	0	1.28	0.62
	T50	2.65	2.62	2.63	1.63	2.22	3.06	2.73	1.85	1.7	2.08	0.21	1.19	0	0.69	0	0.9	0.6	0.62	0	0	0	1.47	0.95
	T100	2.8	2.7	2.79	1.79	2.3	3.18	2.82	1.93	1.8	2.18	0.63	1.29	0	0.79	0	1.05	0.68	0.7	0	0	0	1.61	1.08
S-R	T10	2.09	2.01	2.01	1.01	1.48	2.36	2.02	1.18	1	1.35	0	0.52	0	0	0	0.57	0.01	0.01	0	0	0	0.86	0.35
	T50	2.19	2.18	2.18	1.18	1.72	2.51	2.19	1.38	1.2	1.5	0.01	0.78	0	0.16	0	0.67	0.18	0.18	0	0	0	1.02	0.44
	T100	2.28	2.28	2.28	1.28	1.88	2.61	2.3	1.45	1.3	1.61	0.01	0.83	0	0.27	0	0.68	0.28	0.28	0	0	0	1.13	0.52
	T500	2.41	2.41	2.41	1.41	2.13	2.75	2.45	1.59	1.4	1.76	0.01	1.04	0	0.41	0	0.75	0.39	0.41	0	0	0	1.3	0.62
P-NR	T2	0.06	0.06	0.05	0	0	0.02	0.06	0.03	0	0.03	0	0	0	0.05	0	0.04	0.05	0.05	0	0	0	0.14	0.02
	T10	0.13	0.12	0.12	0	0	0.05	0.13	0.07	0	0.07	0	0	0	0.12	0	0.09	0.12	0.12	0	0	0	0.2	0.05
	T50	0.15	0.14	0.13	0	0	0.06	0.15	0.08	0	0.08	0	0	0	0.13	0	0.09	0.14	0.14	0	0	0	0.21	0.06
	T100	0.16	0.15	0.14	0	0	0.06	0.16	0.08	0	0.08	0	0	0	0.14	0	0.1	0.14	0.14	0	0	0	0.21	0.06
P-R	T2	0.71	0.71	0.71	0	0	0.69	0.71	0.03	0	0.03	0	0	0	0	0	0	0	0	0	0	0	0	0
	T10	1.37	1.37	1.37	0.37	0.41	1.41	1.37	0.38	0.4	0.38	0	0.01	0	0	0	0.01	0	0	0	0	0	0.13	0
	T50	1.55	1.55	1.55	0.55	0.66	1.66	1.55	0.55	0.6	0.59	0	0.01	0	0	0	0.25	0	0	0	0	0	0.37	0
	T100	1.61	1.61	1.61	0.61	0.74	1.74	1.61	0.61	0.6	0.66	0	0.01	0	0	0	0.29	0	0	0	0	0	0.44	0

Table 3-9: The water depth values at points in Namuapala.

Recognizing the complexity of interpreting tabular data, graphical plots were employed to visualize the variations and trends in water depth at these specific point locations. This approach helped present the results clearly and accessibly, enabling a more insightful understanding of the impact of peak discharge values and terrain geometry across all the model sets.

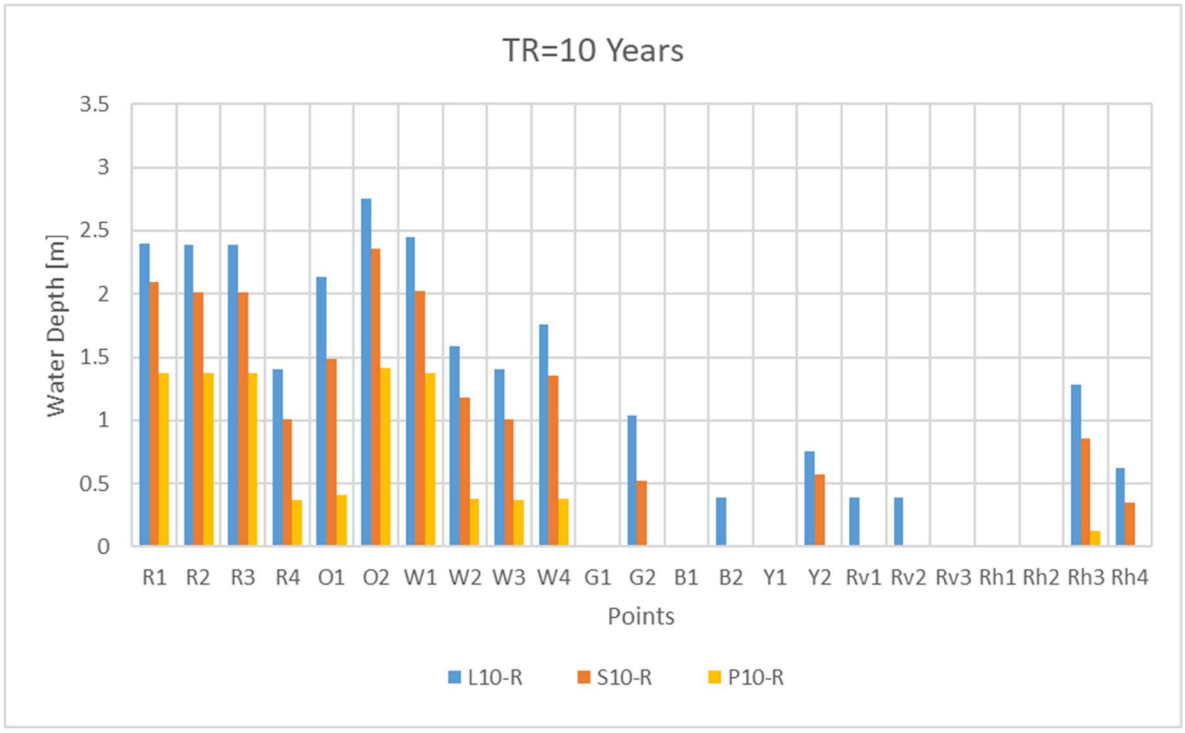

Graph 3- 1: The water depth values at points for TR=10 years considering the L10-R, S10-R, and P10-R models.

Graph 3-1 was employed to examine the variations in water depth values, focusing on model sets with different peak flow discharge values, considering the L-R, S-R, and P-R models for the return period of 10 years. Since models from L to P are characterized by progressively lower flow rates, the

comparison obviously shows the decrease in maximum water depth for decreasing discharge. The L10-R and S10-R models have closer trend alignment than the P10-R model again reflecting closer values of the peak flow rate. However, according to the results of three models (L10-R, S10-R, P10-R), the highest water depth value was obtained in the southern zone at point O2 while considering the results based on the areas, the most critical one is the red one corresponding to the old part of the village. Lastly, there is no water inundation recorded according to three models in the location of the hospital at point B1.

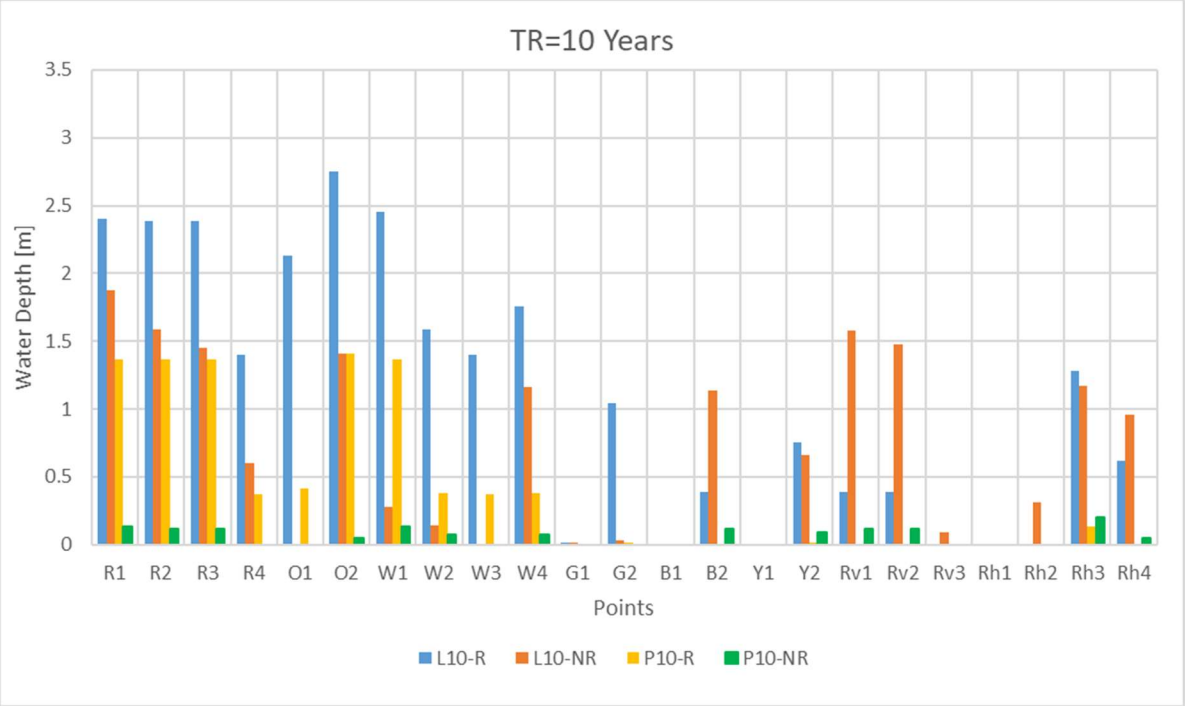

Graph 3-2: The water depth values at points for TR=10 years considering the L10-R, L10-NR, P10-R and P10-NR models.

Graph 3-2 was created to examine the variations in water depth values determined by the inclusion or exclusion of the culverts and elevated roads in the terrain geometry, considering the L-R, L-NR, P-R, and P-NR models (again for the return period of 10 years). The absence of culverts and road height from the terrain geometry results in a significant reduction in water depth heights at certain points (R1 to G2). Conversely, water depth values increase considerably at some points along the roads (Rv1, Rv2, Rh2, Rh4) and at point B2 in the hospital area. This is again attributed to the fact that the elevated roads acted as a barrier in the L10-R and P10-R models. For that reason, their absence allowed water to flow through and reach the other side, causing a rise in water depth values at certain points along the roads and a decrease in depth on the opposite side of the road in the models L10-NR and P10-NR. In particular, it is seen that the effect of peak flow values has a more significant effect on water depth changes in the L10-NR and P10-NR models compared to the L10-R and P10-R models. A notable distinction is clearly visible in the P10-NR model, where water depth values are consistently minimal, often measuring only a few centimeters across the village. In fact, in all the P-NR models the water depth values are very low. The water depth values at specific points considering all the return period scenarios of the model set of P-NR are represented in Graph 3-3. As can be seen from the results of the models, no significant change was observed in water heights even though the return period increased.

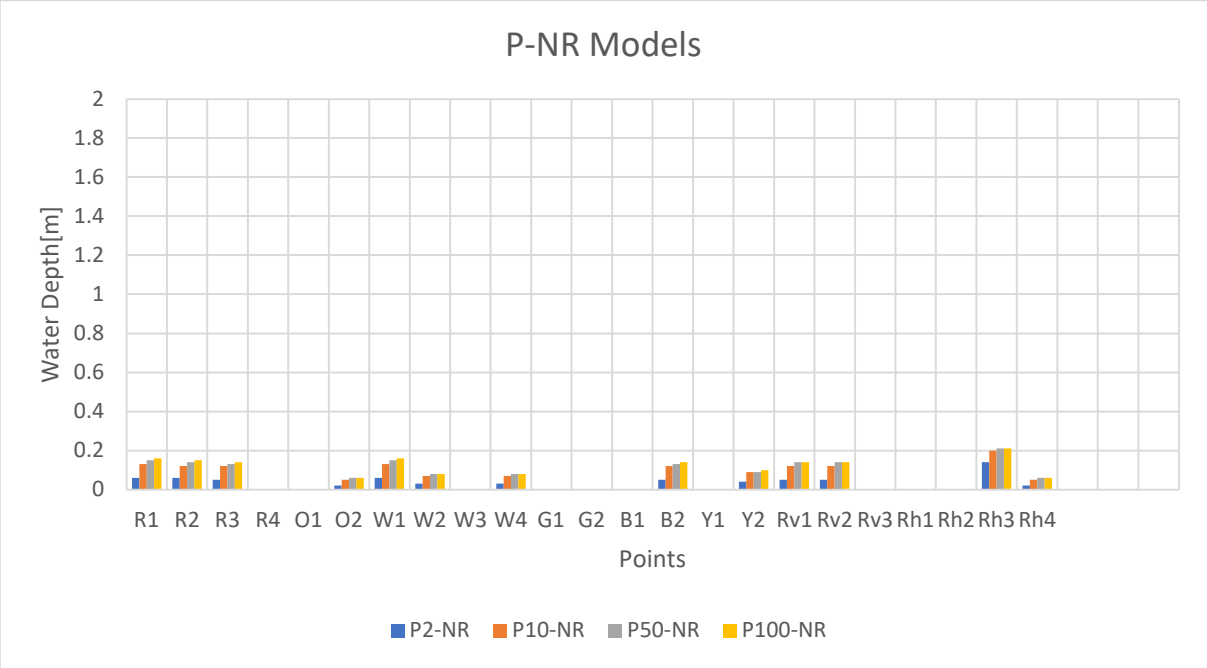

Graph 3-3: The water depths in P-NR Models

3.1.3.3 Comparison of Peak Flow Rates

The comparison of the peak flow discharges employed in the class of models L, P, and S was made by utilizing the scaling plot prepared in the SIXHIARA Project. The scaling plot presented in Figure 3-27 was developed to establish the regional relationship between discharge values and the drainage areas by using the corresponding values of the stations in Malawi (8 stations), Zambia (15), Zimbabwe (6), and South Africa (72) (iCarto & ARA-NORTE, 2017).

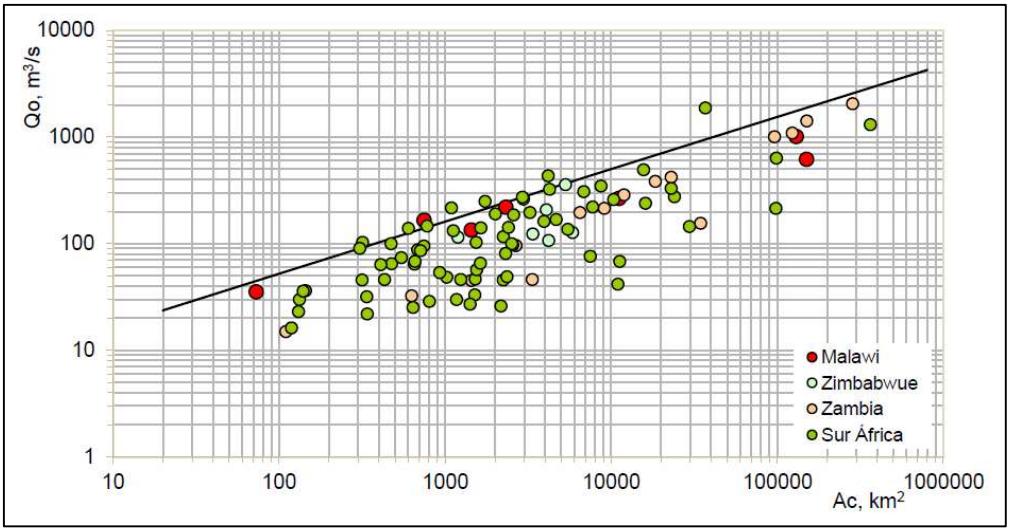

Figure 3-27: Plot of mean annual flood discharges and basin area. Source: (iCarto & ARA-NORTE, 2017)

The plot in Figure 3-27 has been digitalized, and the peak flow rate values of the L, P, and S models have been included in the plot as presented in Graph 3-4 below.

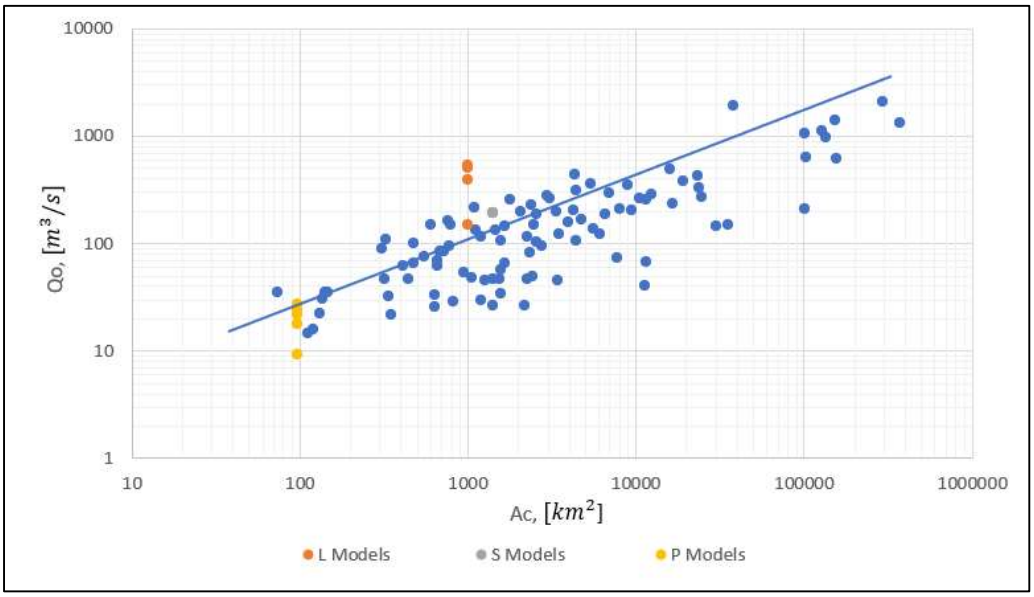

Graph 3-4: Scaling plot of peak flow rates

It can be concluded from Graph 3-4 that the peak flow rate values of the models using a large sub-basin are in relative agreement with this data population, but the values are somewhat high; on the other hand, the peak flow rate values of the models using a small sub-basin are the lowest. Another important factor to note is that the peak flow rate values of both models (L and P) deviate from the probabilistic representation of the Gumbel distribution. This deviation can be attributed to the inadequate applicability of the normalization involving the probability-dependent coefficient used in the Sixhiara Project due to the rainfall-runoff transformation process.

3.2 Results of Damage Assessment

The results of the damage assessment presented in this chapter were obtained using the methods described in Chapter 2. The assessment of damage to residential buildings was conducted at the micro-scale level, ensuring that each building was covered, while the evaluation of roads was performed at the district level. The absolute damage results are illustrated quantitatively in terms of the Repair Cost Maps. Estimates are presented for the affected population, taking into account all return periods of all models.

The damage assessment results were used to generate damage probability curves specific to residential buildings, roads, and the population. Subsequently, these curves were employed for the computation of Annual Average Damage (AAD) values expressed in monetary terms.

The damage assessment for the residential buildings, roads, and population in Namuapala village was carried out for the model sets of L-NR, L-R, P-R, and P-NR. The exclusion of the S-R model set from this assessment was decided due to its hydraulic modeling results, which demonstrated an intermediate trend compared to the other model sets. Moreover, the S-R model set considered the

10, 50, 100, and 500-year return periods, differing from the 2, 10, 50, and 100-year return periods considered by all the other model sets. This decision thus aimed at conducting damage assessment for model sets that exhibit more distinct characteristics and share comparable parameters, ensuring a more meaningful and relevant analysis.

Lastly, a sensitivity analysis was conducted based on the risk in terms of annual average damage (AAD) estimation for residential buildings, roads, and population to investigate the impact of varying sub-basin selection and terrain geometry among model sets (L-NR, L-R, P-R, and P-NR) on damage assessment results (beyond the sensitivity analysis for the hazard shown above).

3.2.1 Relative and Absolute Damages of Residential Buildings

The results of the relative damage to the residential buildings are presented as Building Damage Level Maps (Figure 3-28, Figure 3-29, Figure 3-30, Figure 3-31) regarding four models corresponding to 2, 10, 50, and 100-year return periods in terms of expected damage level. The layout of the maps depicts the flood water depth and damage levels. Water depths below 0.15 m were excluded from the analysis as they were considered not to cause damage to buildings.

According to all the damage level maps, the very high damage level is most observed in the L-R, while for the P-NR model, only a low damage level is observed for residential buildings. Additionally, by excluding the L-R model, it is observed that there is a safe zone with no damage to some buildings in the southern part of the village. When the results are investigated zonally within the village the most affected residential buildings were observed in the northeastern area of the village.

The absolute damage results of residential buildings considering four return periods for all models are represented as maps in Figure 3-32, Figure 3-33, Figure 3-34 and Figure 3-35. These maps present the estimated repair cost for each building according to their water depth level for four different models. The layout of the maps contains the water depth and repair cost.

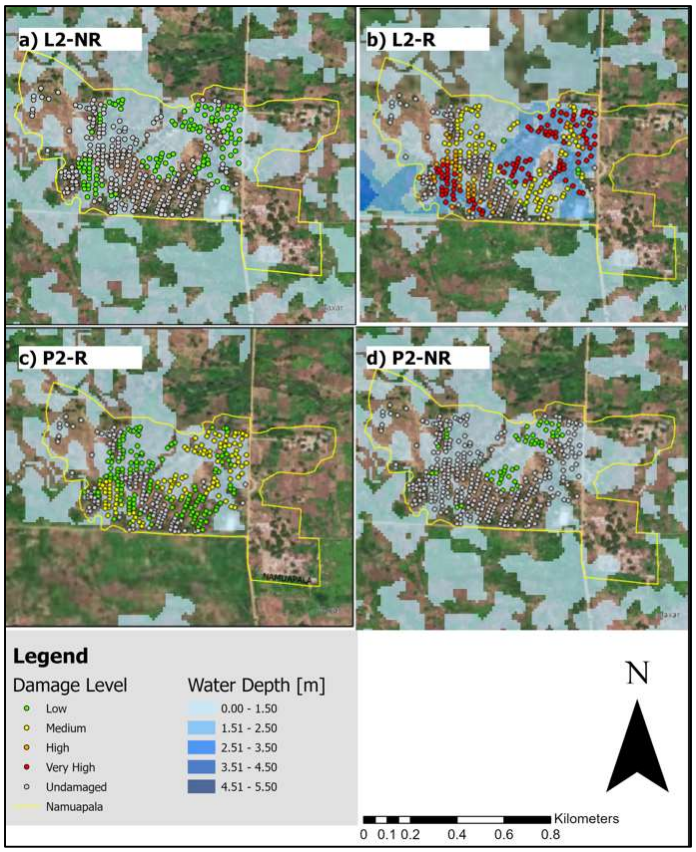

Figure 3-28: Building Damage Level Maps of Models (a-d) for TR=2 years

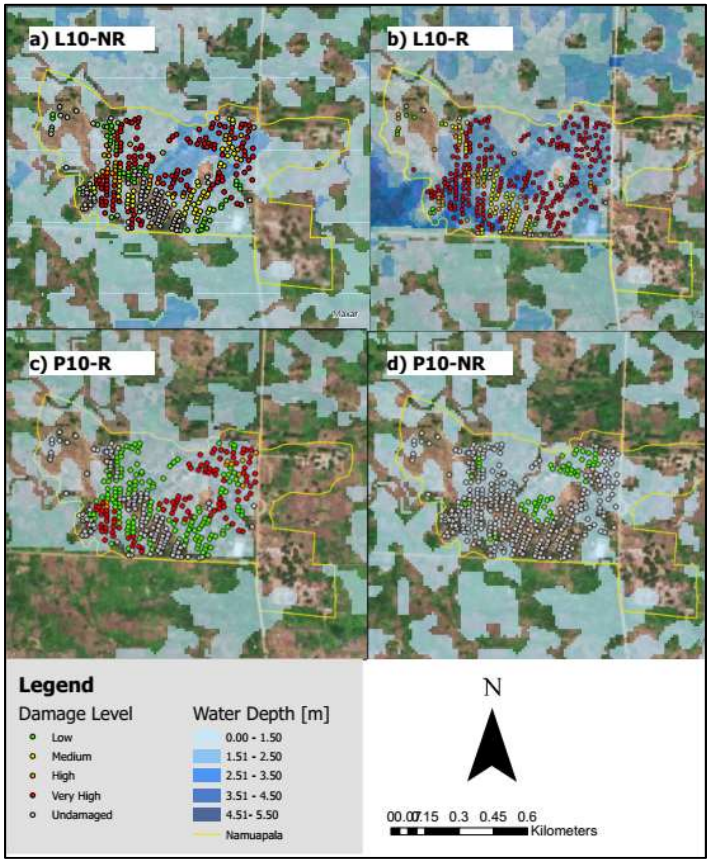

Figure 3-29: Building Damage Level Maps of Models (a-d) for TR=10 years

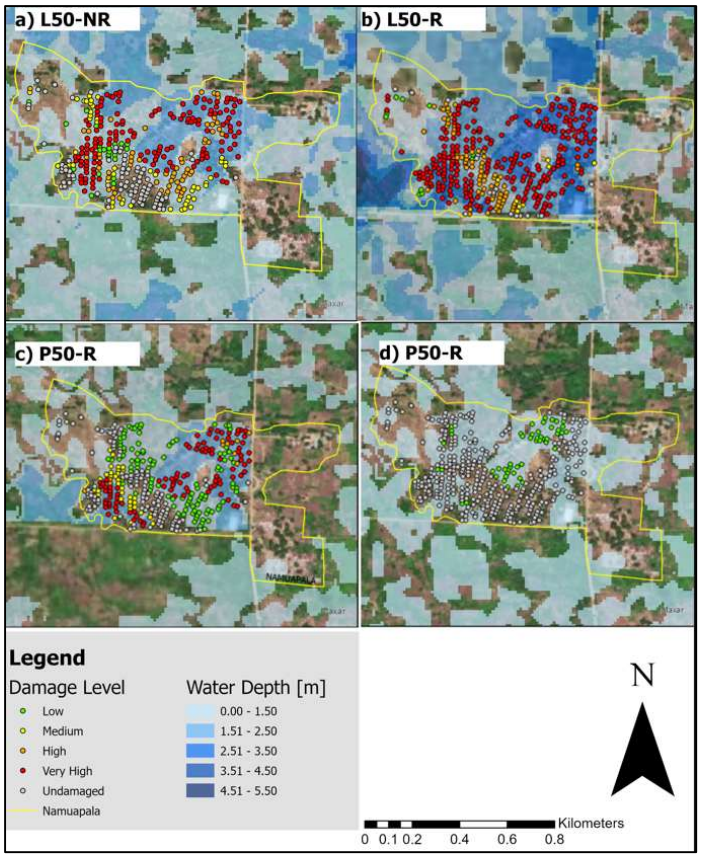

Figure 3-30: Building Damage Level Maps of Models (a-d) for TR=50 years

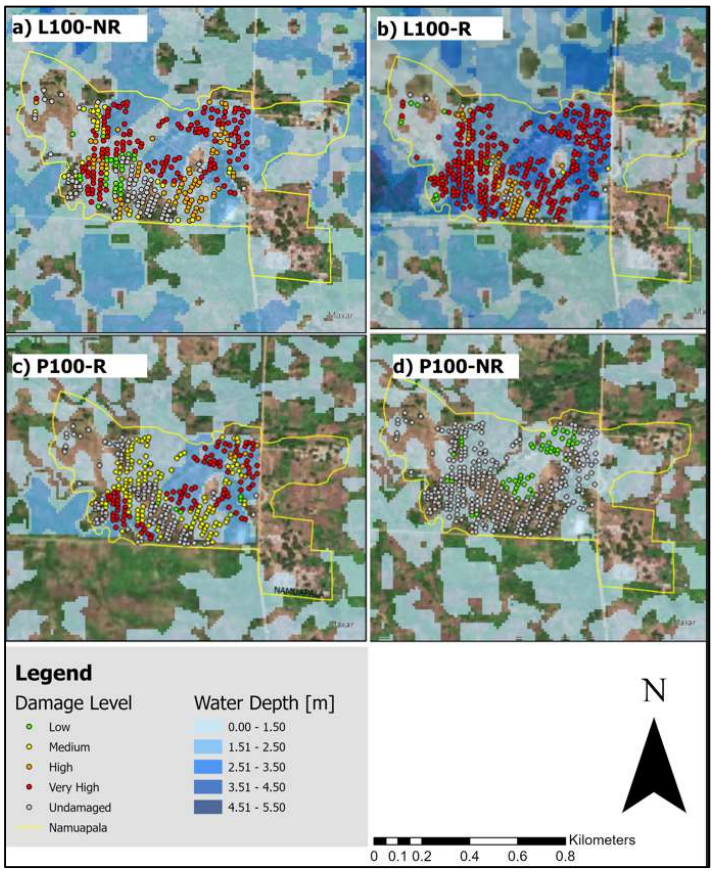

Figure 3-31: Building Damage Level Maps of Models (a-d) for TR=100 years

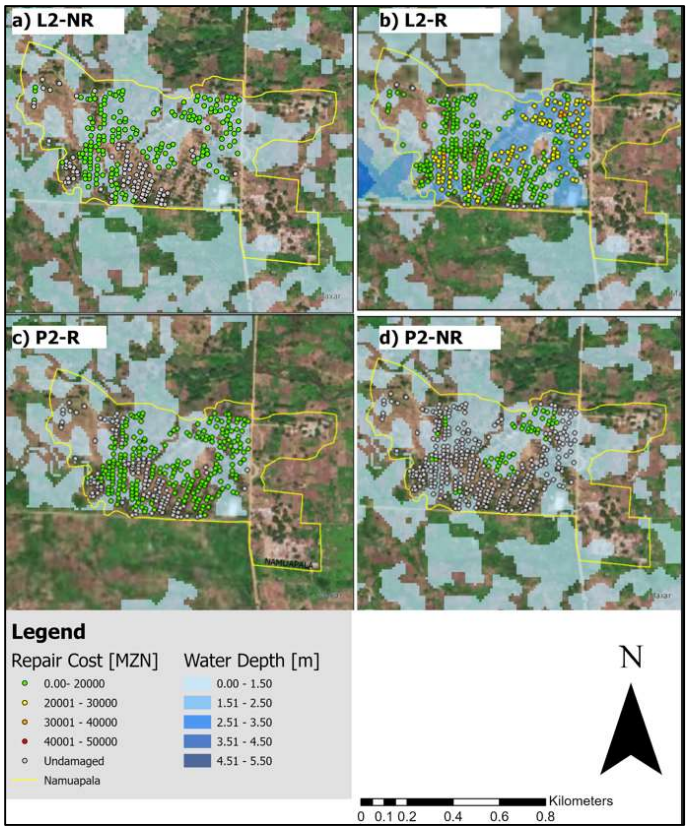

Figure 3-32: Building Repair Cost Maps of Models (a-d) for TR=2 years

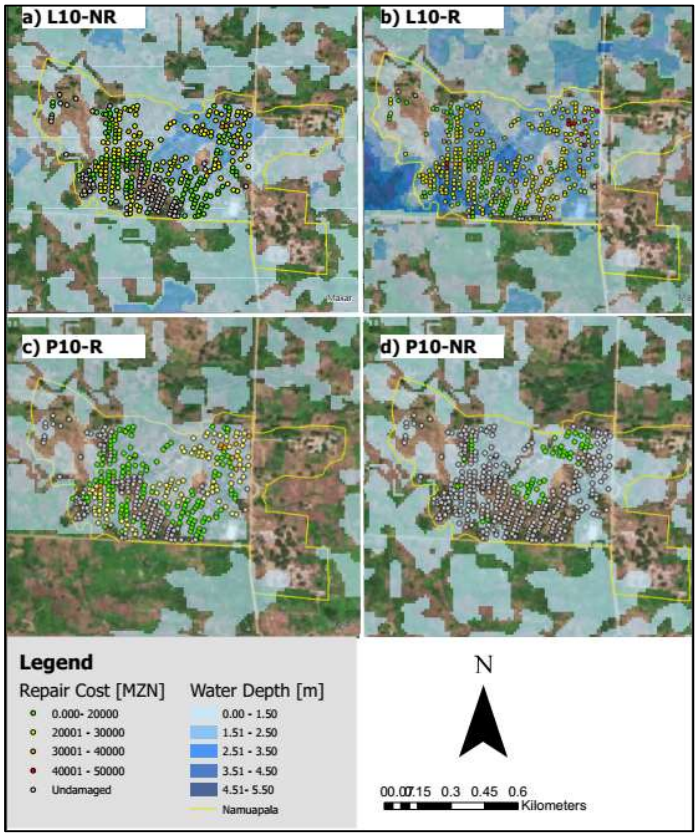

Figure 3-33: Building Repair Cost Maps of Models (a-d) for TR=10 years

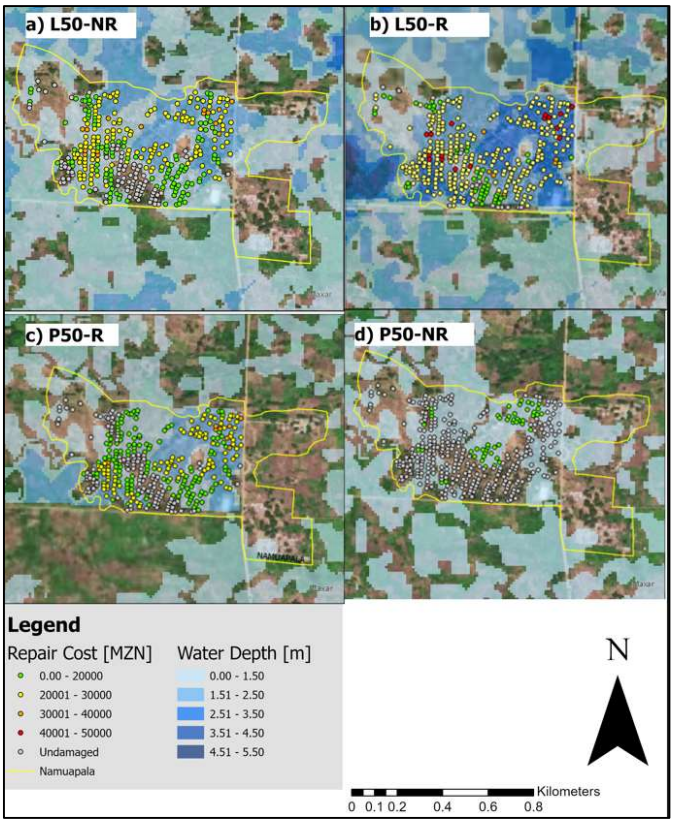

Figure 3-34: Building Repair Cost Maps of Models (a-d) for TR=50 years

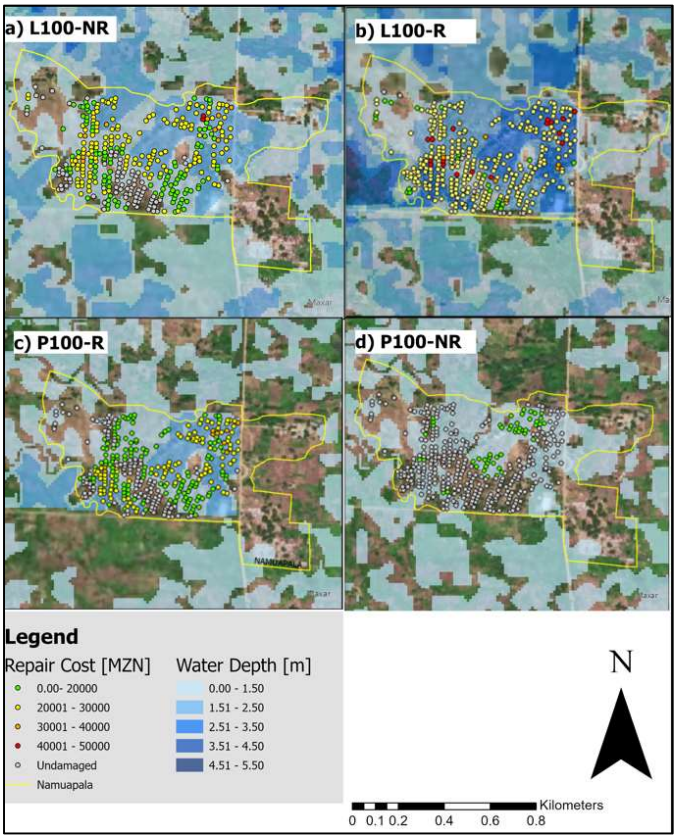

Figure 3-35: Building Repair Cost Maps of Models (a-d) for TR=100 years

3.2.2 Affected Population

As mentioned above, the estimated affected population was calculated by taking into account the number of residential buildings impacted by each damage level, the return periods of each model, and the average number of inhabitants per house. The results are presented for each model set as charts (Chart 3-1, Chart 3-2, Chart 3-3, and Chart 3-4) indicating the return period of the model sets and the number of people affected for each damage level. According to the results, Chart 3-2 provides the highest number of affected individuals across all return periods among other model sets, and as can be seen, the majority of the affected population is at a very high damage level. On the other hand, according to the results of Chart 3-4, it has the least number of affected individuals compared to other model sets, and all affected people are observed to be at a low damage level across all return periods. It is worth noting that the total population of the village is 2368 people when interpreting these results.

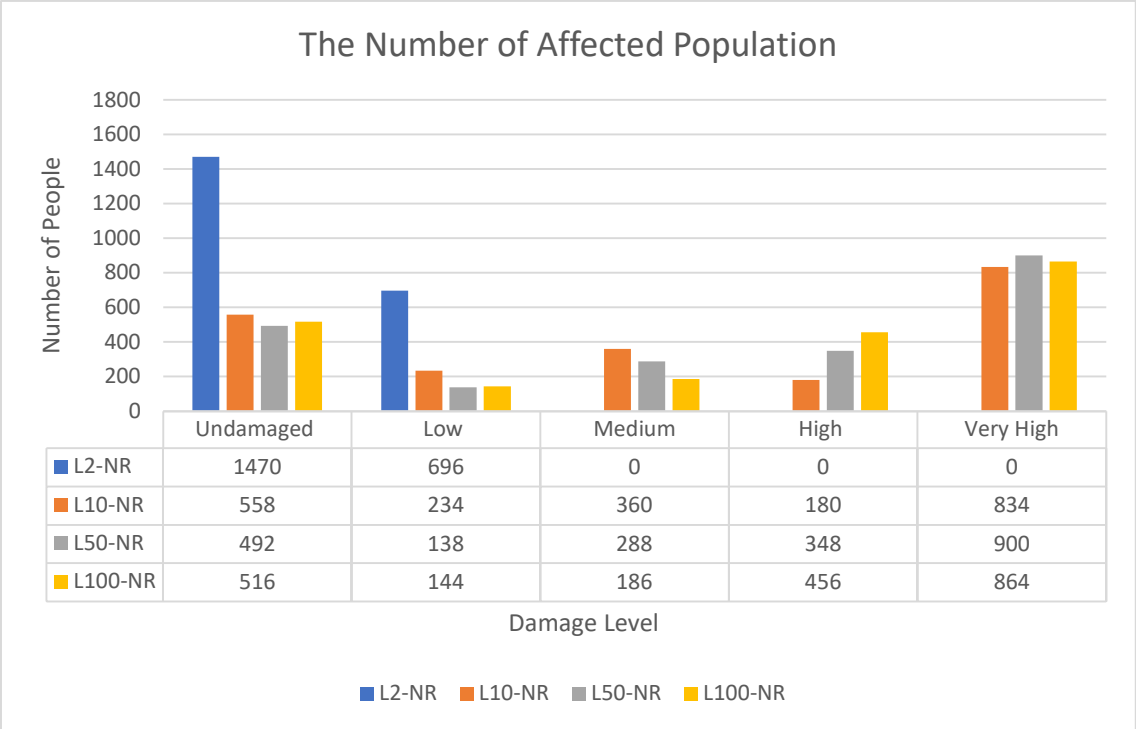

	Undamaged	Low	Medium	High	Very High
L2-NR	1470	696	0	0	0
L10-NR	558	234	360	180	834
L50-NR	492	138	288	348	900
L100-NR	516	144	186	456	864

Chart 3-1: The number of affected people for the L-NR models

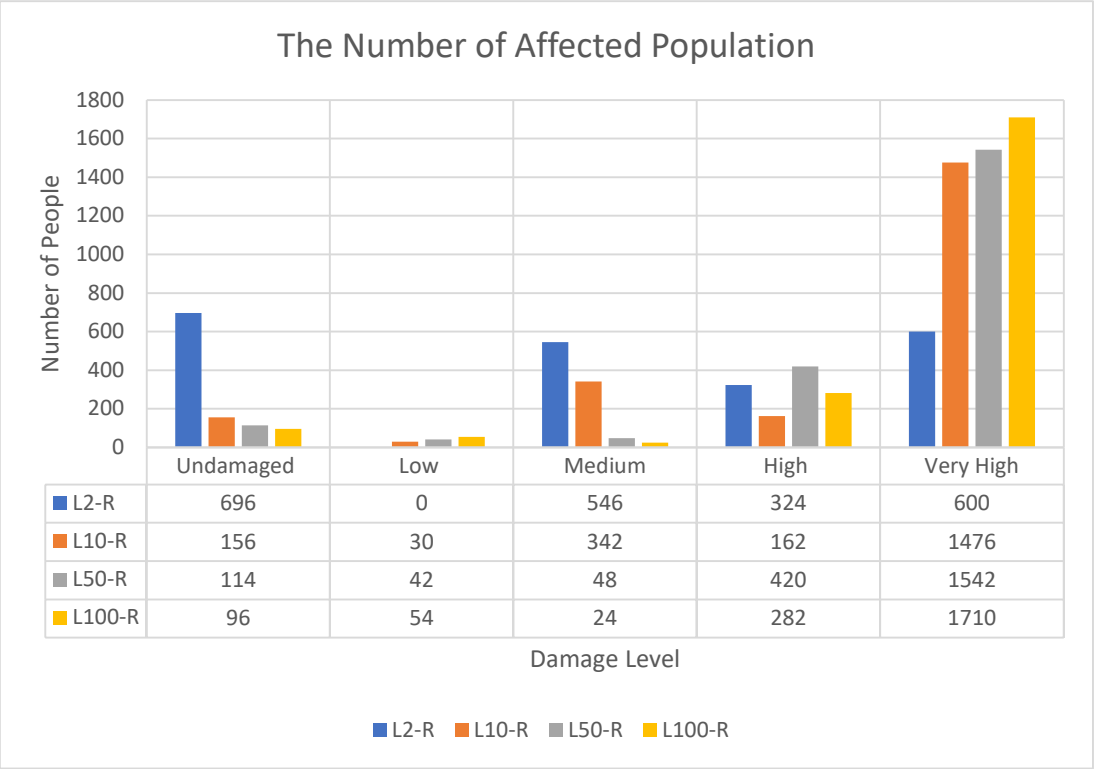

Chart 3-2: The number of affected people for the L-R models

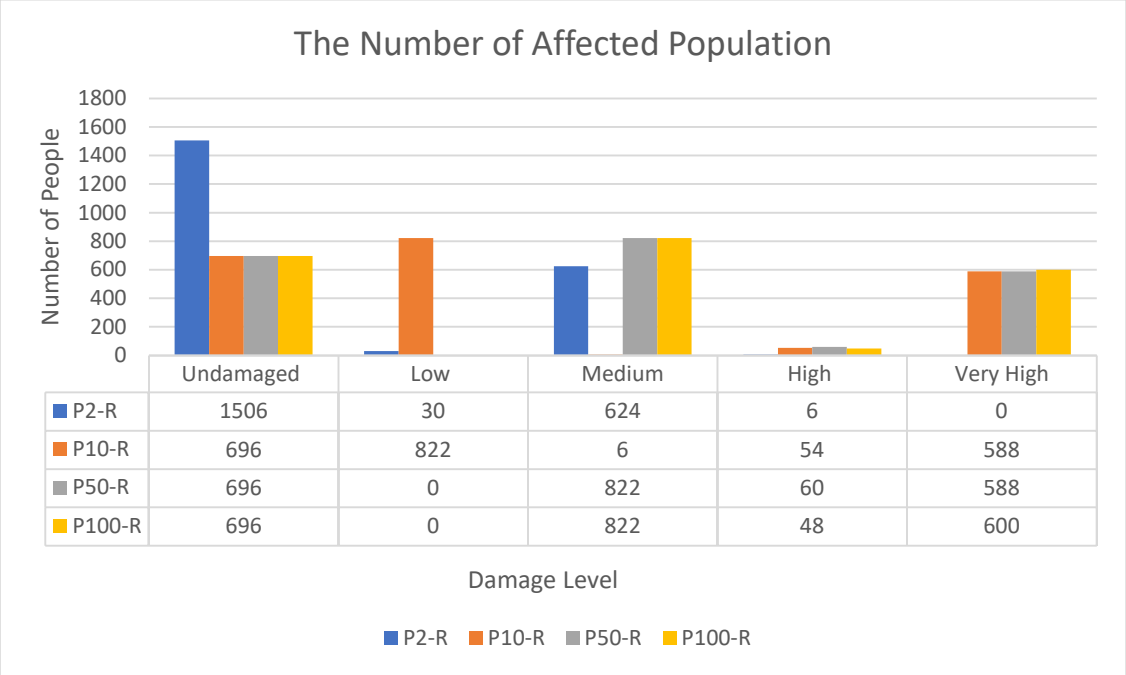

Chart 3-3: The number of affected people for the P-R models

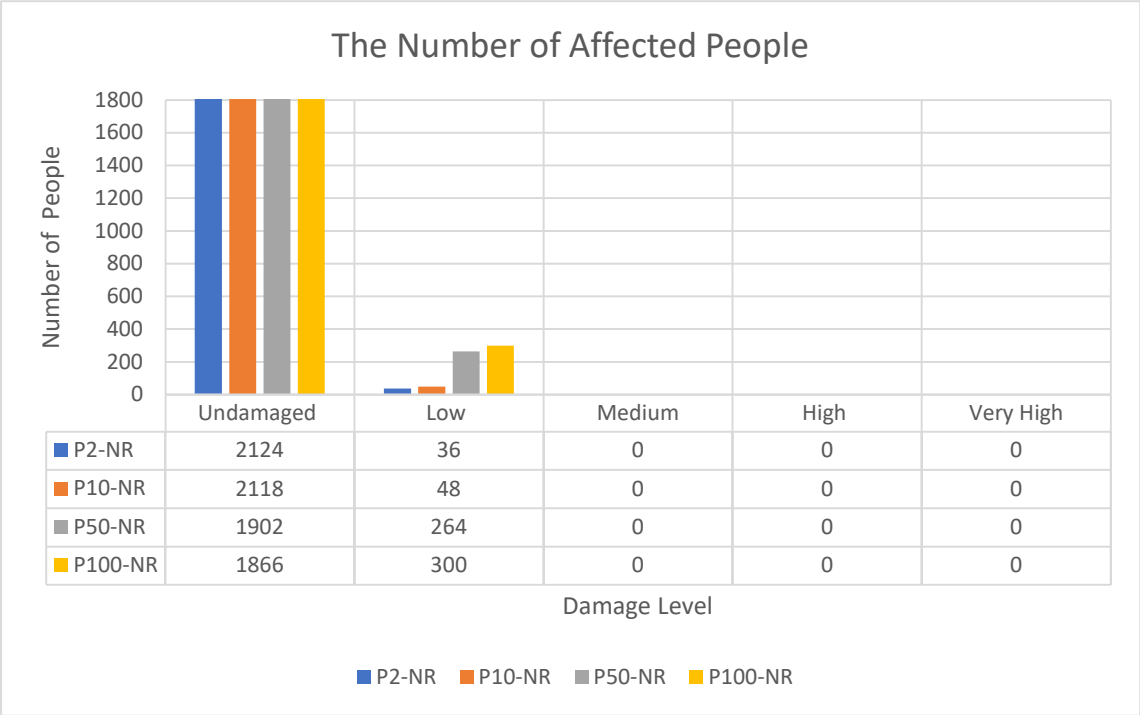

Chart 3-4: The number of affected people for the PN-R models

3.2.3 Relative and Absolute Damages of Roads

The results of the estimated damage to roads for each model according to four different return periods are shown as Road Damage Level Maps in Figure 3-36, Figure 3-37, Figure 3-38 and Figure 3-39. The layout of the maps depicts the damage level and flooded area, and as in the case of residential buildings, the same ranges for the damage level representation were chosen. The road passing through the center of Namuapala village is depicted in Figure 3-37 to have some sections with a high to very high damage level according to the L-NR model, a very high damage level according to the L-R model, medium to low damage levels according to the P-R model. In the case of the P-NR, no damage is obtained to that relevant road.

The absolute damage results of the roads are represented in Figure 3-40, Figure 41, Figure 42, and Figure 4, as Road Repair Cost Maps corresponding to 2, 10, 50, and 100-year return periods, respectively, for all models, illustrating the expected repair cost of the road segments. In this case, the layout of the map includes the repair cost and flooded area.

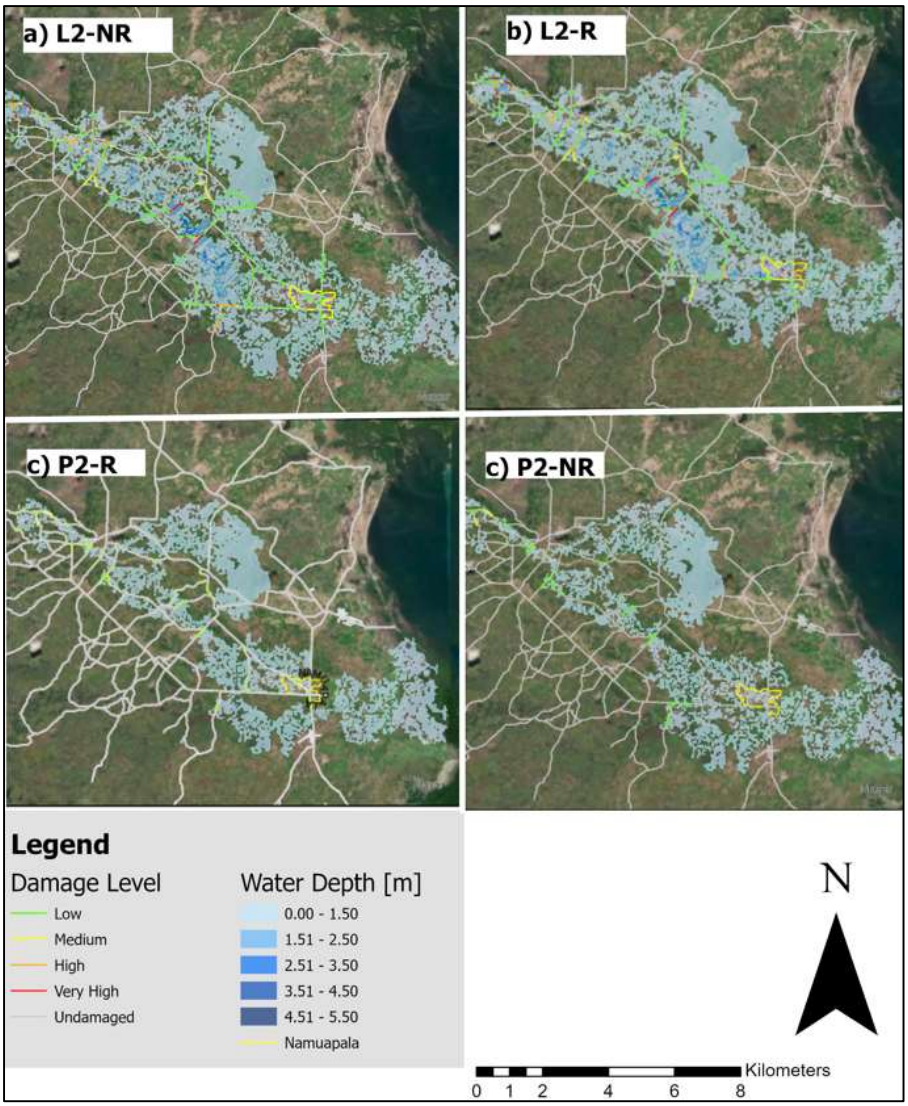

Figure 3-36: Road Damage Level Maps of Models (a-d) for TR=2 years

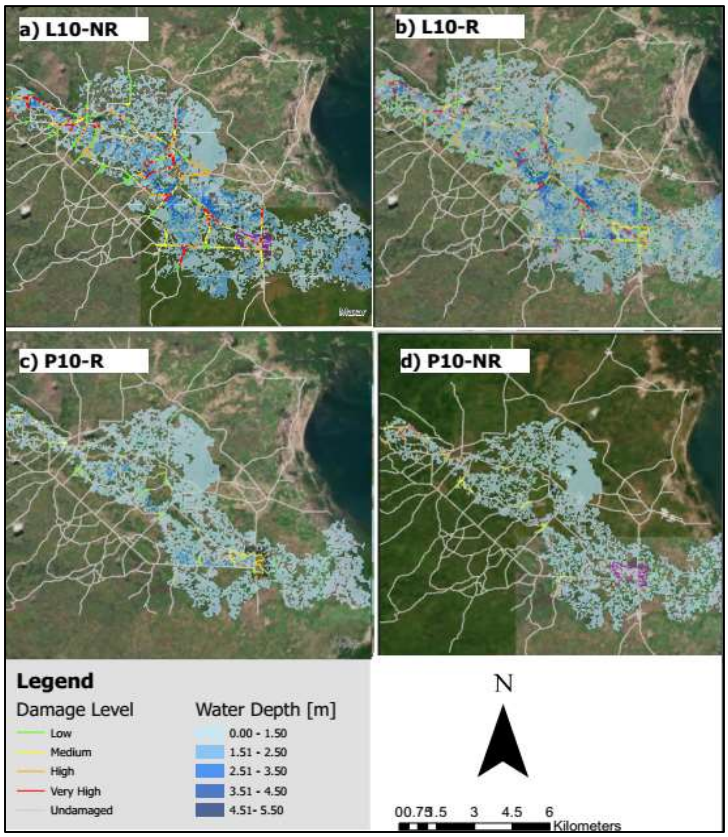

Figure 3-37: Road Damage Level Maps of Models (a-d) for TR=10 years

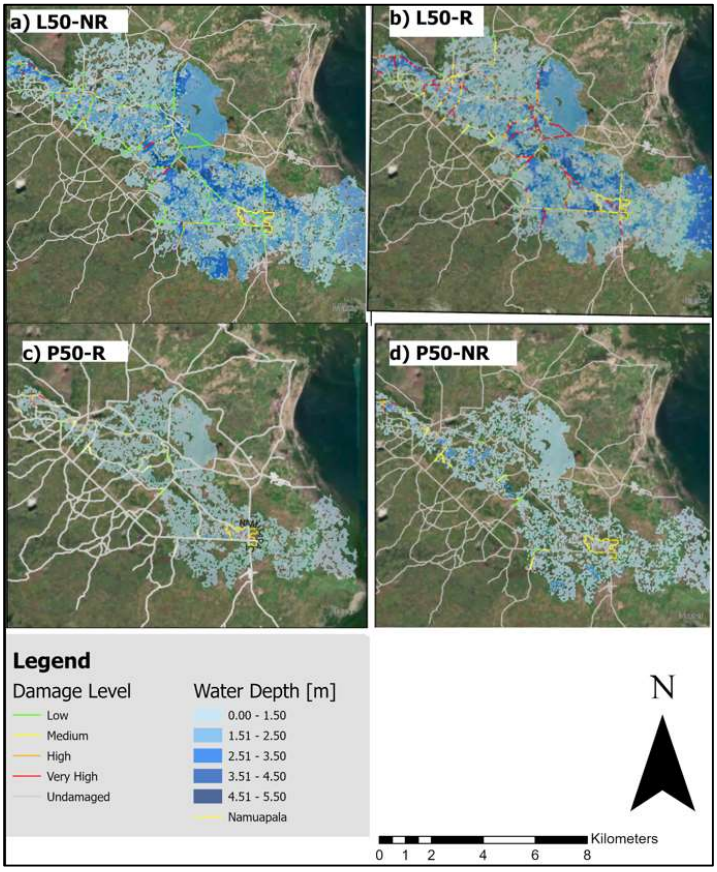

Figure 3-38: Road Damage Level Maps of Models (a-d) for TR=50 years

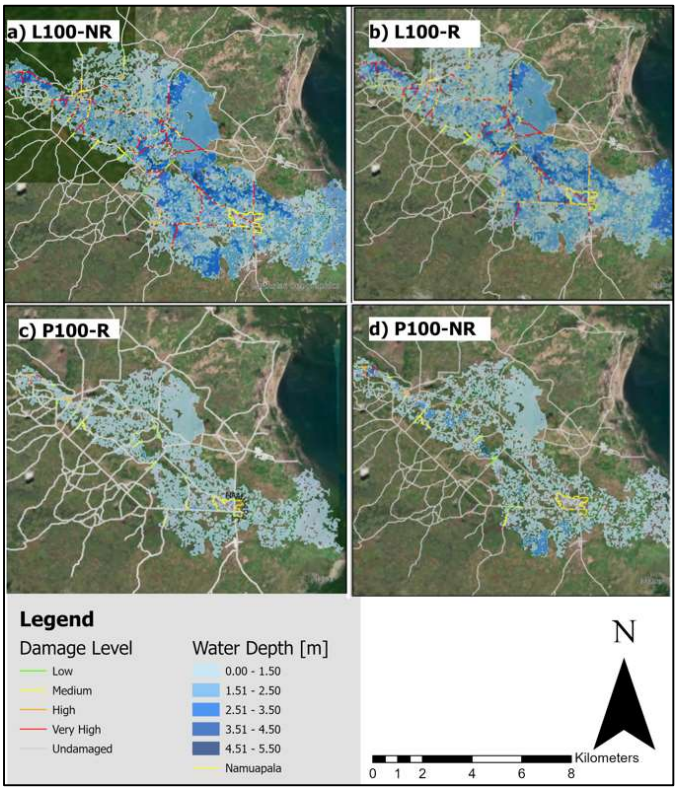

Figure 3-39: Road Damage Level Maps of Models (a-d) for TR=100 years.

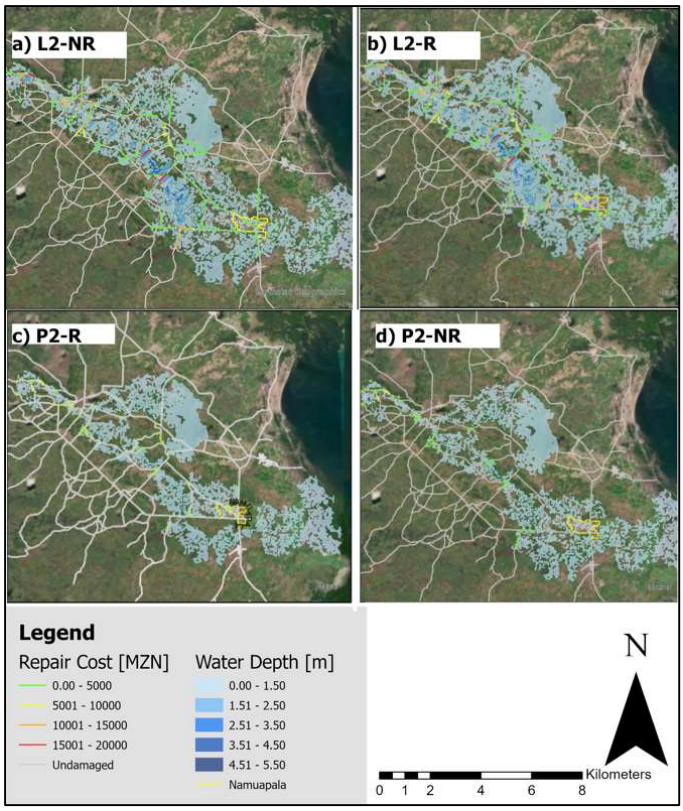

Figure 3-40: Road Repair Cost Maps of Models (a-d) for TR=2 years

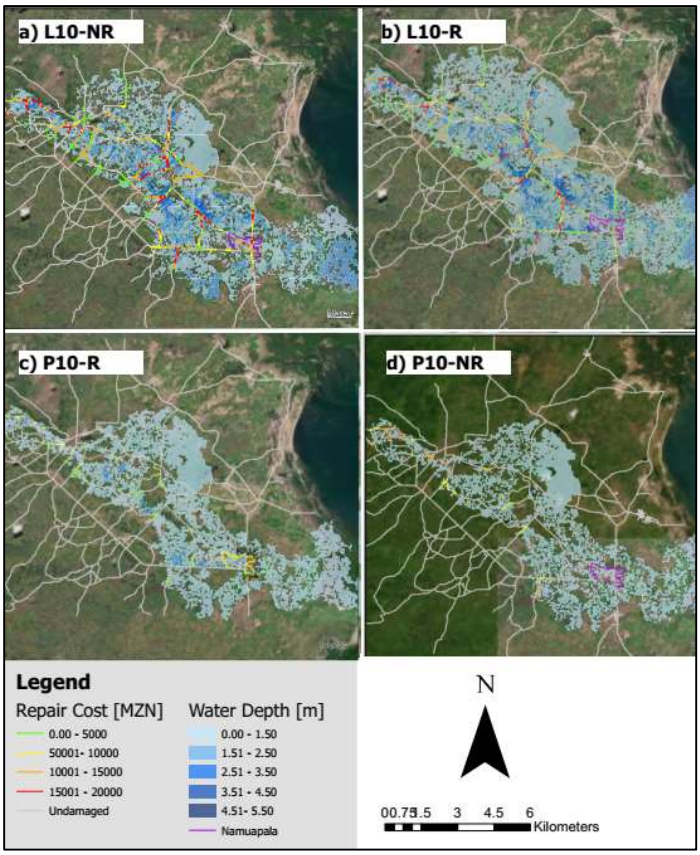

Figure 3-41: Road Repair Cost Maps of Models (a-d) for TR=10 years

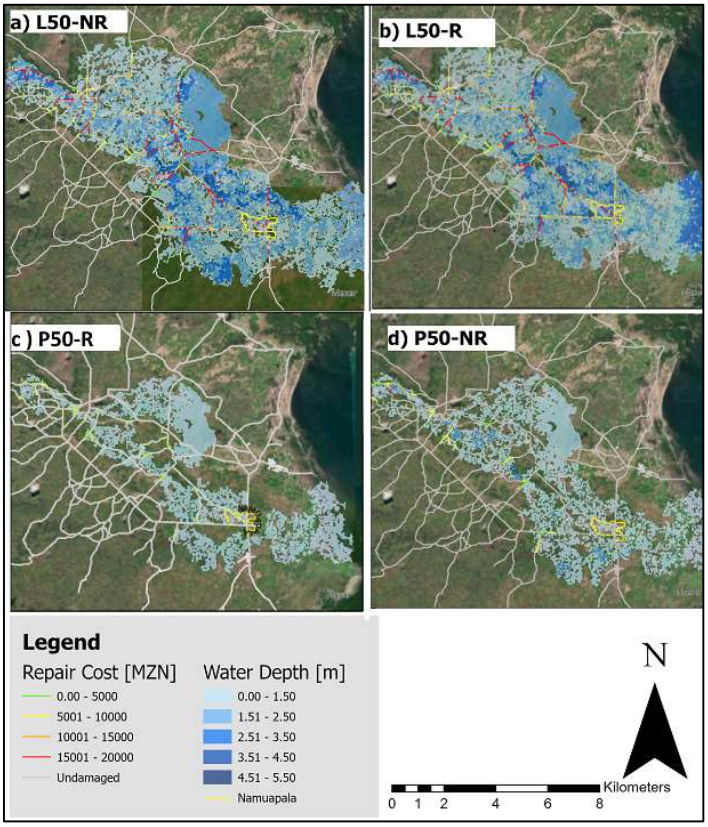

Figure 3-42: Road Repair Cost Maps of Models (a-d) for TR=50 years

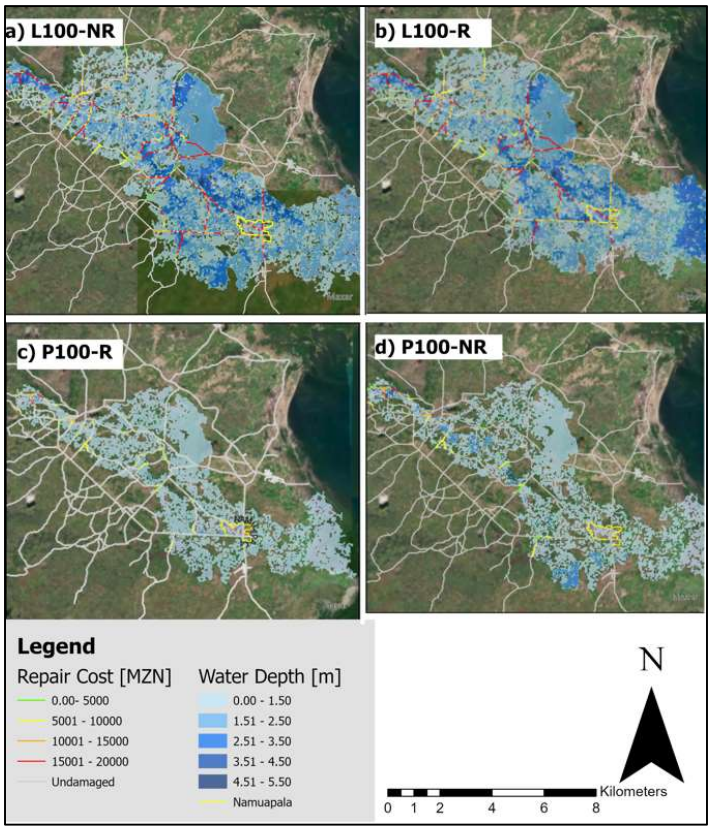

Figure 3-43: Road Repair Cost Maps of Models (a-d) for TR=100 years

3.2.3 Sensitivity Analysis to Annual Average Damage (AAD)

The estimated absolute damage to residential buildings, roads, and the population for each model set served as the basis for constructing damage-probability curves. These curves are obtained considering all return periods present in each model set; by calculating the integral of the area under these curves, the risk in terms of the average annual damage (AAD) is determined in economic terms for residential buildings and roads. In the case of the population at risk, annual average damage is expressed in terms of the expected affected number of people per year.

The comparison of the obtained values shows how the different assumptions used in the hydrologic (sub-basin selection) and hydraulic (geometry of the terrain) models affect the AAD estimation for the considered categories.

The damage-probability curves and corresponding AAD values of residential buildings for each model set are represented in Figure 3-44. The model with the highest annual average damage value for residential buildings is observed to be L-R, which incorporates a large sub-basin in hydrological modeling and elevated roads in hydraulic modeling. As a result of selecting a large sub-basin, it led to higher peak flow discharge values, consequently resulting in higher water levels. This situation, while causing more damage to buildings, has increased the annual average damage value; for instance, in P-R, which considers a small sub-basin, the AAD value has significantly decreased by a factor of approximately three. Another factor influencing the attainment of the highest AAD value in L-R is the elevated roads in hydraulic modeling. Elevated roads hinder the flow of water, causing water to accumulate in the area where buildings are located and resulting in further damage. This situation is

better understood through a comparison of AAD values and damage-probability curves between L-R and L-NR. Elevated roads lead to an approximately threefold increase in the AAD value, and the exclusion of these roads in the L-NR has caused the expected damage to decrease, especially for the 2-year return period (0.5 exceedance probability). The terrain geometry used in hydraulic modeling has a more significant impact on the annual average damage values for residential buildings in models that assess small sub-basins than in models that assess large sub-basins. This can be clearly seen from the decision not to elevate roads in the terrain geometry, which has led to a significant decrease in the annual average damage for the P-NR, up to a hundredfold reduction. Unlike the other curves, in P-NR, there is an evident difference after 0.1 exceedance probability until 0.01 and it resulted in a drastic trend in the curve therefore, the highest impact on the AAD values is due to the 0.01 and 0.02 exceedance probabilities.

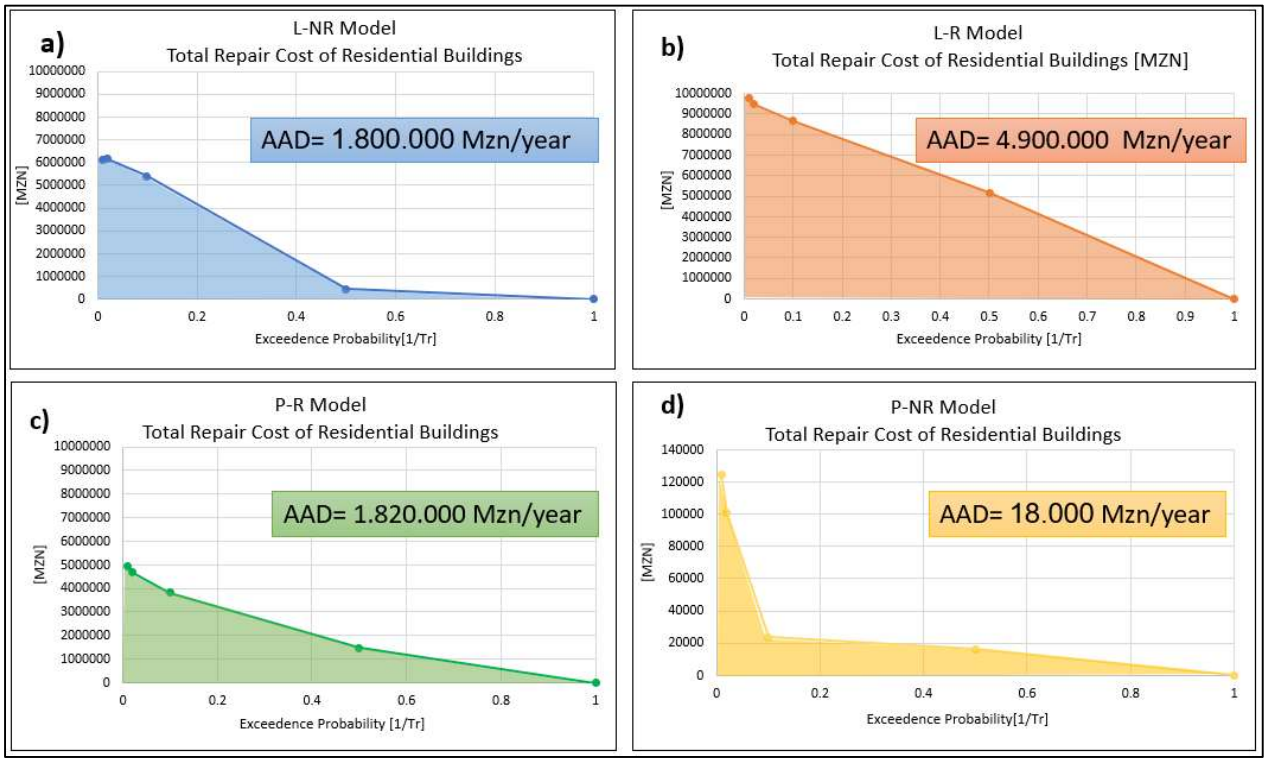

Figure 3-44: Damage-probability curves for residential buildings. a) Damage-probability curve of L-NR Model b) Damage-probability curve of L-R Model c) Damage-probability curve of P-R Model d) Damage-probability curve of P-NR Model

The expected annual average damage considering the population in people/year was calculated based on the damage-probability curves for each model set, as shown in Figure 3-45. As in the case of residential buildings, the highest AAD value for the population was obtained in L-R, with the number of 1247 people in a year. While elevated roads cause the AAD of affected people to increase almost twice as much as in models using large sub-basins, the most significant effect is observed in the 0.5 exceedance probability. Since the calculation of the affected population is obtained based on the number of affected buildings at each damage level, the barrier effect created by elevated roads has led to a significant increase in the water level at the 2-year return period compared to other exceedance probabilities. This has resulted in a substantial rise in damage levels of buildings and, consequently, the number of affected population. On the other hand, the most significant impact of elevated roads on AAD values is observed in models that use small sub-basins (P-R and P-NR). In P-NR, the removal of elevated roads leads to a dramatic decrease in the AAD value by approximately fifteen times. When examining the damage-probability graphs of models that exhibit variations in elevated roads, it is observed that the graph trends of L-R and L-NR models are similar, whereas the

same cannot be said for P-R and P-NR, which significantly diverge from each other. The reason for this divergence is attributed to the almost absence of the affected population in the 0.5 and 0.1 exceedance probabilities evaluated in P-NR. It is clearly evident from the AAD values and curve graphs that the selection of sub-basins nearly doubles the damage affecting the population considering L-R and P-R. In summary, it has been observed that the impact of terrain geometry used on damage outcomes in models using large sub-basins is found to be less sensitive compared to models using small sub-basins.

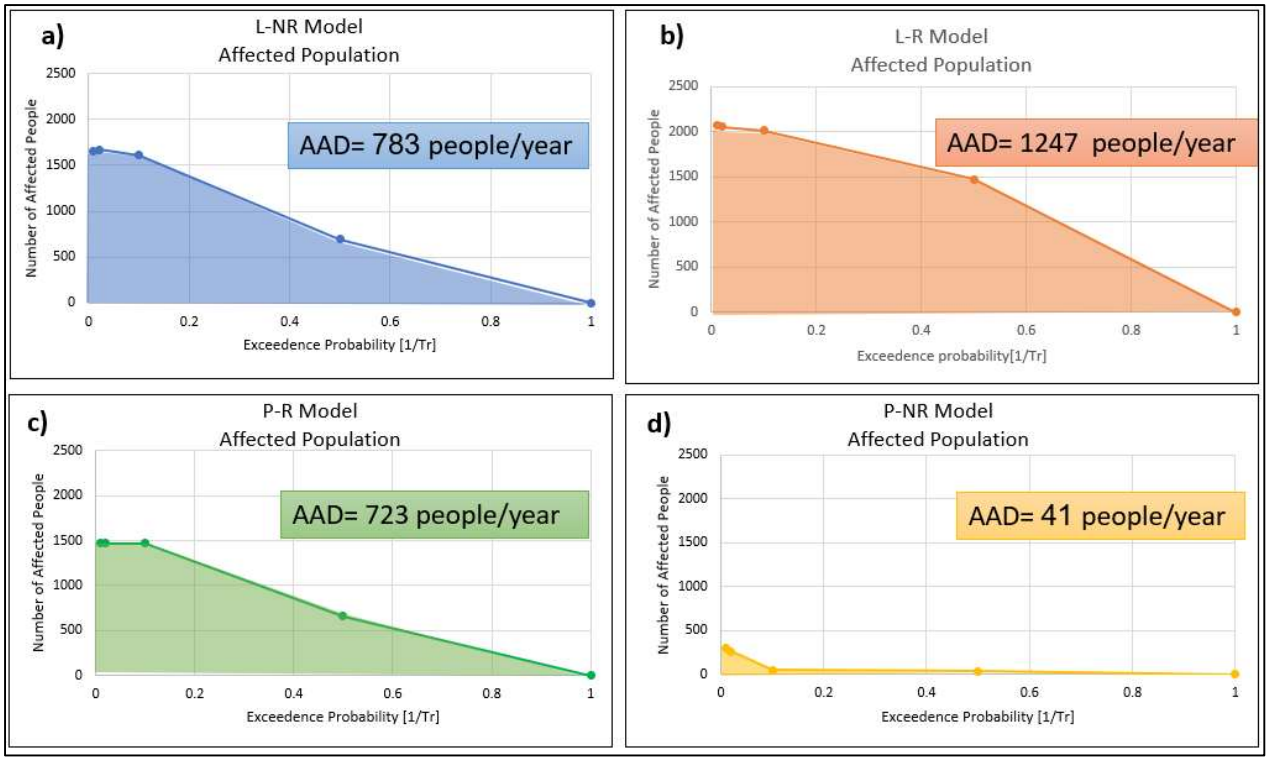

Figure 3-45: Damage-probability curves for population. a) Damage-probability curve of L-NR Model b) Damage-probability curve of L-R Model c) Damage-probability curve of P-R Model d) Damage-probability curve of P-NR Model

The expected annual average damage to roads in terms of MZN per year is finally estimated for each model set, again through obtained damage-probability curves, as shown in Figure 3-46. The highest calculated average annual damage for roads was obtained in the L-NR that utilized the large sub-basin and unelevated roads. As can be seen, the AAD value of L-R, which uses the same large sub-basin but includes elevated roads, is only slightly lower than the value of L-NR. This can be explained by considering that in L-R, the roads did not suffer from damage if the water levels reaching the roads were less than 2 m because those roads were raised by 2 m in the terrain geometry used in hydraulic modeling. In addition, considering that damage assessments of the roads were at the district level, the absence of the barrier effect created by the elevated roads in L-R also amplified the estimated damage. This is because the water flow continued from Namuapala village, and the roads in the lower parts of the district were exposed to higher water levels than L-R.

As seen from Figure 3-46, unlike the residential buildings and population curves, the damage-probability curve trends of the roads in all models are quite similar. This indicates that the increment in damage rate as the exceedance probabilities decrease is quite similar across all models. The sub-

basin selection has a significant impact on damage assessment outcomes for roads. The AAD values and curves of L-R and P-R clearly demonstrate this impact. The selection of a large sub-basin, compared to small sub-basins, has resulted in higher water depth and inundation areas, leading to an increase in the expected annual average damage for roads by up to approximately four times.

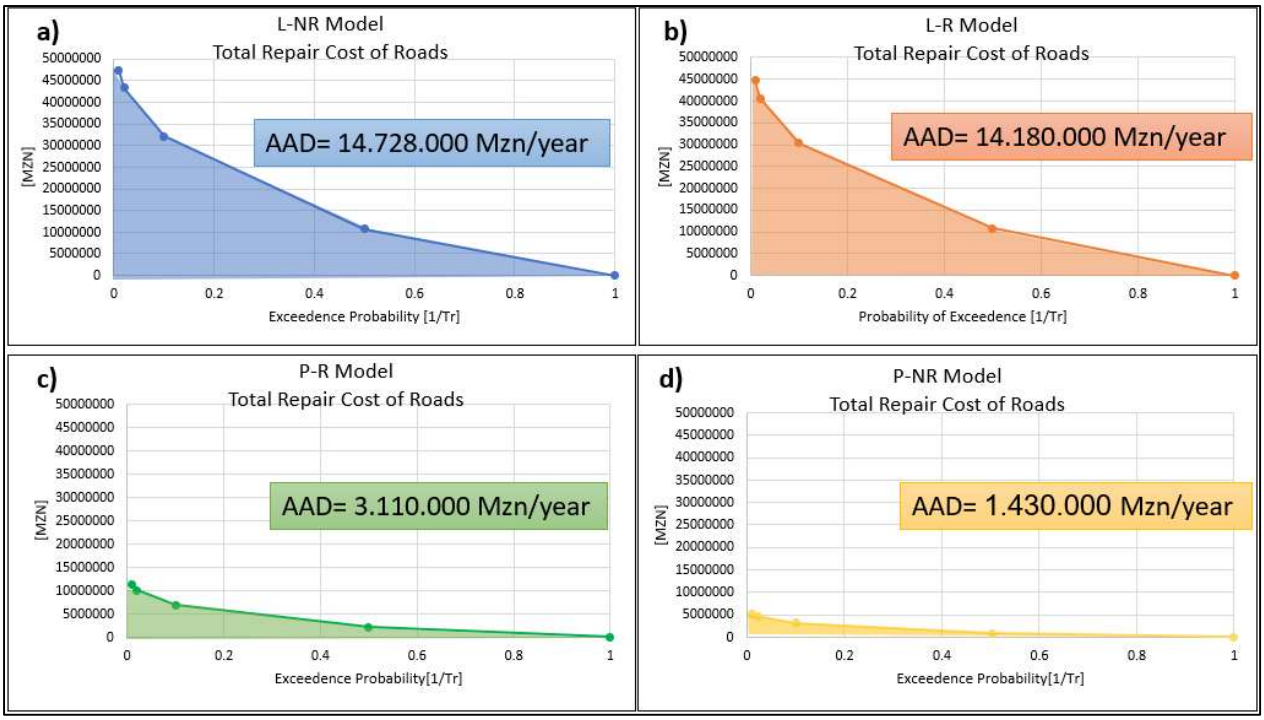

Figure 3-46: Damage-probability curves for roads. a) Damage-probability curve of L-NR Model b) Damage-probability curve of L-R Model c) Damage-probability curve of P-R Model d) Damage-probability curve of P-NR Model

There is a distinct difference in the behavior of buildings and population compared to roads. This divergence arises from the fact that the evaluation of buildings and population occurs at a local scale, while the assessment of roads takes place at a district scale. Additionally, it's important to consider that the assessment of Namuapala is influenced by the specific location of the village. If the village were situated elsewhere, its sensitivity to model parameters would likely be different. However, this does not apply to roads, as a district-scale assessment encompasses all locations.

3.3 Discussion

Within a sensitivity analysis, that was performed because the participatory approach spotted some underestimation of the flood magnitude and impact by the prior studies, the present thesis has been focused on sub-basin selection and local geometry of the terrain. Since large uncertainties in flood hazard modeling are due to the complex and dynamic nature of hydrological processes, sub-basin selection plays a crucial role in the assessment. The water level depths and flooded areas obtained in the previous study were quite limited; therefore, a more traditional approach of considering rainfall distributed on the entire watershed was applied. Furthermore, the identified contradiction between information obtained from ad hoc surveys and the previous manipulation of terrain geometry in the hydraulic model, along with the evidence of highly underestimated damage at a micro-scale, led to prioritizing the analysis of changes in local geometry.

Quite reasonable results have been obtained for the effects on the hazard and damage assessment of employing a larger sub-basin in the hydrological model as well as removing the elevated roads in local geometric data. Employing a larger sub-basin as intended returned higher peak discharge values and, thus, an increase in water depths and flooding area. Moreover, removing the roads that were functioning as barriers created dynamics in which the places that are immediately upstream of these barriers are in a better condition and the places that are immediately downstream of these barriers are in a worse condition. The quantification of these effects has been evaluated by identifying the water depths at specific locations in the village and by developing the damage-probability curves for each considered asset to estimate risk in terms of AAD for each model set. The changes in the AAD, determined by the modeling choices, were also reasonable.

According to the hazard and damage assessment results of all model sets, it was determined that, for the time being, the most appropriate model set to describe the flood impact in Namuapala is the L-NR model set. The reason behind this determination was according to the information from ad hoc surveys conducted by local technicians and outcomes of the participatory meeting held with local stakeholders. The definition of the so-called safe area in the village by the local stakeholders showed that the results of the L-R model set were not compatible because there was no such safe area in the village according to the results. Conversely, in the P-R and P-NR model sets this safe zone was obtained, but the general level of safety was overestimated in terms of damage and water depth levels. In the hazard and damage assessment results of the L-NR model, it was possible to see the safe area, even though it was maybe narrower than expected by stakeholders.

Every time one performs any kind of modeling, calibration would be a necessary process to ensure the accuracy and reliability of model predictions by adjusting model parameters to match observed data. Unfortunately, in this study, model calibration could not be performed because the necessary detailed data were not available. In fact, the indications given by the locals during the participatory approach, though precious at a qualitative level, could not be considered as quantitative drivers for model tuning.

Other sources of uncertainty are obviously present but were not considered within the sensitivity analysis (for example, the roughness of the surfaces or geometric changes to be applied at a larger scale). These were not investigated because roughness was considered a secondary effect compared to that of many irregularities still present in the terrain model. Second, the other terrain data that were found in prior works have a lower spatial resolution than that used in the models.

However, a local geometric change had a significant impact on the flood pattern and impact (obviously, this is true as long as a village very close to where the change was applied is considered). This indicates that the modeling approach would be suitable for exploring the effect of other

geometric changes, for example, those related to building some mitigation measure, which can be a major focus to follow-up studies.

Chapter 4: Conclusions

This study, conducted in collaboration with the NGO Oikos in Mozambique, addressed challenges associated with flood risk assessment, with a specific focus on the rural community of Namuapala, Cabo Delgado province. The research was part of a series of theses aimed at enhancing the reliability of flood risk assessments in this data-scarce region. In particular, the participatory approach outlined in the study of Paz Idarraga & Rotaru (2023) served as a foundation for this research. Some assumptions made in prior studies required reassessment. Above all, the feedback received during the meeting with local authorities emphasized that the flood damages were underestimated.
The process of creating flood inundation maps is affected by uncertainties in data, modeling approaches, and parameters. It is important to note that these uncertainties in the mapping process subsequently impact the accuracy and reliability of damage assessments. To address these uncertainties, the study employed a comprehensive modeling chain, integrating hazard and damage assessment. The main objective was to assess the influence of geometric, hydraulic and hydrologic modeling assumptions on the water depth levels in the village and the expected monetary loss incurred annually (average annual damage, AAD) due to flooding events.

This study thoroughly investigated the selection of sub-basins in hydrological modeling. This analysis was focused on understanding the uncertainties associated with upstream boundary conditions for hydraulic modeling, where the input flow plays a pivotal role. The entire flood inundation process is indeed mainly influenced and propelled by the input flow; therefore, it was decided to choose a larger (compared to prior studies) sub-basin in hydrological modeling to provide higher volumes of water into hydraulic modeling. In this way, the obtained inundation areas and water depth levels were expected to be higher. Simultaneously, the uncertainty of terrain geometry in hydraulic modeling was assessed, recognizing its crucial significance for accurate local-scale predictions of water depth. After conducting ad hoc surveys along the two main roads intersecting Namuapala, it became apparent that they were not as high as previously modeled. The discrepancy between the actual topography and the previous representations was identified and, to analyze the local effects of the geometry on modeling outcomes, additional hydraulic simulations were performed by removing the elevated roads.

Expanding the sub-basin size in the hydrological model and excluding elevated roads from local geometric data in the hydraulic model had significant and reasonable effects on hazard and damage assessment results. Enlarging the sub-basin led to higher peak discharge values, resulting in increased water depths and widerflooding areas. Additionally, as expected, the removal of roads acting as barriers altered the flooding dynamics, with areas immediately upstream experiencing lower water depths and those downstream facing higher water depths. These effects were quantified by assessing water depths at specific locations in the village and estimating the Average Annual Damages (AAD) for residential buildings, affected people, and roads for the different models.

This study focused only on the selection of the sub-basins and the local geometry since they emerged as the main source of uncertainty. Other aspects, such as the effects of roughness, were not considered. This was due to the fact that for localized water depths, the spatial resolution and DEM become much more influential. Unfortunately, analyzing the effects of a more detailed DEM on results was hindered by the unavailability of such data for the study area.

Despite the participatory approach yielding water depth data for Namuapala's various significant buildings (such as schools, hospitals, mosques, churches, etc.) during two preceding events - Cyclone Kenneth in 2019 and a flood in 2021 - this information was not utilized for model calibration. Firstly,

the return period of the two prior events remained unknown. Secondly, the information, reported orally by local residents, carried an inherent uncertainty in terms of reliability.

However, this approach not only facilitates a comprehensive understanding of the direct implications of different assumptions on flood risk but also provides an opportunity for broader application. By incorporating the calculation of the AAD (annual average damage), this methodology would enable a more thorough assessment of the impacts of various mitigation measures. Analyzing how the introduction of any protective infrastructure would affect flood risk, may not only yields valuable insights for designing effective mitigation strategies but also set the stage for a comprehensive cost-benefit analysis. When extended to other local geometry variations, this methodology has the potential to significantly contribute to the development of context-specific and economically viable flood risk mitigation measures.

Overall, this study represents a crucial milestone in the Institute Oikos' project, which aims at addressing the climate crisis in Mozambique by actively involving local communities and institutions in preparing for and mitigating the impacts of climate change. The insights gained from this study serve as a foundational framework for subsequent actions in the district. The methodology outlined in this study serves as a guide on how to confront the issue of uncertainties and data scarcity and is adaptable to similar contexts.

Chapter 5: BIBLIOGRAPHY

Almeida, Isabel & Kaufmann Almeida, Aleska & Anache, Jamil & Steffen, Jorge & Alves Sobrinho, Teodorico. (2015). Estimation on Time of Concentration of Overland Flow in Watersheds: A Review. Geociencias. 33. 661-671.

Cea, L., Álvarez, M., & Puertas, J. (2022). Estimation of flood-exposed population in data-scarce regions combining satellite imagery and high resolution hydrological-hydraulic modelling: A case study in the Licungo basin (Mozambique). *Journal of Hydrology: Regional Studies*, *44*, 101247.

Coulibaly, T., Islam, M., & Managi, S. (2020). The impacts of climate change and natural disasters on agriculture in African countries. *Economics of Disasters and Climate Change*, *4*, 347-364.

Copernicus Land Monitoring Service, & European Environment Agency (EEA). (2021). https://land.copernicus.eu/pan-european/corine-land-cover

Docampo, E., Pascual-Ferrer, J., Mera, I., Penas, V., Peña, E., Vilanova, E., & Pérez-Foguet, A. A Multidisciplinary Partnership to support Water Resources Management in Cabo Delgado: stakeholder's participation as a key factor.

Eckstein, D., Künzel, V., & Schäfer, L. (2021). *Global Climate Risk Index 2021: Who Suffers Most Extreme Weather Events? Weather-Related Loss Events in 2019 and 2000-2019*.

Halwatura, D., & Najim, M. M. M. (2013). Application of the HEC-HMS model for runoff simulation in a tropical catchment. *Environmental modelling & software*, *46*, 155-162.

iCarto, & ARA-NORTE. (2017). Seminário de Apresentação da ARA-Norte e Resultados do Projecto SIXHIARA.

Istituto Oikos. (2023). Prontidao Project. www.istituto-oikos.org

Lazzarin, T., Viero, D. P., Molinari, D., Ballio, F., & Defina, A. (2022). Flood damage functions based on a single physics-and data-based impact parameter that jointly accounts for water depth and velocity. *Journal of Hydrology*, *607*, 127485.

Lugeri, N., Kundzewicz, Z. W., Genovese, E., Hochrainer, S., & Radziejewski, M. (2010). River flood risk and adaptation in Europe—assessment of the present status. *Mitigation and adaptation strategies for global change*, *15*, 621-639.

Lumbroso, D., Ramsbottom, D., & Spaliveiro, M. (2008). Sustainable flood risk management strategies to reduce rural communities vulnerability to flooding in Mozambique.Journal of Flood Risk Management,1(1), 34 42. https://doi.org/10.1111/j.1753-318x.2008.00005.x

Maranzoni, A., D'Oria, M., & Rizzo, C. (2022). Quantitative flood hazard assessment methods: a review. Journal of Flood Risk Management, 16(1). https://doi.org/10.1111/jfr3.12855

Matej Vojtek & Jana Vojteková (2016) Flood hazard and flood risk

assessment at the local spatial scale: a case study, Geomatics, Natural Hazards and Risk, 7:6,

1973-1992, DOI: 10.1080/19475705.2016.1166874

Meyer, V., Haase, D., & Scheuer, S. (2007). *GIS-based multicriteria analysis as decision support in flood risk management* (No. 6/2007). UFZ Discussion Paper.

Mondlane, A. I. (2004). Floods and droughts in Mozambique–the paradoxical need of strategies for mitigation and coping with uncertainty. *WIT Transactions on Ecology and the Environment*, *77*.

Mucova, S. A. R., Azeiteiro, U. M., Lopes, C. L., Dias, J. M., & Pereira, M. J. (2021). Approaching Sea-Level Rise (SLR) change: strengthening local responses to sea-level rise and coping with climate change in Northern Mozambique. *Journal of Marine Science and Engineering*, *9*(2), 205.

Operation Update: Mozambique| Floods and Cyclones. (n.d.). Retrieved from https://go.ifrc.org/emergencies/5787/details#details

Paz Idarraga & Rotaru (2023). Flood hazard and risk assessment in data-scarce regions: the case of the Metuge district in northern Mozambique

Rentschler, J., Salhab, M., & Jafino, B. A. (2022). Flood exposure and poverty in 188 countries. *Nature communications*, *13*(1), 3527.

Rrokaj, S., & Corti, B. (2019). Flood risk assessment and mitigation for Rio Muaguide in Cabo Delgado, Mozambique. Politecnico di Milano

Savage, J. T. S., Pianosi, F., Bates, P., Freer, J., and Wagener, T. (2016), Quantifying the importance of spatial resolution and other factors through global sensitivity analysis of a flood inundation model, Water Resour. Res., 52, 9146–9163, doi:10.1002/2015WR018198.

Thapa, S., Shrestha, A., Lamichhane, S., Adhikari, R., & Gautam, D. (2020). Catchment-scale flood hazard mapping and flood vulnerability analysis of residential buildings: The case of Khando River in eastern Nepal. *Journal of Hydrology: Regional Studies*, *30*, 100704.

The World Bank. (2019) Disaster Risk Profile Mozambique

The World Bank. (2019) Mozambique Disaster Risk Management and Resilience Program Technical Assessment Report

UNHRC. (2022) Annual Results Report Mozambique

UNICEF. (2023) MOZAMBIQUE Humanitarian Situation Report No. 5

UNDP. (2019) Mozambique Cyclone Idai Post Disaster Needs Assessment

United States Department of Agriculture (USDA). (1986). Urban Hydrology for Small Watersheds - TR55

World Food Programme. (2022) Mozambique Annual Country Report 2022

Wouters, L., Couasnon, A., De Ruiter, M. C., Van Den Homberg, M. J., Teklesadik, A., & De Moel, H. (2021). Improving flood damage assessments in data-scarce areas by retrieval of building characteristics through UAV image segmentation and machine learning–a case study of the 2019 floods in southern Malawi. *Natural Hazards and Earth System Sciences*, *21*(10), 3199-3218.

Zeufack, Albert G.; Calderon, Cesar; Kubota, Megumi; Korman, Vijdan; Cantu Canales, Catalina; Kabundi, Alain N. 2021. “Africa’s Pulse, No. 24” (October), World Bank, Washington, DC.